The Role of Cholesterol in Cell Signaling

BY

EWA STEC

B.S., University of Illinois at Chicago, 2010

THESIS

Submitted as partial fulfillment of the requirements
for the degree of Doctor of Philosophy in Chemistry
in the Graduate College of the
University of Illinois at Chicago, 2015

Chicago, Illinois

Defense Committee:
Prof. Wonhwa Cho, Chair and Advisor
Prof. Richard Kassner
Prof. Lawrence Miller
Prof. Jung-Hyun Min
Prof. Irena Levitan, Pulmonary Medicine

This thesis is dedicated to my mommy, Danusia Stec, who gave me endless support and love.

ACKNOWLEDGMENTS

I would like to thank to my advisor, Prof. Wonhwa Cho, for giving me an opportunity to research, raising my scientific capability, and giving motivations and encouragements to accomplish PhD program. He always has served as a good role model to me as a professor and a scientist. And also I appreciated my committee members, Dr. Kassner, Dr. Miller, Dr. Min, and Dr. Levitan, being my committee, and their valuable suggestions and supports.

I want to give thanks to all the former and current lab members, Mrs. Cho, Dr. Chen, Dr. Yoon, Dr. Surajit, Dr. Lucas, Dr. Tao, Dr. Sheng, Dr Kurilova, Park-Joo, Kate, Marian, Anthony, Hamid, Huda, Hyunjin, Yao, Charlie, Liz, Yusi, Indira who study and work together with me in Cho's group.

I would like to show my gratitude to my mom and my friends who always have given me concerns and loves. It always has been a huge motivation and energy to accomplish my study.

May 21, 2015

Ewa Stec

CONTRIBUTION OF AUTHORS

Chapter 1 represents published paper (Nature communication 3, (2012) 1249) where I greatly contributed to all aspects of the project, and was secondary author. I played a large role in measuring the binding of PDZ domains containing the CRAC motif to cholesterol and executed functional studies of NHERF-1 PDZ1 domain. I performed almost all Surface Plasmone Resonance (SPR) measurements. I assisted Dr. Ren Sheng in microscopy experiments and image analysis shown in Figure 2 and 4. I also participated in fluorescence anisotropy measurements. Dr. Hui Lu and his graduate student Morten Kallberg performed computational modeling that was used to generate Figure 6 and 11. The monolayer measurements (Figure 5) and radiolabeled studies (Figure 7A) were performed by Dr. Takahiro Fujiwara and Dr. Akihiro Kusumi from Kyoto University. My adviser, Dr. Wonhwa Cho, supervised the project and wrote the manuscript.

Chapter 2 represents a series of my own unpublished experiments. Dr. Shu-Lin Liu assisted me in the image analysis and Dr. Ren Sheng in cholesterol sensor design. Dr. Shu-Lin Liu, Dr. Li Wang, and other members of the laboratory will continue to investigate the remaining set of experiments after my defense. The data collected by my colleagues and I are planned for a future publication, in which I will serve as first co-author. My research mentor, Dr. Wonhwa Cho, is preparing the final draft of the manuscript.

TABLE OF CONTENTS

LIST OF TABLES

LIST OF FIGURES

LIST OF ABBREVIATIONS

27-HC	27- hydroxycholesterol
ABC	ATP-binding cassette
ACAT	acyl-CoA cholesterol acyl transferase
Acrylodan	6-acryloyl-2-dimethylaminonaphthalene
ATP	adenosine triphosphate
CFTR	cystic fibrosis transmembrane regulator
Chol	cholesterol
CRAC	cholesterol recognition amino acid consensus
D4	Domain 4
DAN	2-dimethylamino-6-acyl-naphthalene
DMEM	Dulbecco's modified Eagle's medium
DO	dioleoyl
DOPC	dioleoyl-phosphatidylcholine
DP	dipalmitoyl
DPPC	dipalmitoyl-PC
EGFP	Enhanced Green Fluorescent Protein
ER	endoplasmic reticulum
ERC	endosomal recycling compartment
GST	Glutathione S-transferase
GUV	Giant Unilamellar Vesicle
HDL	high-density lipoprotein
HMGR	3-hydroxy-3-methyl-glutaryl-CoA reductase

IPTG	Isopropyl β-D-1 -thiogalactopyranoside
K_d	dissociation constant
LDL	low-density lipoprotein
LE	late endosome
LUV	Large unilamellar vesicle
MβCD	methyl β-cyclodextrin
NPC	Niemann-Pick type C
NR-3	Nile Red 3
OSBP	oxysterol-binding protein
PC	phosphatidylcholine
PDZ	(PSD95/DLG1/ZO1)
PE	phosphatidylethanolamine
PFO	perfringolysin O
PI	phsphoinositide
PM	plasma membrane
POPC	1 -Palmitoy l-2-oleoyl-sn-glycero-3 -phosphocholine
POPE	1 -palmitoyl-2-oleoyl-sn-glycero-3 –phosphoethanolamine
PS	phosphatidylserine
PtdIns(4,5)P_2	Phosphatidylinositol 4,5-bisphosphate
PtdInsPs	phosphoinositides
PtdSer	phosphatidylserine
RU	Resonance Unit
SM	sphingomyelin

SM	sphyngomielin
SMase	sphyngomielinase
SPR	surface plasmon resonance
StAR	steroidogenic acute regulatory protein

SUMMARY

Membrane lipids regulate a wide range of biological processes, including cell signaling. Cholesterol is a major lipid component of the mammalian plasma membrane. Although the metabolism and transport of cholesterol and its role in cardiovascular disease have been extensively investigated, the exact cellular function of cholesterol is yet to be fully explored. Cholesterol plays a pivotal role in the stability and architecture of the plasma membrane, most notably the formation of cholesterol-rich membrane microdomains, and structural and functional modulation of integral proteins embedded in plasma membrane. The role of cholesterol in the plasma membranes extends beyond the modulation of the fluidity and permeability of the bilayer. Accumulating evidence suggests that changes in cellular cholesterol levels in the plasma membrane modulate functionality of proteins involved in signaling pathways. However, the direct involvement of cholesterol in cellular activities through specific interactions with cellular proteins has remained unclear. Also, quantitative information about its cellular spatiotemporal dynamics and its local concentration changes under pathophysiological conditions is surprisingly scarce, making it difficult to elucidate how potential changes in the local concentrations of cholesterol may affect cellular processes in health and disease.

Our laboratory has recently made two breakthroughs that should greatly help address these important questions. First, we discovered that cholesterol specifically interacts with various cytosolic scaffold proteins containing PDZ (PSD95, DLG1, and ZO1) domains and regulate their diverse cellular signaling activities. This important finding not only demonstrates that cholesterol can directly interact with major cellular regulatory proteins but also offers excellent systems to investigate the direct correlation

between membrane cholesterol levels and cell cellular activities. Second, we develop a new fluorescence imaging technology for accurate *in situ* quantification of cholesterol in a spatiotemporally resolved manner under physiological and patho-physiological conditions. The specific and sensitive cholesterol quantification was achieved by engineered sensor derived from the D4 domain of perfringolysin O toxin and favorable spectral and membrane-binding properties of DAN and Nile Red 3 probes. This simultaneous quantification of cholesterol provides us with physiologically important data and new insight unattainable by conventional methodologies. Collectively, our discovery of a new class of cholesterol binding proteins and our new quantitative cholesterol imaging technology represent an important technical advance toward understanding of complex cholesterol-mediated cell regulation.

CHAPTER 1

CHOLESTEROL MODULATES CELL SIGNALING AND PROTEIN NETWORKING BY SPECIFICALLY INTERACTING WITH PDZ-DOMAIN-CONTAINING SCAFFOLD PROTEINS

Experimental procedures, Figures (1, 3, 4, 5, 6A, 7, 8, 9, 10, 11, 12, 13A,B and 18) with descriptions, and Tables (Table 1 and Table S1) were extracted from the following paper:

Sheng, R., Chen, Y., Gee, H. Y., **Stec, E**., Melowic, H.R., Blatner, N.R., Tun, M.P, Kim, Y., Kallberg, M., Fujiwara, T., Hong, J.H., Kim, K.P., Lu, H., Kusumi, A., Lee, M.G., and Cho, W. Cholesterol Modulates Cell Signaling and Protein Networking by Specifically Interacting with PDZ Domain-Containing Scaffolding Proteins. Nature Communications. 2012; 1249(3).

1. INTRODUCTION

Effective signal transduction in cellular systems relies on scaffolding proteins, which organize diverse cell signaling assemblies [1]. Proteins that are part of these signaling hubs are not only equipped with catalytic activities but also with binding capacities for other proteins or even lipids [2]. By tethering multiple members of a signaling pathway, scaffold proteins can not only help to localize signaling molecules to specific compartments of the cell but also coordinate and guide the flow of cellular information. Understanding these protein networks is crucial for defining most of the key signaling pathways that functionally control cellular responses to external stimuli, but it is a very challenging task due to complexity of individual components and specific interactions in which each protein can be engaged [2]. Scaffolds are usually composed of multiple modular interaction domains [3]. Recently, it has become clear that modular protein interaction domains, the PDZ family members in particular, play key role in mediating assembly of macromolecular complex.

PDZ domains are one of the best-characterized protein interaction modules that are predominantly found in eukaryotes but also in some prokaryotes, bacteria, and yeasts. Their name originates from the three proteins in which these domains were first identified: post-synaptic density 95 protein (PSD-95), Discs Large protein (DLG), and zona occludens 1 protein (ZO-1) [4]. In human, 270 PDZ domains have been documented in over 150 different proteins [2] that are implicated in regulation of multiple biological processes such as establishment and maintenance of cell polarity, cell migration, regulation of cell junctions, ion channel signaling, and signal transmission in neurons [5]. These domains consist 80-100 amino acids and encompass two α helices (αA and αB)

and six β strands (βA~ βF). PDZ domains can be present in one or several copies or additionally flanked by other interaction modules. PDZ-containing proteins are classified into three major families according to their modular topology [7]. To the first category fall proteins with PDZ domains only, whereas second family associates PDZ domain(s) with SH3 and guanylate kinase (GuK) domains. The third family contains proteins with PDZ domains flanked by other modular domains, such as, PH, DEP, C2, WW, and LRR domains [7]. The primary function of PDZ domains is to recognize a specific carboxyl-terminal sequences present in their partner proteins. More recently, internal-motif-mediated PDZ interaction (sequences that structurally mimic a C-terminus motif) has also been identified and reported in few cases [8]. C-terminal recognition is found to fall into at least three discrete functional categories, depending on the identity of critical binding residues [9]. Class I PDZ domains distinguish the motif T/S-X- ψ -COOH (where X is any amino acid and ψ is a hydrophobic residue). Category II has ability to bind to ψ X ψ-COOH motifs whereas class III PDZ domains to D/E-X- ψ-COOH [10]. PDZ domains bind to the COOH-termini of target proteins in extended groove situated between βB-strand and αB-helix, known as the "peptide-binding groove" that contains well-conserved R/KXXXGLGF signature [11]. In this motif, the first glycine residue is variable among the vast majority of PDZ domains and can be substituted with Thr, Phe, or Ser [12]. The second and the fourth residues, on the other hand, are hydrophobic (Phe, Val, Ile, or Leu) [12] and are conserved among species. Such sequence and the conformational properties of amino acid residues firmly position the peptide in the binding groove. Accumulating studies show, however, a more complex landscape for PDZ interactions as many of them are able to interact with the peptide ligands that do not share the canonical consensus

sequence at their COOH-termini [10]. Subsequently, adding to their versatility, more recent investigations have demonstrated that many PDZs interact with other PDZ domains (hetero-dimerization), intrinsically disordered regions within proteins, and finally lipids [13]. These structural features permit PDZ domains to transport appropriate proteins to sites of cellular signaling and thereby coordinate signaling complex formation. Consequently, significant measurements have been undertaken to decipher their binding preferences, as such knowledge would allow to gain insights into PDZ-mediated biological processes that govern the intracellular signaling at the molecular level.

The PDZ family members are often associated with the plasma membrane (PM), a compartment where majority of signaling lipids are located. Recent advances suggest that membrane lipids play a central role in the formation of structural and functional supramolecular networks through direct collaborations with scaffolding proteins [9,10]. This conundrum is further complicated by the latest notion that PDZ domains have dual binding specificities and can facilitate not only protein-protein but also protein-lipid interactions [16]. This property promotes a new mode of action of PDZ domains in the control of cell signaling. Defining the molecular mechanisms by which PDZ domains interact with biological membranes will be essential for understanding how lipids can orchestrate these interactions. The first reports indicating that numerous PDZ domains interact with plasma membrane and phosphoinositides (PIPs) as a main signaling lipid in particular [17,18] came 10 years ago. Although PIPs represent a small portion of the cellular phospholipids, they are important regulators of vast cellular activities like cell growth and differentiation, vesicular trafficking, cytoskeletal organization, and ion channels and transporters functionality [19]. Until now, only few research groups were

successful in providing insight on the molecular details of PDZ-PtdInsPs binding-interactions. In the one of the first well-known studies, Wu et al assessed that 20 percent of PDZ domains from the human genome interact with membrane lipids [20]. In subsequent investigation involving a pool of 70 PDZ domains from various species, Chen et al reported that 40 percent of PDZ domains display membrane binding [16]. In addition, when he measured PtdInsPs selectivity of 28 PDZ domains, only 4-tested domain showed some degree of selectivity toward this lipid [16]. Although, different attempts were undertaken to identify the PDZ-PtdInsPs interactions, the promiscuity and specificity of these interactions and their impact on PDZ recruitment to plasma membrane have not been foreseen [3]. It became very clear that many PDZ domains do not possess high enough affinity for PIPs, and that is why they cannot act alone to navigate their target proteins to specific membrane compartments. To become powerful signal integrators, they most likely need to act together with other modular domains [6] or membrane lipids to form complexes with greater avidity for biological membranes. Based on these observations, a critical question is raised: What other lipids play a crucial role in assembly of multi-protein platforms on or in very close proximity to membranes through direct association with scaffolding proteins containing PDZ domain? One candidate is cholesterol, which is a major lipid constituent of the mammalian plasma membrane. Cholesterol present in cell membranes has been proven to be essential in regulating neurotransmission [21] and protein sorting [22], and an imbalance in the cholesterol level has similarly been implicated in many diseases, such as cancer [23], diabetes mellitus type 2 [24], and Alzheimer's disease (AD) [25]. Since membrane cholesterol content has a specific effect on certain physiological processes, mammals

have developed sophisticated but only partially characterized molecular machineries to sustain cellular cholesterol levels in membranes within a narrow range [26]. However, a molecular understanding of how cholesterol regulates cell signaling is still lacking. Interestingly, we discovered that numerous PDZ domains contain a "cholesterol recognition/interaction amino acid consensus (CRAC) motif" which is represented by the pattern "(**L/V**-(X)(1–5)-**Y**-(X)(1–5)-**R/K**-," and which occurrence was reported in some cholesterol-binding integral membrane proteins and ion channels [27] but never in cytosolic proteins. Thus, the primary goal of our investigation was to determine PDZ domains with the CRAC motif could actually bind cholesterol and how this potential cholesterol binding regulates physiological function of those PDZ domain-containing proteins. The recruitment and targeting of PDZ-protein complexes to the plasma membrane most likely rely on specific cholesterol recognition. Therefore, elucidating the cholesterol induced PDZ-plasma membrane clustering will improve our knowledge on the potential significance of this interaction in cell signaling.

2. EXPERIMENTAL PROCEDURES [28]

2.1. Materials

All lipids were purchased from Avanti Polar Lipids except for the 1,2-dipalmitoyl derivative of PtdIns(4,5)P_2 that was from Cayman Chemical. The rabbit polyclonal antibody against NHERF1 was from Thermo Fisher Scientific. Horseradish peroxidase-conjugated goat anti-rabbit IgG was purchased from Cayman. The horseradish peroxidase conjugate substrate kit was from Bio-Rad. Forskolin, 3-isobutyl-1-methylxanthine, and bumetanide were from Sigma. 6-Methoxy-N-(3-sulfonropyl) quinolinium was from Molecular Probes.

2.2. Plasmid construction

Constructs for bacterial expression were prepared by subcloning cDNAs of the full-length NHERF1 and its PDZ1 domain into pET21a (+) (Invitrogen). Mammalian expression platforms were obtained by subcloning the same cDNAs into pEGFPC1 (BD Clonetech) vector. Constructs for other PDZ domains were prepared using either the pET21a (+) vector or were tagged with enhanced green fluorescent protein (EGFP) on the C-terminus and then subcloned into pRSET-b vector (Invitrogen). The D1 domain (residue K391-N500) of perfringolysin O was subcloned into the pGEX-4T-1 (Invitrogen) vector to generate bacterial expression plasmid containing an N-terminal glutathione S-transferase (GST) fusion. Mutations were done with a QuickChange kit from Stratagene. After positive results each construct was sent and verified by DNA sequencing.

2.3. Protein expression and purification

For protein expression, the constructs for all PDZ domains with a C-terminal His_6 tag were transformed into Escherichia coli BL2 (DE3) pLysS (Novagen) cells. Cells are cultured using Luria broth when optical density at 600nm was 0.6 units at 37°C. Induction of expression machinary is initiated with addition of 0.2mM isopropyl 1-thio-β–D galactopyranoside (IPTG) and culture was shaken for additional 16 hours at 25°C. The cells were harvested by centrifugation for 10 min at 500rpm. To purify the PDZ domains, cell pellet was vortexed and resuspended in lysis buffer (50mM Tris, 300mM NaCl, 10mM Immidazole, 10%(v/v) Glycerol, pH 7.9) containing 20 µl of 2-mercaptoethanol. The solution was sonicated (Branson Sonifier 450) for 5 minutes on ice (15 s sonication and 15 s rest period). The supernatant was collected by a 30 min centrifugation at 16,000 rpm at 4°C and added to 1.0 mL Ni-NTA agarose from (QIAGEN) and mixed for 1 hr. Using 50mM Tris pH 7.9, containing 300mM NaCl, 20mM imidazole and then with 20mM Tris pH 7.9, containing 160mM NaCl, 20mM imidazole the resin was washed. The protein was eluted by 50mM Tris pH 7.9, containing 160mM NaCl, 300mM imidazole and purified on Q-Sepharose ion-exchange chromatography. SDS-PAGE gel and bicinchoninic acid method (Pierce), respectively were used to determine protein concentration and overall purity.

The D_1 domain of perfringolysin O was transformed into E. coli RIL cells and expressed as a glutathion- S-transferase-tagged protein. Growth of E. coli was initiated by inoculating 1 L flask of sterile Difco Luria broth (containing 100 µg/mL ampicillin) with 10ml of an overnight culture grown at 37°C. The 1L culture was incubated at 37°C with constant shaking. Expression of D_1 domain of PFO was induced by adding isopropyl β-

D-thiogalactopyranoside to a concentration of 0.2 mM when A_{600}nm of the suspension was at 7.0. The induced culture was further grown for 16 h at room temperature, and the cells were harvested by centrifugation at 5000 rpm for 10 min. The pellets were resuspended in 20ml lysis buffer (50mM Tris, 300mM NaCl, 10mM Immidazole, 10%(v/v) Glycerol, pH=7.9) containing 20 µl of 2-mercaptoethanol and subjected to tip sonication with a cell disruptor (Branson Sonifier 450) for 15 s while cooled on ice, followed by the rest period of 15s as well. The sonication and cooling steps were repeated 15 times. Next, the mixture centrifuged at 16,000 rpm for 30 min. The supernatant from this step was incubated for 1 h at 4°C while mixing with 1 ml glutathione S-transferase tag^{TM} resin (Novagen, Madison, WI). The resin solution was transferred to chromatography column and washed with 150ml washing buffer (20mM Tris, 160mM NaCl, pH=7.4) with occasional pipetting. Purification was fallowed by thrombin treatment. 1 µl of thrombin (Invitrogen) was added to the column containing 1ml of 20 mM Tris-HCl buffer with 0.16 M KCl (pH=7.4) solution and the mixture was incubated at 4°C for 12h. After overnight incubation, the protein was eluted and concentration was determined by the bicinchoninic acid method (Pierce).

2.4. Lipid vesicle preparation

PM-mimetic vesicles are formulated with 1-palmitoyl-2-oleoyl-sn-glycero-3-phosphocholine (POPC), 1-palmitoyl-2-oleoyl-sn-glycero-3-phosphoethanolamine (POPE), 1-palmitoyl-2-oleoyl-sn-glycero-3-phosphoserine (POPS), cholesterol, 1-palmitoyl-2-oleoyl-sn-glycero-3-phosphoinositol (POPI), and 1,2-dipalmitoyl derivatives of PtdIns(4,5)P_2 using a molar ratio 12:35:22:22:8:1. Solution for PM-cholesterol vesicles contains POPC/POPE/POPS/PI/PtdIns(4,5)P_2 in a molar ratio of 23:46:22:8:1. To prepare

large unilamellar vesicles (LUVs) Liposofast (Avestin) microextruder with a 100-nm polycarbonate filter was used. Giant unilamellar vesicles (GUVs) were prepared by the electroformation. The lipid mixture (POPC/POPS/cholesterol= 80-x:20:x, x = 0-30 mole%) was dissolved in chloroform to the final concentration of 100 μg/ml. The lipid solution was spread onto the indium-tin oxide electrode surface and dried under vacuum for 1.5 hour. By applying an electric field at 3V with 20 Hz frequency, the vesicles were developed in 350 mM sucrose solution the vesicles at room temperature for 4 hours. 1μl sucrose-loaded GUV solution was added into a well containing 200 μl of buffer (20 mM Tris, 0.16 M NaCl, pH 7.4). Protein was added after GUVs were sedimented at the bottom of the well, and the entire well was scanned with an automated x-y stage (2-min scan time).

2.5. Determination of PDZ domain bound to GUV by fluorescence microscopy.

All fluorescence microscopy measurements were carried out at 37 ºC using a custom-built multi-photon microscope that was described previously. Both instrument control and data analysis were performed by the SimFCS. GUV composed of POPC/POPS/cholesterol (80-**x**:20:**x**; **x** = 0-30 mole%) were mixed with 200 nM EGFPNHERF1-PDZ1 in 20 mM Tris-HCl, pH 7.4, contains 0.16 M NaCl. For each cholesterol concentration, 10 GUVs were selected and for each GUV, an averaged image of a total of 10 frames was collected for further analysis by MATLAB (MathWorks, Inc). The total photon counts in blue and green channels of the image were read into a M x N (typically 256 x 256) matrix: $(\mathbf{I})_{i,j}$ ($0 \leq \mathbf{I} \leq M - 1$ and $0 \leq \mathbf{j} \leq N - 1$) to recreate the averaged image. Each matrix element (one pixels, ai,j) represents the raw photon counts. Then a binary image mask (**I**') was created on the lipid bilayer of GUV using this image matrix

by analyzing the photon count histogram of the image.

For any $a'_{i,j}$ Î **I'**, either $a'_{i,j}$ =0 or $a'_{i,j}$=1. So the result of element by element multiplication of **I** and **I'** (i.e., **I''=I** x **I'**) will be $a_{i,j}$ x $a'_{i,j}$ = $a_{i,j}$ where $a'_{i,j}$ = 1 and $a_{i.j}$ x $a'_{i,j}$ = 0 where $a'_{i,j}$ = 0. The total photon counts of GUV ($\mathbf{F}_{B(total)}$) and $\mathbf{F}_{G(total)}$)were divided by the total area of the pixels that constitute each GUV to yield the photon counts per area.

2.6. Surface Plasmon Resonance (SPR) Measurement

All SPR measurements were performed at 23°C in running buffer (20 mM Tris, pH 7.4, containing 0.16 M NaCl). Lipids were immobilized on L1 chip in the BIACORE X system purchased from GE Healthcare. The active channel (Fc-2) was coated with PM-mimetic (or others) vesicles and control surface with POPC vesicles (Fc-1). Equilibrium SPR measurements required extended time for association equilibration for reliable R_{eq} results, thus a flow rate of 5 μL per minute was used. Each sensorgram was background-corrected by subtracting the response units (RU) of control surface from the active surface ones. The Langmuir-type binding, represented as P + M <--> PM, is concerning the protein, P, and vesicle binding site for protein, M, was used to analyze sensograms. A plot was generated comparing the equilibrium values, R_{eq}, and concentration of protein, P_0. Using the binding isotherm curve and nonlinear least-squares analysis, R_{eq} = Rmax/(1 + Kd/Po), was solved for dissociation constant, K_d. Kinetic SPR measurements were preformed at 30 μL per minute flow rate for both association and dissociation phases. The measurement was repeated three times to obtain average and standard deviation values.

2.7. Monolayer measurement

Surface pressure of solution in a circular Teflon trough (4 cm diameter x 1 cm deep) was measured using a Wilhelmy plate attached to a computer-controlled Cahn electrobalance (Model C-32) as described previously 2. Five to ten µl of lipid solution (POPC/POPS/cholesterol = 6:2:2) in ethanol/hexane (1:9 (v/v)) was spread onto 10 ml of subphase (20 mM HEPES, pH 7.4, containing 0.16 M KCl) to form a monolayer with a given initial surface pressure. Once the surface pressure reading of monolayer stabilized, the protein solution (typically 40 µl) was injected into the subphase through a small hole drilled at an angle through the wall of the trough and the change in surface pressure was measured as a function of time with gentle stirring until it reached a maximal value. The maximal change in surface pressure value at a given initial surface pressure depended on the protein concentration and thus protein concentrations in the subphase were maintained high enough (typically **Ñ**1 **µ**g/ml) to ensure that the observed change in surface pressure represented a maximal value. The critical surface pressure was determined by extrapolating the change in surface pressure versus initial surface pressure plot to the x-axis 3.

2.8. Binding to radiolabeled cholesterol

Binding of PDZ domains to 1,2-3H-labeled cholesterol (Perkin-Elmer) was performed in 20 mM Tris-HCl, pH 7.4, with 160 mM NaCl and 1 µM of protein as reported previously 5. Cholesterol in ethanol was added to the protein solution to a final concentration ranging from 0 to 10 µM and the mixture was incubated at 25 °C for 1 hour. A His SpinTrap column (GE Healthcare) was pre-equilibrated with 20 mM Tris-HCl pH 7.4

with 160 mM NaCl, and the reaction mixture was added to the column and incubated for 5 minutes. The column was washed three times by 600 µl of the same buffer, and the protein was eluted using 600 µl of 20 mM Tris-HCl pH 7.4 with 160 mM NaCl and 300 mM immidazole. 200 µl of the washed (free cholesterol) and eluted (protein-bound cholesterol) solutions were taken for radioactivity measurement using the Beckman LS6500 liquid scintillation counter.

2.9. GST pull-down experiment

Glutathione S-transferase (GST) and GST-fusion CFTR peptides (GST-QDTRL) were expressed in BL21 (DE3) pLysS (Novagen) and purified. The proteins were mixed with glutathione beads in the incubation buffer (20 mM Tris-HCl, pH 7.4, 0.16 M NaCl, 1% Triton X-100) and the beads with the bound proteins were washed three times with the buffer and re-suspended in the buffer. Purified human recombinant NHERF1 proteins (0-5 **µ**g) were incubated with 5 **µ**g of GST and GST-CFTR bound to the beads for 30 min at 4°C. The bound proteins were collected by brief centrifugation, washed 3 times with the incubation buffer, extracted with the Laemmli buffer, and subjected to dodecylsulfate-polyacrylamide gel electrophoresis and immunoblotting using the rabbit polyclonal antibody against NHERF1 and horseradish peroxidase-conjugated goat antirabbit IgG.

2.10. Cellular Culture and Methyl-β-cyclodextrin Treatment

MDCKII cells were seeded into 50 mm round glass-bottom plates and grown in 37 °C in humidified atmosphere with 95% air and 5% CO2. Growth medium Dulbecco's modified Eagle's medium (DMEM) (Life Technologies) was supplemented with 10% (v/v) fatal

bovine serum (FBS), 100 units per milliliter penicillin G, and 100 microgram per milliliter streptomycin sulfate (Life Technologies) and passaged every other day. For cholesterol depletion, MDCKII cells were incubated in 5 mM MβCD, methyl-β-cyclodextrin, (Sigma) for 60 minutes in serum free media.

2.11. Confocal Imaging

MDCK2 cell transiently transfected with N-terminal-enhanced green fluorescence protein (EGFP)-tagged NHERF1 were used for confocal imaging. Confocal imaging was performed using Zeiss LSM510 microscope. HEK 293 cells stably expressing the EGFP-CFTR was transfected with HaloTM (Promega)-tagged NHERF-1 and labeled with Halo-Tag tetramethylrhodamine (Promega) for TIRF imaging. The EGFP-tagged human CFTR in pcDNA3.1(-) (Invitrogen) was transfected into HEK293 cell with 1 **μ**g DNA and 0.5 **μ**l of Lipofactamine 2000 (Invitrogen) for each well of 8-well plate (Thermo Scientific). HEK 293 cells stably expressing the EGFP-CFTR was prepared after selection with 1 mg/ml geneticin (Gibco) for 2 weeks and maintained with 200 **μ**g/ml of geneticin. After a few passages, the stable cell line was transfected with 0.05 **μ**g of HaloTM (Promega)-tagged NHERF-1 and 0.3 **μ**l of Lipofactamine 2000 for each well of 8-well plate for 4 hours and kept at 37oC in a 5% CO2 incubator for 12 hours. As a control, one plate was treated only with Lipofactamine 2000. Halo-Tag tetramethylrhodamine (TMR, Promega) diluted 200,000 times with the media was added to each well for labeling Halo-NHERF1 and the plates were kept at 37oC in a 5% CO2 incubator for 15 min. The TMR-containing media were replaced by equal amount of warm fresh media and after 3x washing, the plates were kept at 37oC for 30 min. Finally, the media was replaced with one without phenol red for imaging. An Olympus IX71

microscope was used as the base for the custom-built TIRF microscope. For dual color imaging, two DPSS lasers (488/561 nm, Excelsior, Spectra-Physics) were introduced to an Olympus 100x TIRF oil-immersion objective (numerical aperture 1.49) through the side port parallel but off the optical axis using a dual band dichroic mirror (XF2044 490-575DBDR, Omega Optical). The fluorescence from the sample was split into two channels through a dichroic mirror (565DCXR Chroma) and passed through emission filters (510BP20, Omega and D630/30, Chroma) and finally projected on to the EMCCD cameras (Andor) acquiring images of 512x512 at 30 msec interval. The images were spatially corrected following the algorithm described previously 7. Briefly, the centroids of an array of holes spaced 5 μm on a grid were used to create a lookup table for each channel using a cubic spline interpolation for the correction of the raw images through the remapping of the pixel intensities based on the lookup tables. All particle tracking, data analysis and image processing were carried out with in-house programs written in MATLAB.

2.12. Structural modeling of CFTR and Electrostatic calculation

A structure model of the C-terminal domain of CFTR was constructed using our structure prediction tool RaptorX 8. First, domain parsing of the CFTR protein sequence (P13569) was done to determine the individual folding units of the full protein sequence. From this analysis it was determined that CFTR is composed of a total of 14 domains, with the residues 1423 to 1480 constituting the C-terminal folding unit containing the PDZ binding peptide. Since protein domains are known to act as independent functional units, further analysis focused exclusively on the C-terminal domain (referred to as CFTR-14 hereafter). A series of structure models was constructed for CFTR-14 based

on a multiple sequence alignment with template structures, 1R5I-D and 3KPH-A. The top-ranked structure model used further in this study had a quality score of 54 (a model scoring 30 or higher is normally considered reliable). To better gauge the full interaction context of CFTR-14 with NHERF1-PDZ1, the newly constructed structure of CFTR-14 was superimposed on the docking model of the terminal peptide of CFTR shown in Fig. 1C and the best structure of the CFTR-14-NHERF1-PDZ1 complex was selected as described above for the CFTR-peptide-NHERF1-PDZ1 complex. The full electrostatic profile of the CFTR-14-NHERF1-PDZ1 complex was then determined by solving the Poisson-Boltzmann equation using APBS 9.

2.13. PDZ-peptide binding assay by fluorescence anisotropy

A fluorescein-6-aminohexanoyl (F-Ahx)-labeled peptide, F-Ahx-VQDTLR or F-Ahx-EETEEEVQDTLR, was dissolved in 20 mM Tris buffer, pH 7.9, containing 160 mM NaCl, 300 mM imidazole and 5% dimethylsulfoxide. To each well of Corning 96 flat bottom black polystyrol plate was added 100 **µ**l solution containing each peptide (5 nM final concentration) and each PDZ domain solution (concentration ranging from 100 nM to 1 mM). After incubation for 30 minutes, the plate was inserted into Tecan Genios Pro spectrofluorometer and the fluorescence anisotropy (r) was measured with excitation and emission wavelengths set at 485 and 535 nm, respectively. Since Po ≫ Pepo under our conditions, the Kd for the PDZ domain-peptide binding was determined by the non-linear least-squares analysis of the binding isotherm using the equation:

$$Pep_{bound}/Pep_0 = \Delta r/\Delta_{rmax} = 1/(1+K_d/P_0)$$

where Pepbound , Pep_o , and Po indicate the concentration of bound peptide, total

peptide and total PDZ domain, respectively, and Δr and Δr_{max} are the anisotropy change for each Po and the maximal Δr , respectively.

3. RESULTS

3.1. Many PDZ domains bind cholesterol

Considering that cholesterol is primarily localized to plasma membrane, and using vesicles that are cholesterol rich (see Methods) with available PDZ domains that have increased affinity for cholesterol we quantified their cholesterol preference by testing cholesterol dependency in vesicle binding. The thirty screened PDZ domains (Table S1, Suplementery materials) were analyzed by SPR, which showed that twelve PDZ domains have sub-micromolar affinity for vesicles resembling the inner leaflet composition of the plasma membrane, and eight of them exhibited prominent cholesterol dependency in membrane binding, with different affinities (Figure 1). To further validate our finding, PDZ domains that showed cholesterol-dependent binding were tagged with enhanced green fluorescence protein (EGFP), expressed in MDCK2 cells, and their subcellular distribution was analyzed by fluorescence microscopy. In the majority of the cases, the fluorescent domains were localized on the plasma membrane but in some instances PDZ domains were enriched on the plasma membrane and distributed diffusely in cytosol at the same time. As Figure 2A depicts, the most striking plasma membrane localization was observed for NHERF PDZ-1 and α1-syntrophin PDZ. We next investigated if plasma membrane localization of these domains will be affected by methyl-β-cyclodextrin treatment, a method commonly used to remove cholesterol from the plasma membrane in living cells. The treatment conferred significant loss in apparent plasma membrane binding in line with the *in vitro* data. NHERF PDZ-1 and α1-syntrophin

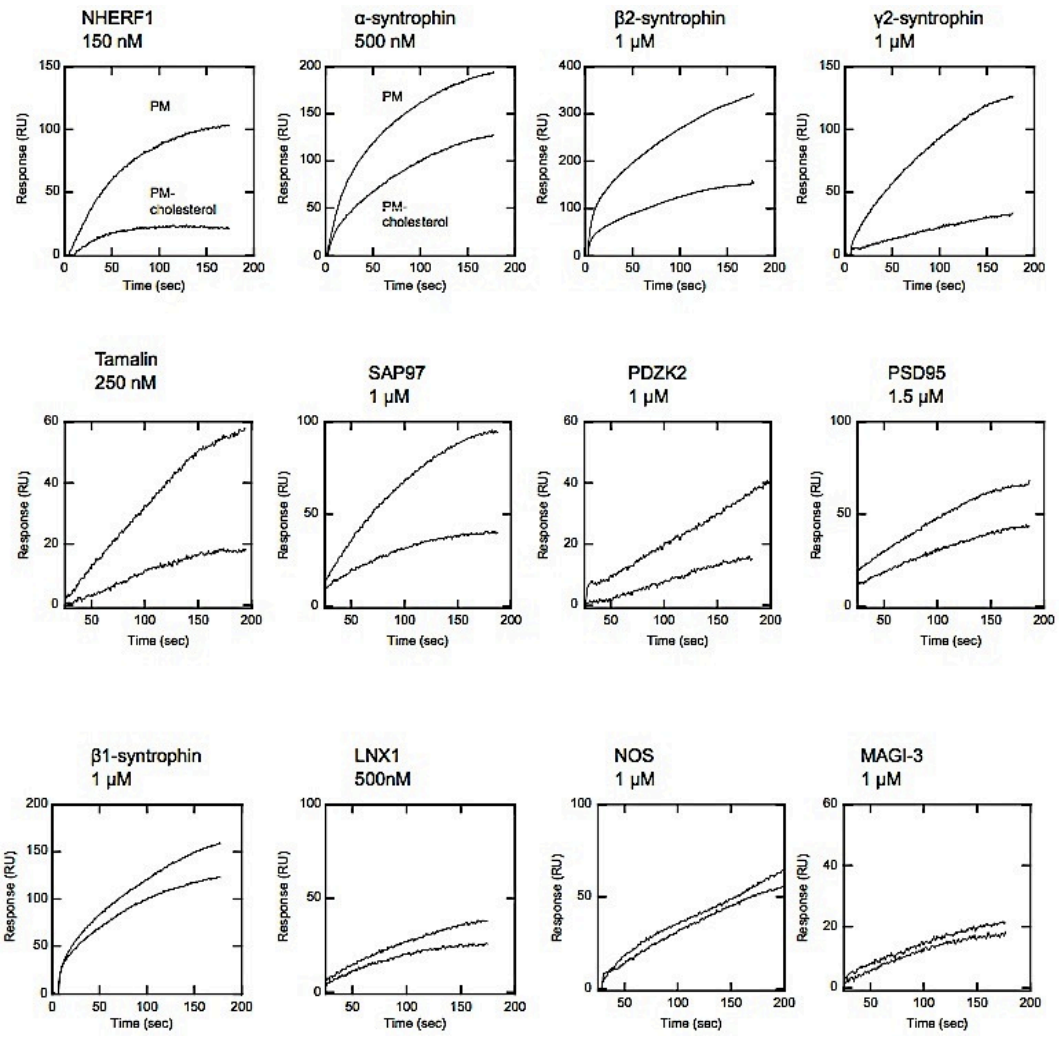

Figure 1. Cholesterol-dependent membrane binding of PDZ domains with the CRAC motif [28].

For all PDZ domains the upper curve is for PM-mimetic vesicles (POPC/POPE/POPS/POPI/Cholesterol/PtdIns(4,5)P_2 (12:35:22:8:22:1)) and the lower for PM-cholesterol vesicles (POPC/POPE/POPS/POPI/PtdIns(4,5)P_2 (19:40:27:13:1)). Protein concentration used for the SPR measurement is shown for each PDZ domain. Vesicle binding affinity was measured in 20 mM Tris-HCl, pH 7.4, containing 0.16 M NaCl While 8 PDZ domains in the first two rows show clear cholesterol dependency in membrane binding, four PDZ domains in the bottom row do not [28].

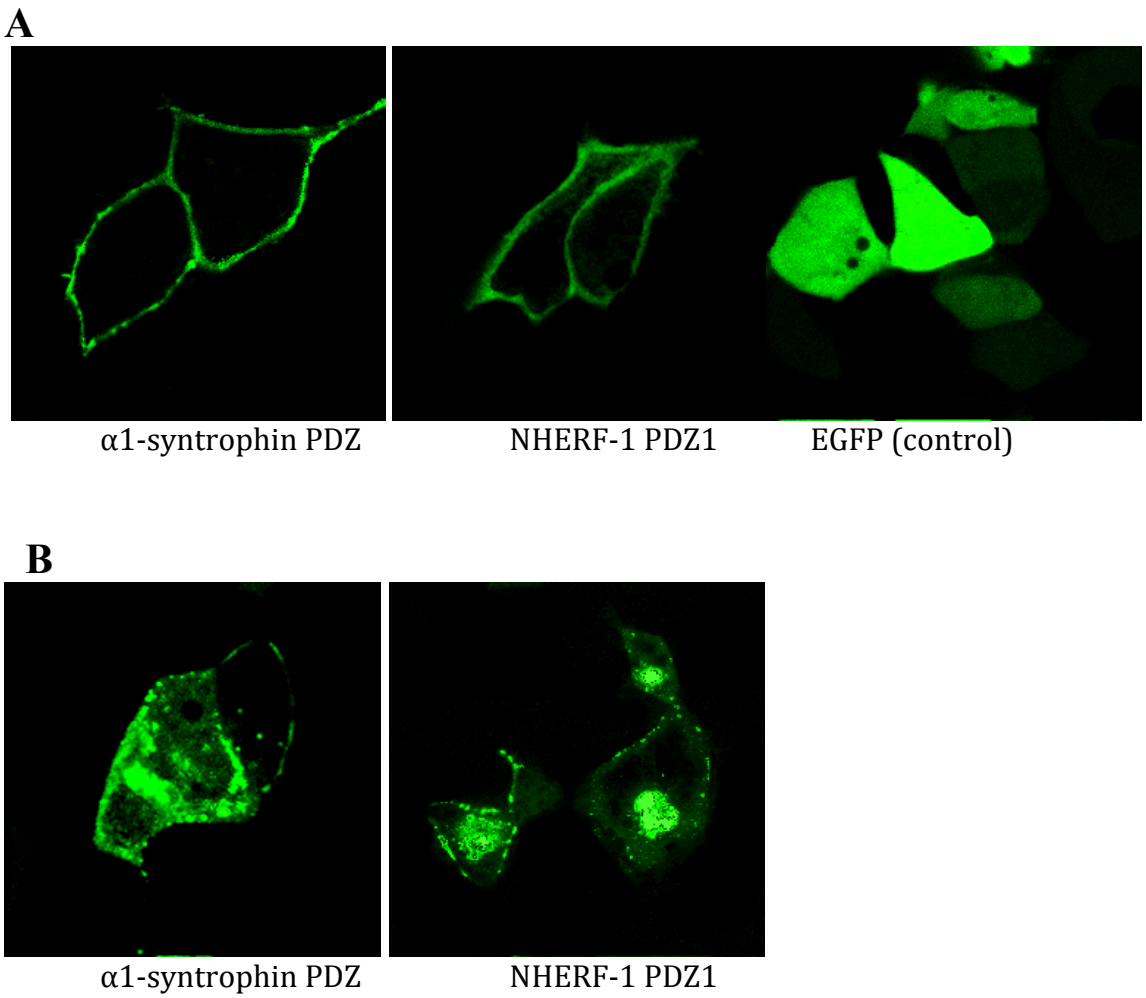

Figure 2. PDZ domains as an enhancer for cholesterol dependent cellular plasma membrane localization.
(**A**) Confocal micrographs of MDCK2 cells over-expressing EGFP tagged PDZ domains. Shown are examples of strong plasma membrane localization of α1-syntrophin PDZ and NHERF-1 PDZ1. (**B**) Neither the α1-syntrophin nor PDZ NHERF-1 PDZ1 was able to localize on the plasma membrane after methyl-β-cyclodextrin treatment.

Table 1. Membrane binding properties of PDZ domains and their mutants measured by SPR analysis. Vesicle binding affinity was measured in 20 mM Tris-HCl, pH 7.4, containing 0.16 M NaCl [28].

Proteins	Lipids	Kd (nM)[a]
NHERF1-PDZ1 WT	PM[b]	38 ± 9
NHERF1-PDZ1 WT	PM-Chol[c]	760 ± 60
NHERF1-PDZ1 WT	PM'[d]	600 ± 80
NHERF1-PDZ1 K32A	PM	87 ± 23
NHERF1-PDZ1 K34A	PM	175 ± 20
NHERF1-PDZ1 K32A/K34A	PM	350 ± 40
NHERF1-PDZ1 L35A	PM	68 ± 5
NHERF1-PDZ1 Y39A	PM	106 ± 9
NHERF1-PDZ1 R40A	PM	255 ± 32
NHERF1-PDZ1 Y39A/R40A	PM	684 ± 45
NHERF1-PDZ1 L41A	PM	800 ± 45
NHERF1-PDZ1 V42A	PM	84 ± 14
NHERF1 FL[e] WT	PM	76 ± 9
NHERF1 FL Y38/R40	PM	24 ± 3
α-syntrophin PDZ WT	PM	860±70
α-syntrophin PDZ Y162A/K164A	PM	NM[f]
SAP102 PDZ3 WT	PM	260 ± 45
SAP102 PDZ3 Y530A/R532A	PM	NM
PSD95 PDZ3 WT	PM	390±30
PSD95 PDZ3 Y439/K441	PM	2700± 320

[a]Mean ± S.D. values determined by equilibrium SPR analysis
[b]PM-mimetic vesicles = POPC/POPE/POPS/PI/cholesterol/PtdIns(4,5)P2 (12:35:22:8:22:1)
[c]PM mimetic - cholesterol = POPC/POPE/POPS/PI/PtdIns(4,5)P2 (23:46:22:8:1)
[d]PM-mimetic vesicles with 5α,6β-dihydroxycholestanol = POPC/POPE/POPS/PI/5α,6β-dihydroxycholestanol/PtdIns(4,5)P2 (12:35:22:8:22:1)
[e]FL, Full-length protein
[f]NM, Not Measurable

showed a substantial decrease in the plasma membrane localization due to cellular cholesterol depletion. (Figure 2B). Taken together, these results depict a substantial proportion of PDZ domains from different proteins and diverse functions bind to the plasma membrane with high affinity, and are cholesterol-dependent.

3.2. NHERF1 PDZ1 domain specifically binds cholesterol

After screening the available PDZ domains it was discovered that NHERF1, specifically the N-terminal region also named PDZ1, displayed maximum affinity for cholesterol based plasma membrane-mimetic vesicles with a K_d of about 40 nM, (Figure 1, Figure 3A,B) and the most noticeable cholesterol dependency (Figure 3C). With this result we selected NHERF1-PDZ1 domain and the full-length NHERF1 for detailed functional studies. Surface plasmon resonance binding experiments with NHERF1-PDZ1 showed dramatically lower affinities towards other lipids like oxysterols or ceramide, therefore confirming the high specificity toward cholesterol (Figure 3D). The cholesterol-dependent nature of NHERF1-PDZ1 was additionally investigated using GUVs or giant unilamellar vesicles with cholesterol at differential concentrations, while the PDZ1 domain was bound to EGFP, enhanced green fluorescence protein, and measured with quantitative fluorescence imaging (Figure 4).

According to literature, subset of PDZ domains exploits a common mechanism to interact with cell membranes. The mechanism is based on the structural properties of the domains and include the following steps: (i) electrostatic interactions between anionic membranes and basic protein residues, (ii) association of hydrophobic residues with the

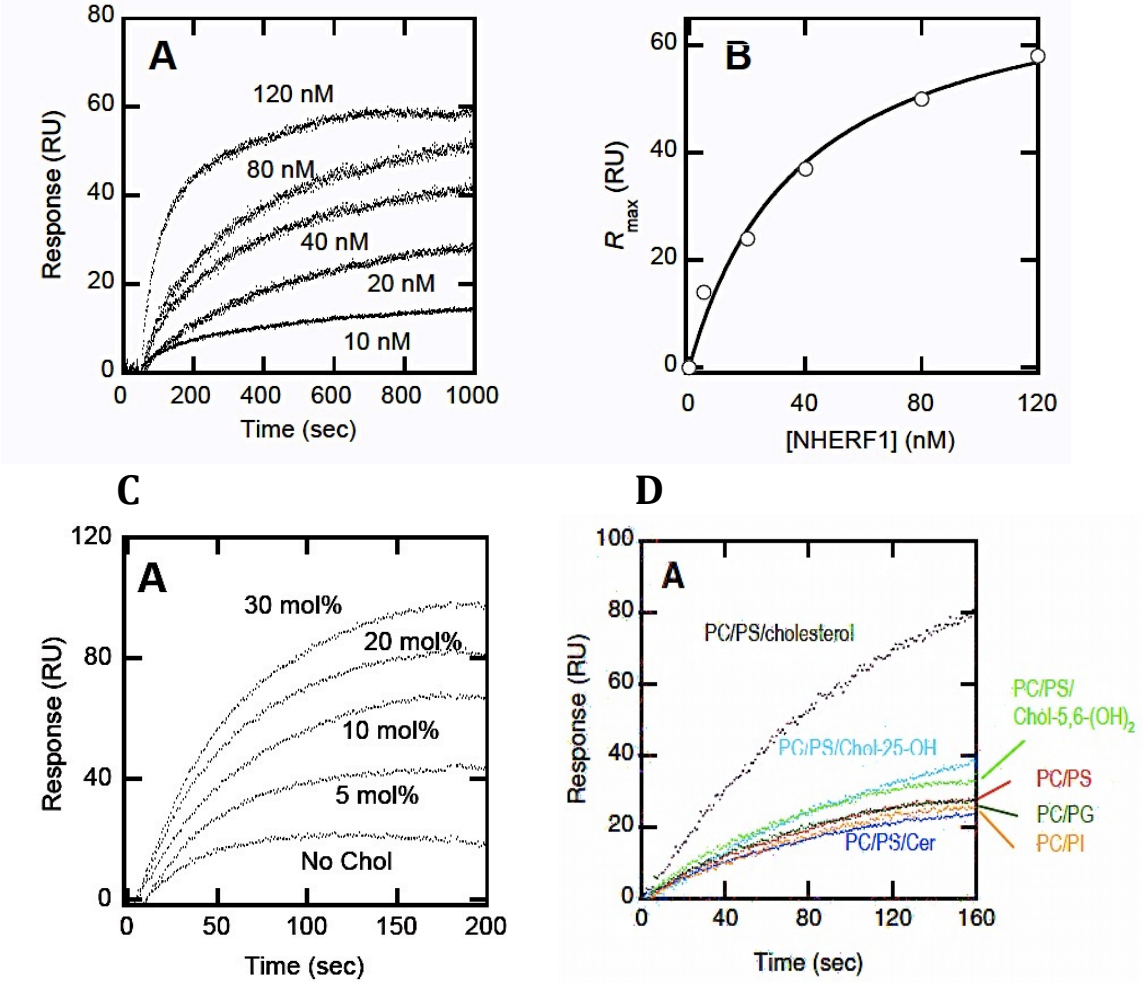

Figure 3. **Determination of Kd for binding of PDZ domains to PM-mimetic vesicles and lipid specificity profiles by SPR analysis** [28].
(**A**) NHERF1-PDZ1 was injected at 5 µl/ min at varying concentrations (1, 10, 25, 40, and 65 nM) over the L1 chip coated with PM-mimetic vesicles, and $\mathbf{R}_{eq}$ values were measured. (**B**) The binding isotherm was generated from the $\mathbf{R}_{eq}$ the concentration ($\mathbf{P}_0$) of NHERF1-PDZ1 plot. A solid line represents a theoretical curve constructed from $\mathbf{R}_{max}$ (= 75 ± 7) and $\mathbf{K}_d$ (= 38 ± 9 nM) values determined by nonlinear least squares analysis of the isotherm using the following equation: $\mathbf{R}_{eq} = \mathbf{R}_{max}/(1 + \mathbf{K}_d/\mathbf{P}_0)$. (**C**) Cholesterol dependence of membrane binding of NHERF1-PDZ1. Protein (300 nM) was allowed to interact with POPC/cholesterol/POPS (80-*x*:20:*x* or 80-*x*:*x*:20) vesicles. (**D**) SPR Sensorgrams of NHERF1-PDZ1 interacting with various lipids. The PDZ domain (50 nM) was allowed to interact with the L1 sensor chip coated with POPC/POPS/cholesterol (60:20:20), POPC/POPS/25-hydroxycholesterol (Chol-25-OH) (60:20:20), POPC/POPS/ceramide (Cer) (60:20:20), POPC/POPS (80:20), POPC/POPG (80:20), and POPC/POPI (80:20), vesicles, respectively. PG and PI indicate phosphatidylglycerol and phosphatidylinositol, respectively. All SPR measurements were performed in 20 mM Tris-HCl, pH 7.4, containing 0.16 M NaCl [28].

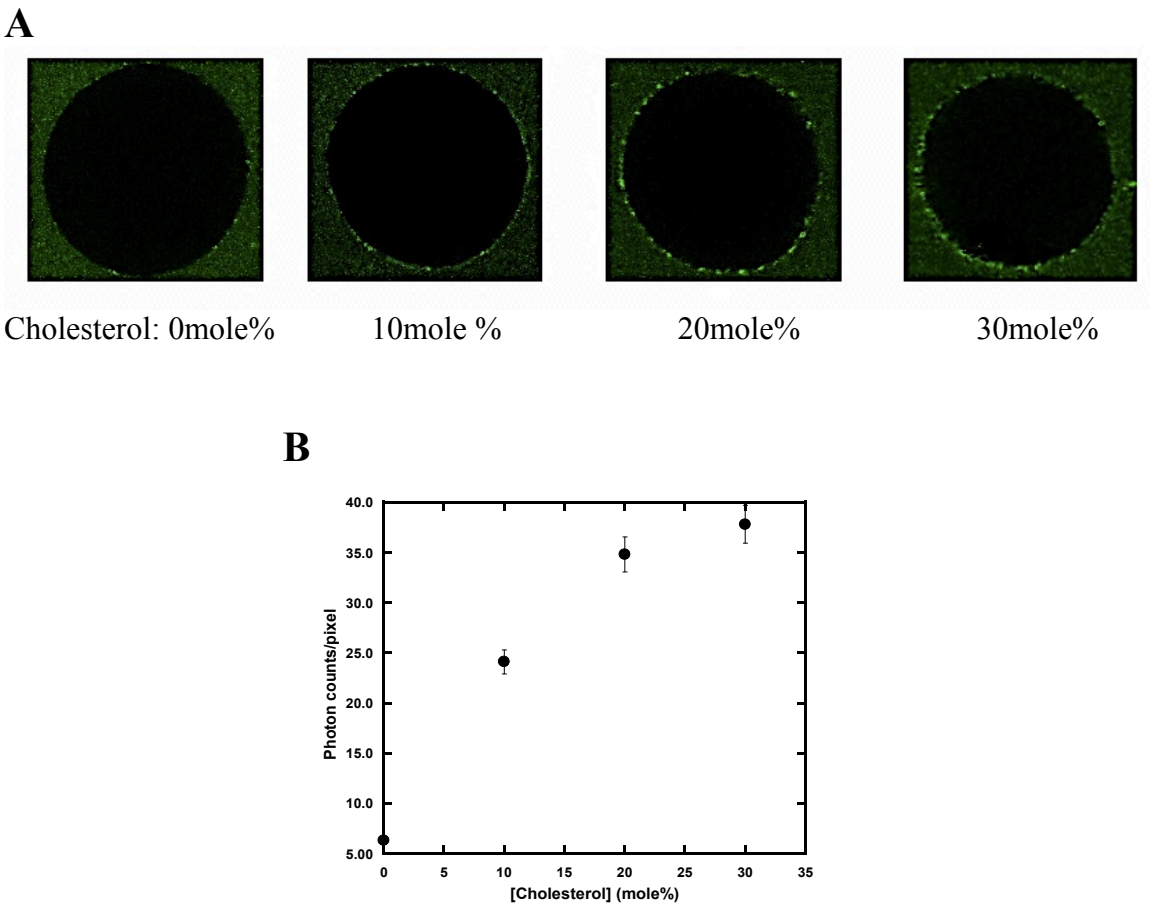

Figure 4. Cholesterol-dependent binding of NHERF1-PDZ1 to giant unilamellar vesicles (GUV) [28].
(**A**) Representative fluorescence images of EGFP-NHERF1- PDZ1 interacting with GUVs with varying cholesterol concentrations. The EGFP tagged PDZ domain (200 nM) was allowed to interact with GUVs composed of POPC/POPS/cholesterol (80-**x**:20:**x**; **x** = 0-30 mole%). Total lipid concentration was 0.6 μg/ml (0.85 μM). The background signals in the external media of GUVs are due to free EGFP-tagged PDZ domain molecules. (**B**) Dependence of the abundance of the GUV-bound PDZ domain on the cholesterol concentration of GUV. The total photon counts on the GUV surfaces are divided by the number of pixels to calculate the average fluorescence intensity of EGFP-NHERF1-PDZ1 per GUV surface. Measurements were performed in 20 mM Tris-HCl, pH 7.4, containing 0.16 M NaCl [28].

membrane hydrocarbon core, and (iii) hydrogen bonds between protein residues and the lipid head group [29]. Cholesterol is largely a hydrophobic molecule with a small polar head group and is readily accessible from outside the membrane, thus it is localized to the hydrophobic core of the membrane. Based on this property the interaction between cholesterol and PDZ domains in plasma membrane will display some penetration into the interior of the membrane because of hydrophobic residues [30]. This process usually initiates with electrostatic attraction between the negatively charged lipids, for example PS, and positive charge amino acids at the membrane level [31]. To see whether NHERF1 PDZ1 domain elucidates the prevalence of this function, lipid dependency needs to be defined. Looking at Figure 8B, NHERF1-PDZ1 binds to the negatively charged PS lipid but depends on cholesterol concentration. The electrostatic binding between lipids and proteins is widespread and NHERF1-PDZ1 is known to bind different anionic lipids, as shown in Figure 3D. The lack of anionic lipids (PS for example) in vesicles, displays diminished NHERF1-PDZ1 binding in vesicles with cholesterol, demonstrating the anionic lipid is necessary in cholesterol based lipids. It was determined that NHERF1-PDZ1 is able to penetrate the cholesterol-containing lipid monolayer, which was possible due to PS binding (Figure 5). Overall, the data shows that NHERF1-PDZ1 binds to and recognizes cholesterol by a non-specific anionic lipid interaction while also having subsequent membrane penetration.

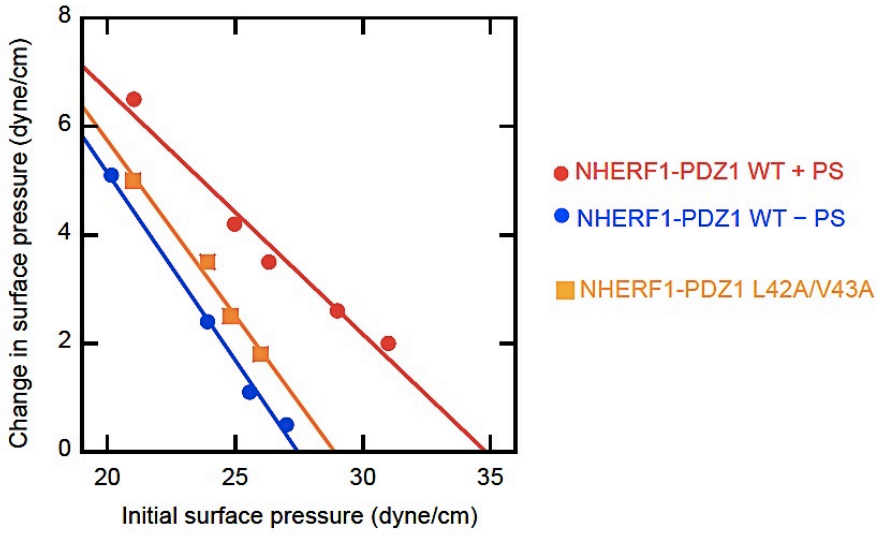

Figure 5. **Membrane penetration of NHERF1-PDZ1 WT and L42A/V43A** [28]. For WT, the monolayer measurements were performed with the POPC/POPS/cholesterol (60:20:20) or POPC/cholesterol (80:20) monolayer with varying initial surface pressure (i.e., different packing density) at the air-water interface. For L42A/ V43A, the POPC/POPS/cholesterol (60:20:20) monolayer was used. The protein was injected into the subphase (20 mM HEPES, pH 7.4, 0.16 M KCl) and the lipid penetration of the protein was monitored as the change in the surface. Since the estimated surface pressure of biological membranes is about 31 dyne/cm, the protein whose critical surface pressure is > 31 dyne/cm is considered to be able to penetrate the biological membranes. Thus, PS enables NHERF1-PDZ1 WT to penetrate cholesterol-containing membranes. Even in the presence of PS, L42A/V43A cannot penetrate cholesterol-containing membranes as effectively as WT [28].

3.3. Interplay between lipid and protein binding sites of NHERF1 PDZ1

Three-dimensional visualization of the electrostatic potential of NHERF1- PDZ1 by Pymol revealed that its domain has a strong positive potential that extends out significantly beyond the molecular surface of the protein along one surface of the molecule (Figure 6A). Such an extended positive potential predicts that, in agreement with our experimental data, the protein will have a significant affinity for negatively charged lipids and suggests that this side of the protein will face the lipid membrane. Accordingly, mutation of positively charged residues in this patch would be expected to have a significant effect on the positive potential and hence reduce the affinity for cholesterol-containing membranes. NHERF1-PDZ1 contains a CRAC motif in residues 35–40 (LGQYIR) [28] that should serve as a cholesterol-binding site. When L35, Y38, and R40 are mutated to alanine (Figure 6B), these mutants conferred significant loss in attraction for membrane affinity (Table 2) with double-site mutant Y38A/R40A having the most prominent effect (Table 2). When using radiolabeled cholesterol reduced binding was also observed (Figure 7A), in conjunction with undetectable cholesterol dependency in membrane binding (Figure 7B). These results demonstrate the necessary residues, Y38 and R40, in defined cholesterol binding and an important tool in non-cholesterol binding variants for further studies. To test the relevance of our mutagenic analysis, we introduced the same mutations into full-length NHERF1 and investigated the effects on plasma membrane binding. The mutation Y38A/R40A utilized the same negative effect on vesicles mimicking the plasma membrane composition as truncated one (Table 2).

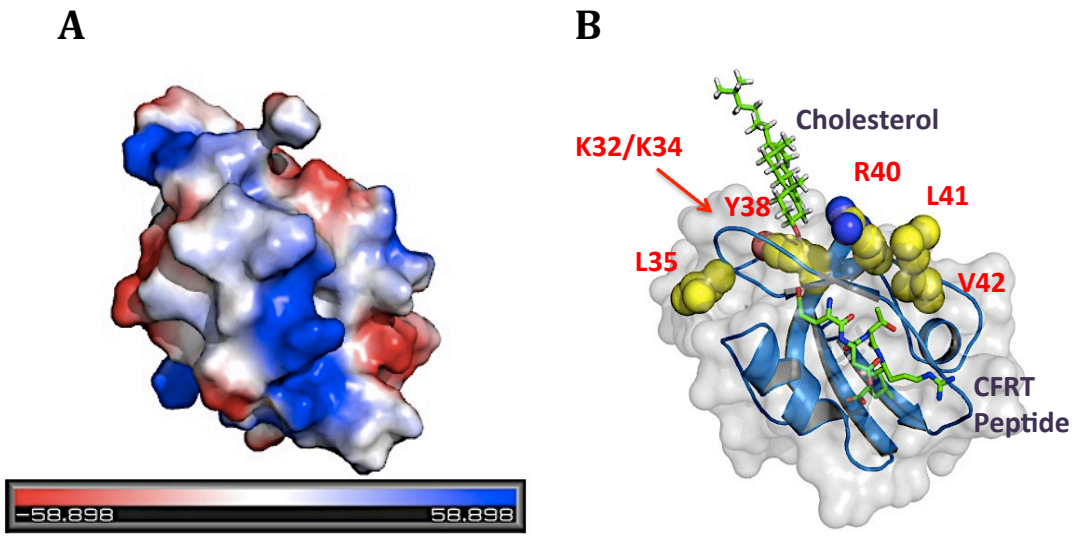

Figure 6. Lipid binding of NHERF1 PDZ1 domain [28].
(A) Accessible surface area representation of the PDZ1 domain of NHERF-1 (PDB code: 1G9O) highlighting the membrane binding site (blue patch). The figure was generated by Pymol software. (**B)** Model structure of the NHERF1-PDZ1-cholesterol-peptide ternary complex. Cholesterol (with its hydrophobic tail pointing upward) and the bound peptide are shown in stick representation. The side chains of putative cholesterol-binding, CRAC motif residues, L35, Y38 and R40 are shown in space-filling representation and labeled. The location of the putative anionic lipid-binding site composed of K32 and K34 is indicated by a red arrow. The side chain conformation of K32/K34 is not fully resolved in the crystal structure, which hampered the modeling with a bound PS molecule. Also shown are L41 and V42 that may be involved in membrane penetration. Notice that the putative lipid binding sites are topologically distinct from the peptide-binding pocket [28].

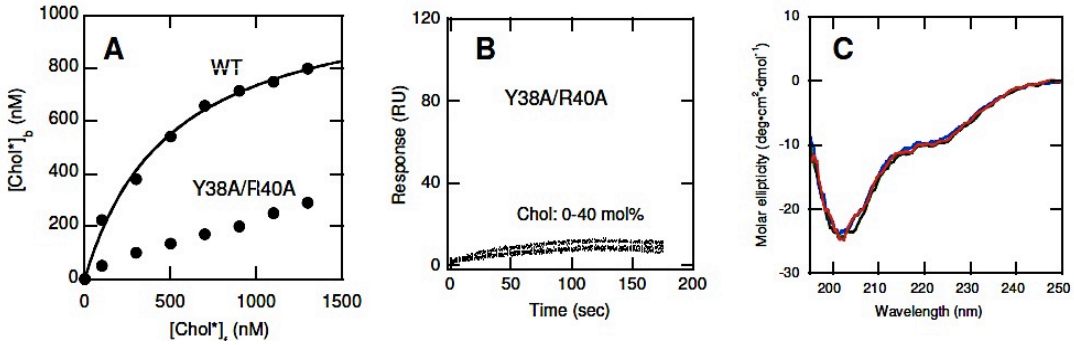

Figure 7. **Cholesterol binding of NHERF1 PDZ1 and Y38A/R40A mutant [28].** (**A**) Binding isotherms of NHERF1-PDZ1 WT and Y38A/R40A mutant. For ^{3}H-labeled cholesterol (*Chol). Each isotherm was fit by non-linear least squares analysis using the equation: $[*Chol]_b = P_0 / (1 + K_d/[*Chol]_f)$ assuming 1:1 PDZ protein-*Chol binding. P_0, $[*Chol]_b$, and $[*Chol]_f$ indicate the concentrations of total protein, protein-bound *Chol, and free *Chol, respectively. Excellent curve fitting corroborates that the PDZ domain binds cholesterol with 1:1 stoichiometry. K_d = 505 ± 70 nM for NHERF1-PDZ1 WT. The mutant showed dramatically reduced binding and thus K_d could not be determined with high confidence by curve fitting. (**B**) Cholesterol dependence of membrane binding of NHERF1-PDZ1 Y38A/R40A mutant. Binding of the PDZ domain to POPC/ POPS/cholesterol (80-x:20:x) vesicles was measured by SPR analysis. See Fig. 3C for comparison with the WT PDZ domain. (**C**) CD spectra of NHERF1-PDZ1 WT (green), Y38A/K40A (blue), and K32A/K34A (red). 300 μg/ml proteins were dissolved in phosphate buffer, pH 7.4, and the averages of six consecutive scans were taken. Notice that three proteins have essentially the same spectra, showing that mutations did not cause deleterious structural changes [28].

Surface analysis of the CRAC motif reveals two important areas, the cationic (K32 and K34) and hydrophobic (L41 and V42) residues (Figure 6B), these properties are most likely involved in anionic lipid binding and partial membrane penetration, respectively. When subjecting these residues to alanine mutations the binding constant significantly increased, thus confirming that all these residues contribute to membrane binding of NHERF1-PDZ1 (Table 2). The double-site mutant K32A/K43A had the most prominent effect on reduced binding to PS-containing membranes, which led to reduced PS dependency versus WT (Figure 8). Noteworthy, the mutated K32 and K34 residues are all located at distinct regions and cluster together to form a defined anionic lipid-binding site that is involved in electrostatic interactions important for membrane avidity. Also, in the monolayer penetration assay the residues L41 and V42 were discovered to be involved in membrane anchoring of NHERF1-PDZ1 as measured by the alanine mutants demonstrating lower activity in membrane penetration versus WT (Figure 5).

NHERF1-PDZ1 has a prominent putative cholesterol binding site located on the opposite side of the peptide binding pocket and as expected can bind simultaneously to cholesterol and protein molecules (Figure 6). A well-known "binding partner of NHERF1 is the cystic fibrosis transmembrane regulator (CFTR)," [32] "a chloride ion channel that regulates the flow of fluid transport across the apical membrane of epithelial cells" [33]. Any mutations or deletions in the *CFTR* gene greatly affect the stability and gating of the transmembrane ion channel that consequently leads to cystic fibrosis" [34]. Thus, we used the CFTR peptide to investigate the interplay between peptide and cholesterol binding. Fluorescence anisotropy assay revealed the mutants Y38A/R40A and

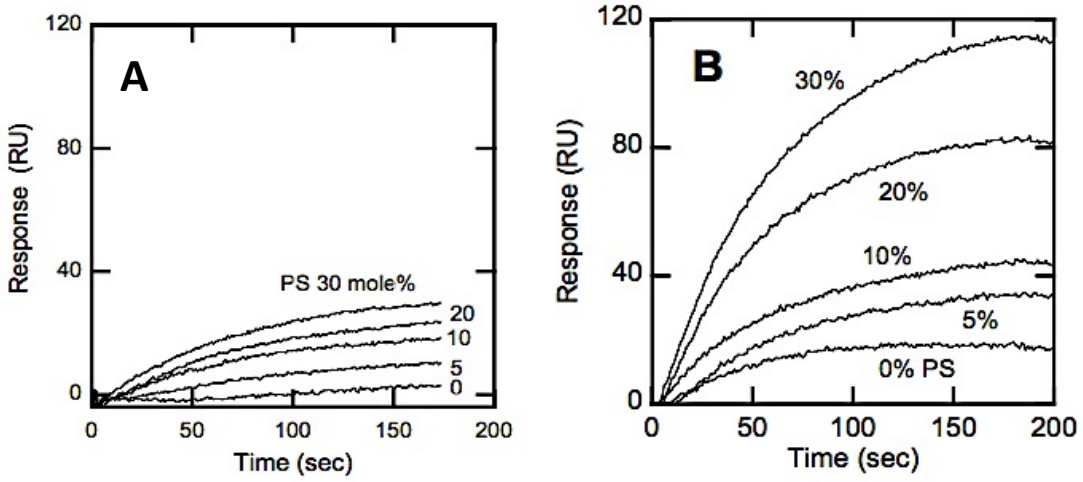

Figure 8. PS binding of NHERF1 PDZ1 and Y32A/R34A mutant [28].
(**A**) PS dependency in membrane binding of NHERF1-PDZ1 mutant K32A/ K34A and (**B**) NHERF1-PDZ1 WT. Both proteins (300 nM) were allowed to equilibrate with vesicles composed of POPC/cholesterol/POPS in molar ratio (80-**x**:20:**x**) [28].

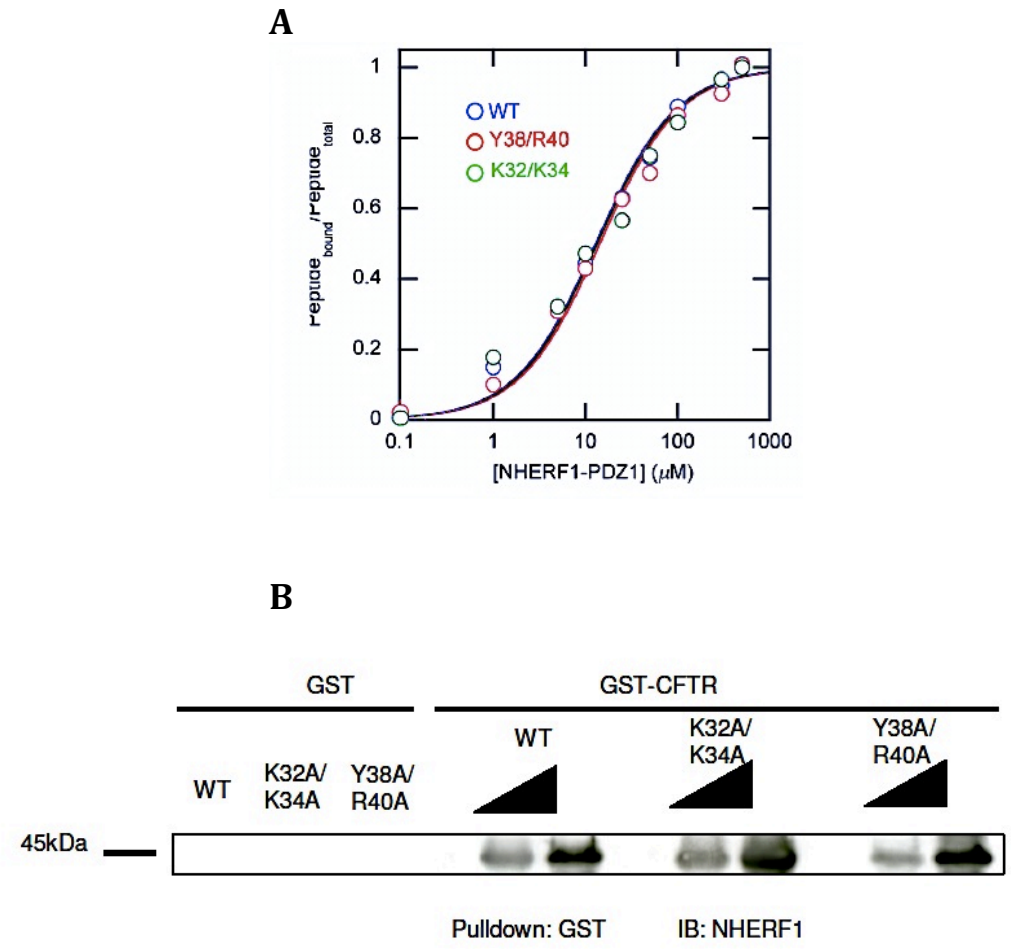

Figure 9. **Interplay between peptide and cholesterol binding.** [28]
(**A**) Effects of mutations of NHERF1-PDZ1 on its CFTR peptide binding. Binding of WT (blue), K32A/K34A (green) and Y38A/R40A (red) to F-Ahx-VQDTLR was monitored by fluorescence anisotropy. Notice that mutations have little to no effect on peptide binding (K_d = 13 ± 1 μM for WT, 13 ± 2 μM for K32A/K34A, and 14 ± 1 μM for Y38A/R40A). (**B)** GST pull-down assay for full-length NHERF1 WT, K32A/K34A, and Y38A/R40A. 5 μg of GST or GST-CFTR peptide was incubated with 0-5 μg of NHERF1 proteins attached to glutathione beads and the bound proteins were analyzed by gel electrophoresis followed by immunoblotting with a NHERF1 [28]

K32A/K34A had no direct effect on the interaction between NHERF1-PDZ1 and the type 1 carboxy-terminal PDZ-binding motif of CFTR (- VQD**T**R**L**) (Figure 9A).

Testing the mutants with full-length NHERF1 using glutathione-S-transferase pull-down assay also had no noticeable effect on the peptide binding (Figure 9B). The relation between peptide and lipid binding was further investigated by SPR experiments. The distinct nature of the anionic lipid and NHERF1-PDZ1 interface was reinforced with the result showing no signal between CFTR and NHERF1-PDZ1 to vesicles recapitulating plasma membrane composition, (Figure 10A) and no interference was observed with the inclusion of PM-mimetic vesicles and NHERF1-PDZ1 with CFTR (Figure 10B). The contact between negatively charged lipids and NHERF1-PDZ1 is maintained by a PDZ motif (*EE*T*EEE*VQDTRL), but CTFR encompasses anionic amino acids directly past this region. These residues could interfere or inhibit the interaction between NHERF1-PDZ1 with negatively charged lipids, but only with the CFTR peptide. To elucidate the molecular determinants of the interactions between NHERF1-PDZ1 and negatively charged patch of the peptide under the investigation; we modeled CFTR (residues 1423 to 1480; referred to as CFTR-14) these residues encompass the negative charge region, PDZ motif, and NHERF1-PDZ1 (Figure 11A) this complex was used to calculate the negative charge density map (Figure 11B). This model proposes that even though there is a negative density area the whole complex is mostly positive. To note the positive density is around the PM area due to the cationic residues from CFTR-14 helix at the c-terminus negate the negative potential from the anionic patch. Finally, we investigated to what degree PDZ-lipid binding was affected by extended C-terminal peptide.

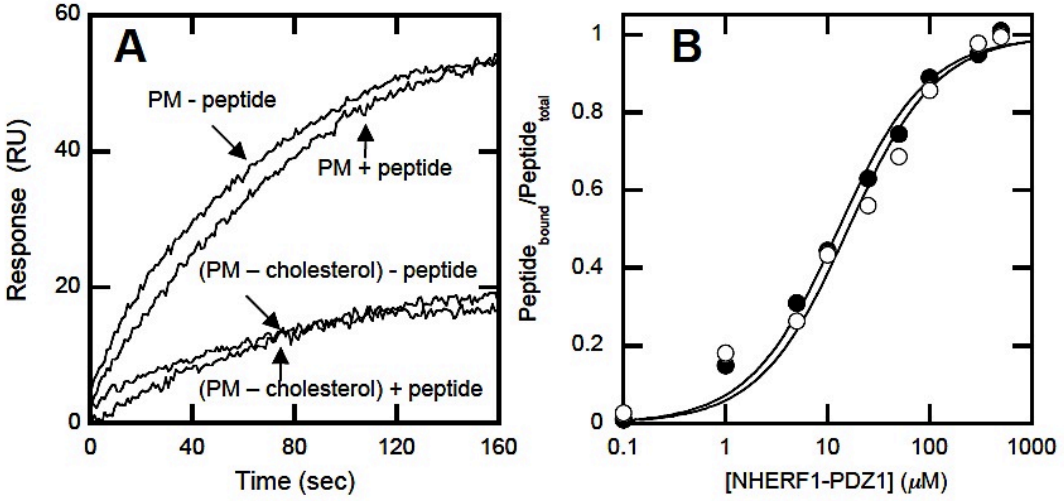

Figure 10. **NHERF1-PDZ1 has topologically distinctive binding sites for lipids and a peptide.** [28]
(A) Effect of the CFTR peptide (F-Ahx-EEVQDTRL) on membrane binding of NHERF1-PDZ1. The PDZ1 domain (50 nM) was allowed to interact with the PM mimetic vesicles or (PM – cholesterol) vesicles before and after 30-minute incubation with 100 μM CFTR peptide. The peptide had negligible effects on the membrane binding of NHERF1-PDZ1 regardless of the presence of cholesterol in the membrane, showing that it does not interfere with cholesterol binding of the PDZ domain. (B) Effects of lipid binding of NHERF1-PDZ1 on its peptide binding. Binding of PDZ1 to F-Ahx-EEVQDTRL in the absence (filled symbols) and presence (open symbols) of 120 μM PM-mimetic vesicles. With 120μM PM-mimetic vesicles, most of NHERF1-PDZ1 molecules would be vesicle-bound; however, the vesicle binding had only a minor effect on peptide binding of the domain (i.e., K_d changes from 13 ± 2 to 15 ± 3μM). Experimental conditions are the same as described for Fig. 9A. PM-mimetic vesicles = POPC/POPE/POPS/POPI/cholesterol/PtdIns (4,5)P_2 (12:35:22:8:22:1). (PM – cholesterol) vesicles = POPC/POPE/POPS/POPI/PtdIns(4,5)P_2 (19:40:27:13:1) [28].

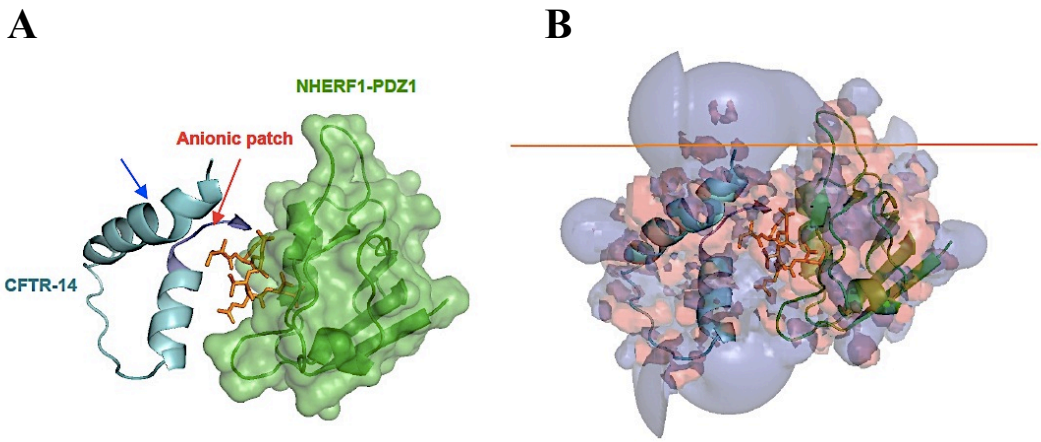

Figure 11. **Effects of the anionic patch of CFTR on membrane binding of NHERF1-PDZ1.** [28]
(A) A structural model of the interaction between the C-terminal CFTR (CFTR-14) domain and NHERF1-PDZ1. The PDZ domain-binding peptide tail of CFTR is highlighted in orange. **(B)** An electrostatic profile of the CFTR-14-NHERF1-PDZ1 complex in the same orientation. Two isosurfaces have been superimposed on the structure complex depicting electrostatic values of 2 KT/e (blue) and –2 KT/e (pink), respectively. An orange line indicates a hypothetical membrane surface. Notice that the putative membrane-binding surface of the complex still possesses a strong positive electrostatic potential despite the presence of the anionic patch in CFTR-14 presumably because cationic residues on the neighboring α-helix (blue arrow) neutralize it [28].

We challenged NHERF1-PDZ1 with the 12-mer EETEEEVQDTRL-COO^-peptide. This longer peptide had similar binding (-VQDTLR) in NHERF1-PDZ1, (Figure 12A) which also showed no interfere between NHERF1-PDZ1 with plasma membrane-mimetic vesicles (Figure 12C). Binding of NHERF1-PDZ1 with the extended peptide was not effected by the addition of PM vesicles (Figure 12B). Accumulated evidences proposes that the anionic region in CFTR would not affect neither affinity nor specificity of the NHERF1-PDZ1-membrane interaction proposed in Figure 6B.

3.4. Cholesterol binding is mediated through the CRAC motif

Despite intense interest in the functions of cholesterol in cell signaling and trafficking, the mechanisms by which this occurs remain little understood. Thus, we investigated the extrinsic factors and structural properties that promote PDZ containing proteins recruitment to cell membranes and examined the impact of association with cholesterol. We identified a putative CRAC motif, which is defined by the consensus (L/V)X_{1-5}YX_{1-5}(R/K) (*X*, any amino acid) in PDZ domains and provide evidence of its functional role in enhancing protein affinity for cholesterol-containing membranes. The current hypothesis is leucine or valine binds to hydrophobic side chain in cholesterol and tyrosine bonds with hydroxyl part in cholesterol, finally, arginine or lysine helps form binding grove [35]. Moreover, aromatic groups are likely important for stacking with cholesterol, but the conformation of the domain is also important in determining its ability to preferentially bind to cholesterol in the membrane. Previously, we performed mutagenesis on an individual NHERF1-PDZ1 to identify mutations that affect specificity of PDZ domain to cholesterol, but it is unknown if the same mutations have the same effects on specificity in similar PDZ domains.

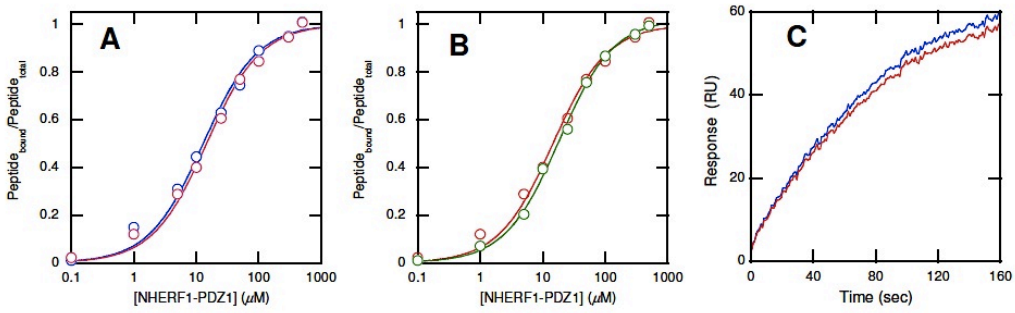

Figure 12. The anionic patch of CFTR does not interfere with membrane/protein binding of NHERF1-PDZ1. [28]
(**A**) Binding of NHERF1-PDZ1 to FAhx-VQDTLR (blue) and F-Ahx-EETEEEVQDTRL (red) monitored by fluorescence anisotropy. NHERF1-PDZ1 binds to both peptides with comparable affinity (Kd = 13 ± 1 μM for VQDTLR and 15 ± 2 μM for EETEEEVQDTRL). Experimental conditions are the same as described for Fig. 9A. (**B**) Binding of NHERF1-PDZ1 to FAhx- EETEEEVQDTRL in the absence (red) and presence (green) of 120 μM PM-mimetic vesicles. The vesicle binding had negligible effect on peptide binding of the domain (i.e., Kd changes from 15 ± 2 to 17 ± 2 μM). Experimental conditions are the same as described for Fig. 9A. (**C**) Binding of NHERF1-PDZ1 to PM-mimetic vesicles in the absence (blue) and presence (red) of F-Ahx-EETEEEVQDTRL [28].

In determining recognition and binding of cholesterol to PDZ domains we experimented with the CRAC motif in context of this interaction. After screening additional proteins, α-syntrophin-PDZ is one such protein that has a CRAC motif besides NHERF1-PDZ1. The "syntrophins are a family of scaffolding proteins that link signaling proteins to the dystrophin protein complex," [36] "the PDZ domain of syntrophins can bind to a variety of signaling proteins, including kinases, various channels, and nitric oxide synthase." [37] Syntrophins are known to complex with actin, calmodulin, and phosphatidylinositols [38] but no remarks about cholesterol. However, our preliminary study revealed that α-syntrophin-PDZ has cholesterol dependent binding to plasma membrane (Figure 1 and 2). α-syntrophin-PDZ contains a CRAC motif in residues 158–164 (***L***EVK***Y***M***K***) [28]. It is important to note that the residues Y162 and K164 of α-syntrophin (Figure 13A) and Y38 and R40 of NHERF1 PDZ1 are similar in side chain orientation. Mutational analysis on tyrosine162 and lysine164 in α-syntrophin-PDZ to alanine lost the ability to bind cholesterol, (Figure 13C) hence the high binding constant when compared to wild type (Figure 13B). This study again supports the notion that the CRAC motif serves as a cholesterol recognition site. Nonetheless, it is important to note that cationic and hydrophobic residues surrounding CRAC motif facilitate cholesterol sensitivity of α-syntrophin PDZ, as Figure 13A depicts, and presumably other PDZ domains as well.

To further confirm the increased affinity of PDZ domains for cholesterol-containing membranes is instigated by CRAC motif presence, we screened PDZ-domain containing protein family, "the discs large (dlg) membrane associated guanylate kinase (MAGUK) family," comprising PSD-95 and SAP-102 [39].

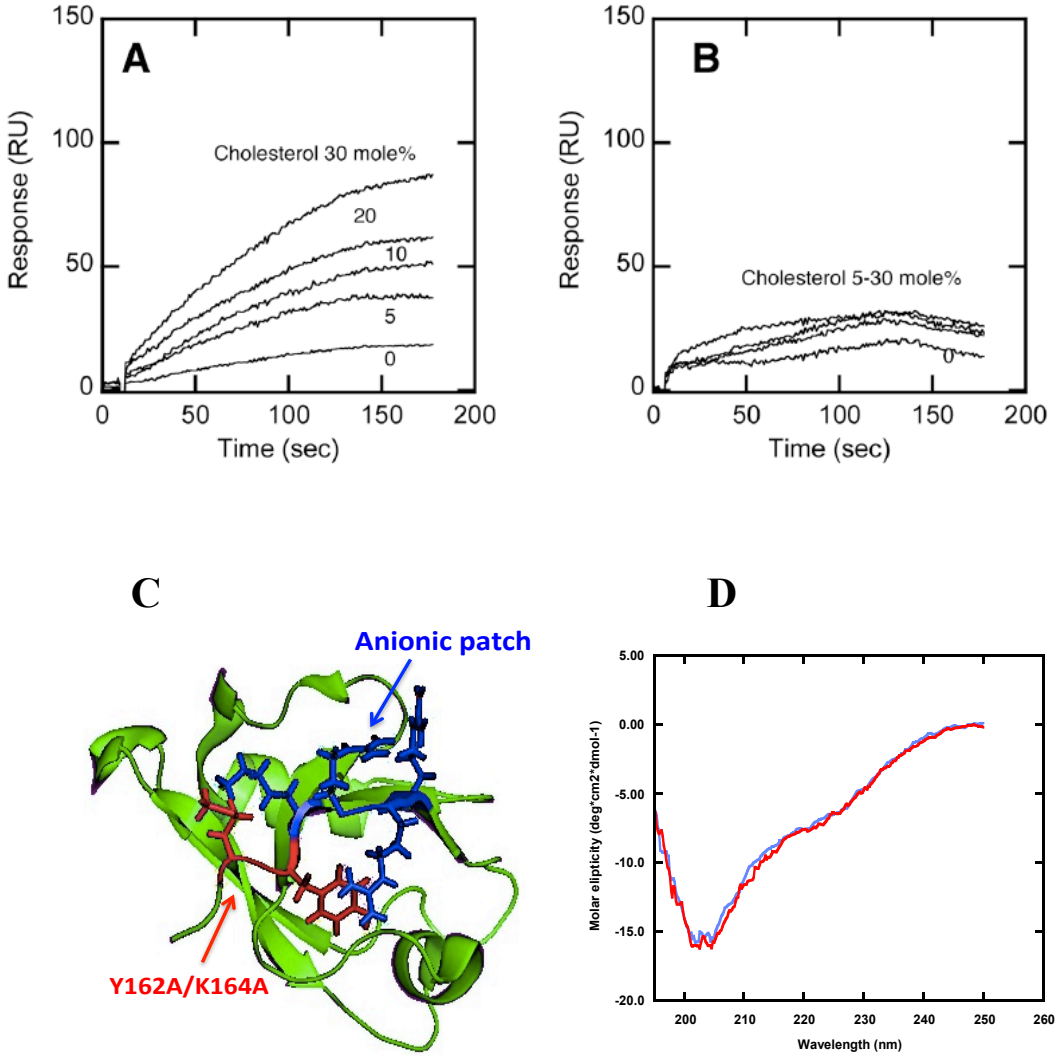

Figure 13. **Membrane binding of α-syntrophin PDZ domain and its CRAC motif mutant.** [28]
(A) Cholesterol dependent membrane binding of α-syntrophin-PDZ WT and (B) its mutant Y162A/K164A. Affinity of the PDZ domain to POPC/POPS/cholesterol (80-x:20:x) vesicles was assessed by SPR analysis. The double-site mutant displays much lower RU's, diminutive cholesterol dependency, and altered binding curves, all consistent with its reduced cholesterol binding. (C) Ribbon diagram of α-syntrophin-PDZ (PDB code: 1Z86). The figure was generated by Pymol software. The amino acid residues Y162 and K164 in the putative cholesterol-binding site are shown as red stick representation and residues in the anionic binding site are highlighted in blue. (D) CD spectra of α-syntrophin-PDZ Y162A/K164A (red) and WT (blue). Protein (300 µg/ml) was solubilized with phosphate buffer (pH 7.4), six measurements were recorded, the average was recorded. WT and its mutant have almost overlapping spectra, proving that the secondary structure was not altered by site-directed mutagenesis [28].

Proteins in the "MAGUK family are involved in receptor trafficking and scaffolding of primarily post-synaptic signaling complexes through their PDZ domains and have been implicated as a therapeutic target for a range of diseases such as chronic pain, stroke, and Alzheimer's disease." [39-42] By measuring binding affinity of SAP102 PDZ3 (Figure 14A) and PSD95 PDZ3 (Figure 1), the preference of these proteins for membranes containing cholesterol has been confirmed. First, we examined the feasibility of the SAP102 PDZ3 with a CRAC motif in residues 527-532 (LFDYDR). WT PDZ domain displayed high affinity with K_d value of 260 ± 45nM for the PM-mimetic vesicles (Figure 14C,D) and defined cholesterol dependency (Figure 14B). With an understanding of modalities of NHERF1-PDZ1 and α-syntrophin PDZ interaction in hand, we presumably can generate non-cholesterol variant of PDZ domains by mutating central tyrosine and arginine/lysine to alanine within the CRAC motif. Accordingly, when Y530 and R532 of SAP102-PDZ3 were mutated to alanine, the Y530A/R532A mutant almost completely abolished cholesterol dependency in membrane binding (Figure 15A). It has significant affinity for anionic membranes as other PDZ domains and displays binding to PS-containing vesicles even with out cholesterol. As Figure 15B demonstrates, the Y530A/R532A affinity towards plasma membrane was significantly reduced and K_d value was not measurable. Another interaction where an increase in specificity is driven by interaction between CRAC motif residues of PDZ domain and cholesterol containing plasma membrane is PDS95 PDZ3 analysis. In agreement with previous studies, we found that when Y439 and K441 in LFD**Y**D**K** motif of PDS95 PDZ3 were substituted with alanine, this mutation abrogated cholesterol dependency (Figure 16B) and conferred a significant loss in affinity for membranes. The K_d value was determined to be 2.7 uM

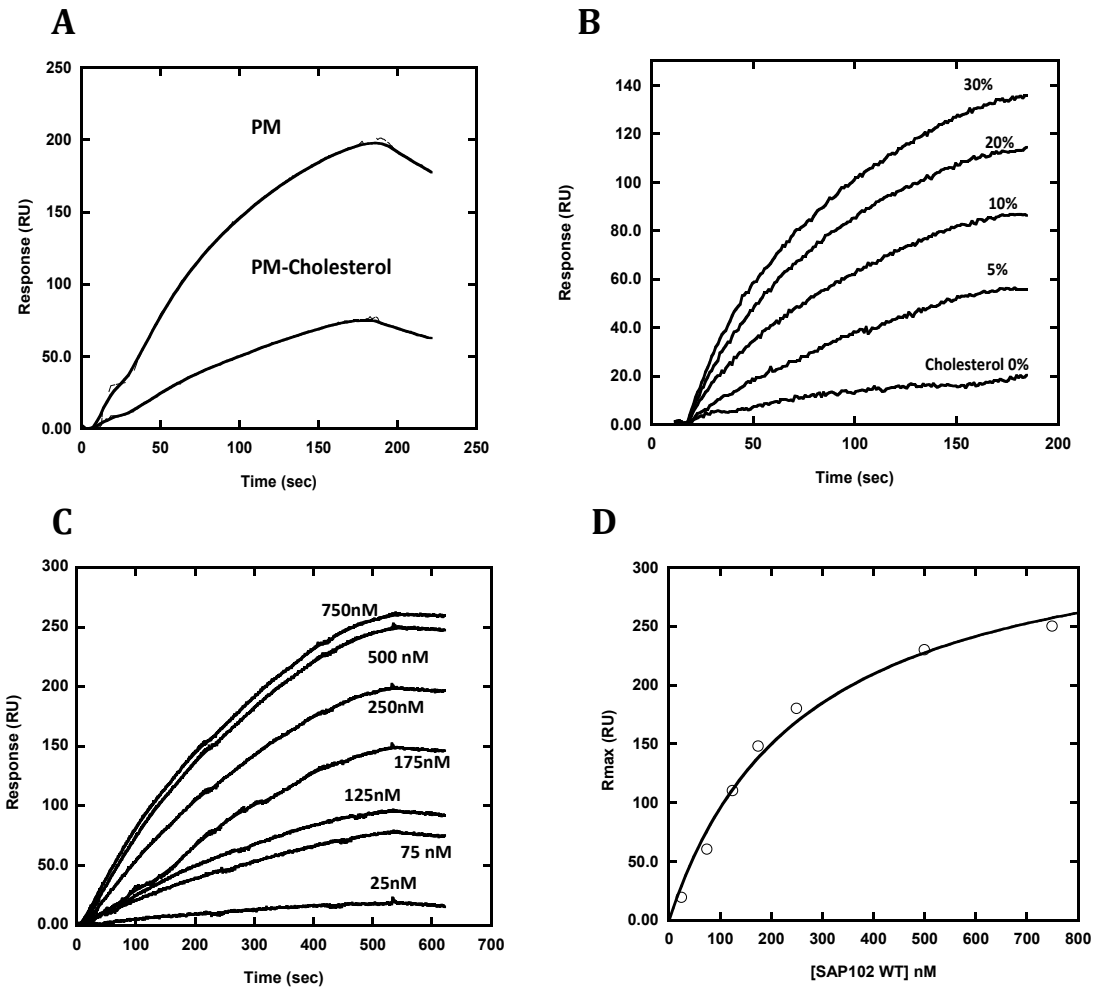

Figure 14. Membrane binding of SAP102 PDZ3 domain and its CRAC motif mutant. (**A**) Cholesterol specific membrane binding of SAP102-PDZ3. The upper curve represents binding of PDZ domain to PM-mimetic vesicles displaying the following composition (POPC/POPE/POPS/POPI/Cholesterol/PtdIns(4,5)P_2 (12:35:22:8:22:1)) and the lower binding to PM-cholesterol vesicles (POPC/POPE/POPS/POPI/PtdIns(4,5)P_2 (19:40:27:13:1)). (**B**) Cholesterol dependence of membrane binding of SAP102-PDZ 3. The PDZ domain (1μM) was allowed to interact with POPC/cholesterol/POPS (80-*x*:*x*:20) vesicles. (**C**) and (**D**) Determination of $\mathbf{K}_d$ for binding of PDZ3 domains to plasma membrane by equilibrium SPR measuremets. SAP102-PDZ3 was passed over the L1 chip coated with PM-mimetic vesicles at the flow rate of 5μl/ min at varying concentrations (25, 75, 125, 175, 250, 500 and 750nM). $\mathbf{K}_d$ =260 ± 45nM value from binding isotherm and equation: $\mathbf{R}_{eq} = \mathbf{R}_{max}/(1 + \mathbf{K}_d/\mathbf{P}_0)$ was solved using nonlinear least squares analysis.

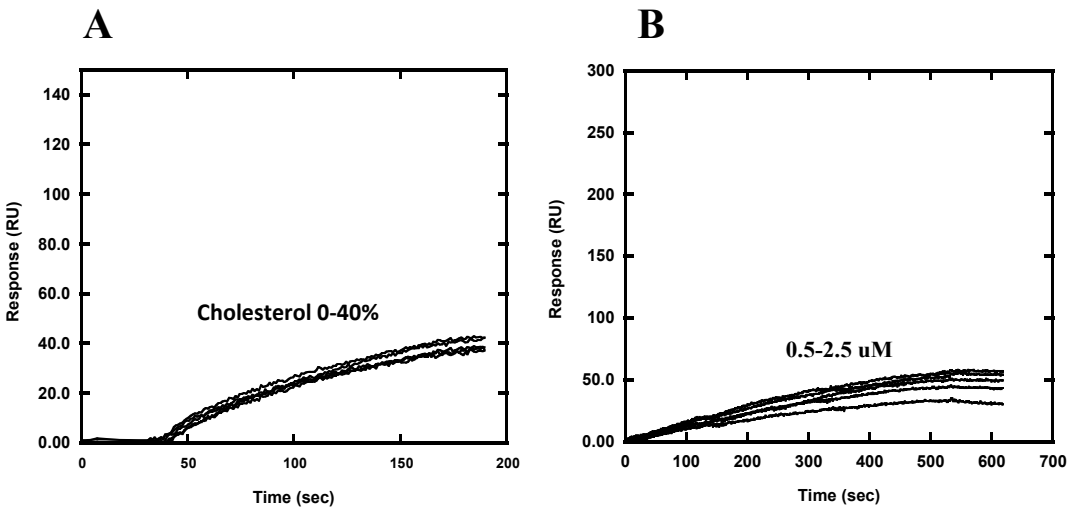

Figure 15. Altered affinities of SAP102-PDZ 3 Y530A/R532A mutant.
(**A)** Cholesterol dependency of SAP102-PDZ 3 Y530A/R532A mutant. The Y530A/R532A mutant almost completely abolished cholesterol dependency in membrane binding. It has significant affinity for anionic membranes as other PDZ domains, and therefore displays some degree of binding to PS-containing vesicles even in the absence of cholesterol. See Fig. B for comparison with the WT PDZ domain. (**B)** Determination of $\mathbf{K}_d$ for binding of SAP102-PDZ 3 Y530A/R532A mutant to plasma membrane by equilibrium SPR analysis. Mutated SAP102-PDZ3 was injected at 5µl/ min at varying concentrations (0.5, 1.0, 1.5, 2.0, and 2.5 µM) over the L1 chip coated with PM-mimetic vesicles. The mutant impaired cholesterol binding abilities to plasma membrane, thus $\mathbf{K}_d$ could not be determined by curve fitting. See Fig. B for comparison with the WT.

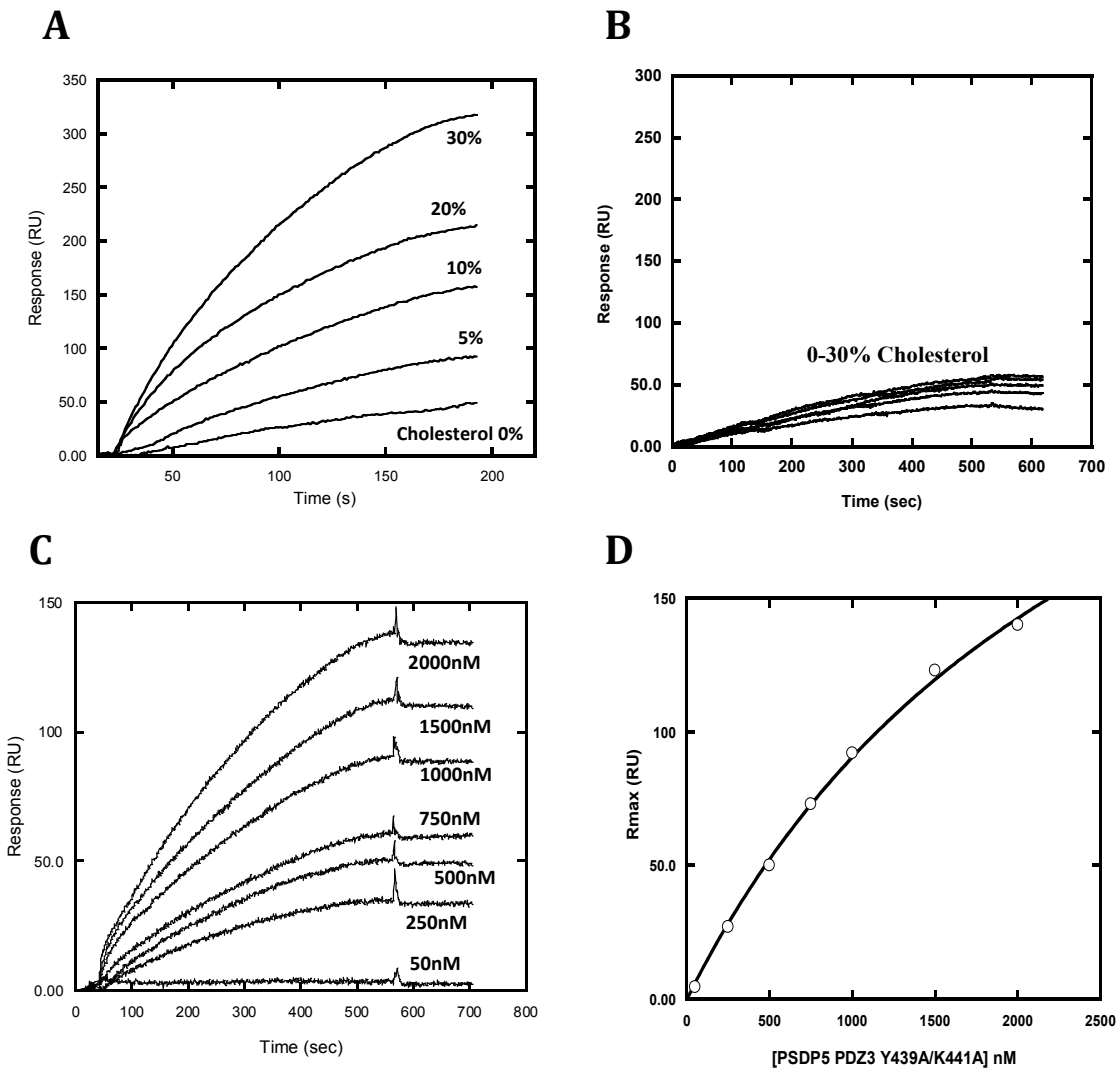

Figure 16. Membrane binding of PSD95 PDZ3 domain and its CRAC motif mutant. **(A**) Cholesterol dependent membrane binding of PSD95 PDZ 3 WT. (**B)** Cholesterol dependent membrane binding of PSD95 PDZ 3 Y439A/K441A. The WT and its mutant (1μM) were allowed to interact with POPC/cholesterol/POPS (80-*x*:*x*:20) vesicles. (**C)** and (**D)** Determination of $\mathbf{K}_d$ for binding of PSD95 PDZ3 Y439A/K441A to plasma membrane by equilibrium SPR analysis. Protein was injected at 5μl/ min at varying concentrations (50, 250, 500, 750, 1000, 1500 and 2000nM) over the L1 chip coated with PM-mimetic vesicles. The $\mathbf{K}_d$ value was determined to be 2.7uM, which is 10-fold lower than the WT (Table 1). The $\mathbf{R}_{eq} = \mathbf{R}_{max}/(1 + \mathbf{K}_d/\mathbf{P}_0)$ equation was used to calculate the value of $\mathbf{K}_d$ by nonlinear least squares analysis of the isotherm.

(Figure 16C,D), which is 7-fold lower than the WT (Table 2). Taken together, we again provided evidence that the CRAC motif is involved in cholesterol binding of PDZ domains.

Cholesterol modulates membrane fluidity and membrane thickness, and is non-randomly distributed in the membrane with a preference for ordered microdomains [43]. Modulation of proteins by cholesterol can either be direct through binding of cholesterol to the protein or indirect through changes in the physiochemical properties of the membrane, such as the fluidity and membrane thickness, or it can be a combination of both [44]. If a domain is able to abrogate its cholesterol sensitivity upon extraction of this lipid from the membrane, then the domain can be classified as having specificity to cholesterol. However, when cholesterol is extracted from the plasma membrane, various changes can occur in the lateral mobility of its components. One can thus argue that difference in binding of PDZ domains to PM-mimetic or PM-cholesterol vesicles (Figure 1) is not necessarily due to specific binding to cholesterol but changes in membrane properties after removing its main component. To distinguish between specific and non-specific binding, we substituted cholesterol with other cholesterol derivatives (structures presented in Figure 17) that have similar physiochemical properties but which may not fit into a cholesterol-binding pocket. Screening of 12 compounds revealed that many PDZ domains have lower affinity for the PM-mimetic vesicles containing all of these sterols except the main yeast sterol, ergosterol, which is known be very similar to cholesterol in both structure and function. As shown in Figure 18, 8 out of 12 tested PDZ domains showed preference for cholesterol to 5α,6β-dihydroxycholesterol , demonstrating their cholesterol specificity.

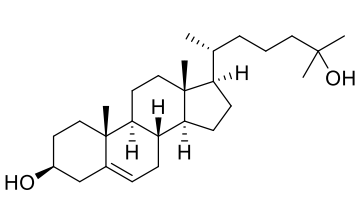

25-hydroxycholesterol

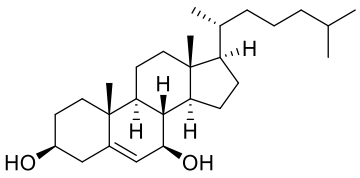

7β-hydroxycholesterol

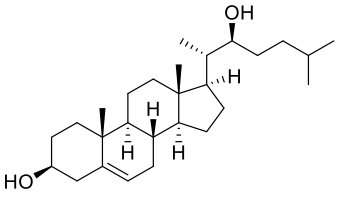

22(S)-hydroxycholesterol

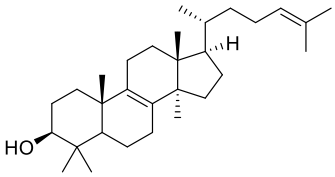

Lanosterol

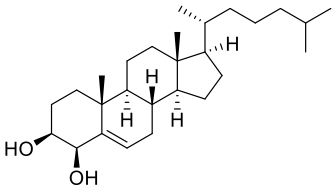

4β-hydroxycholesterol

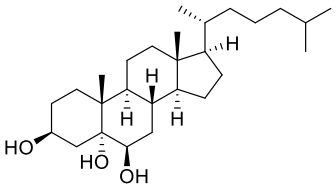

5α, 6 β-dihydroxycholestanol

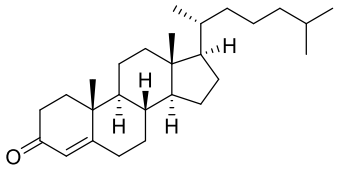

Cholestenone

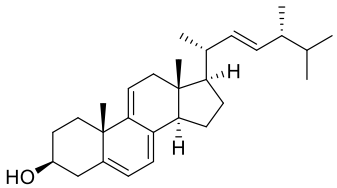

Ergosterol

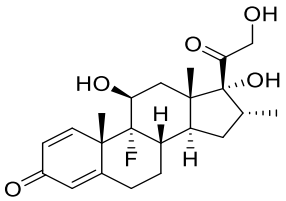

Dexamethasone

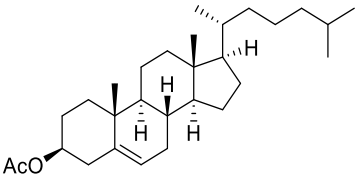

Cholesterol acetate

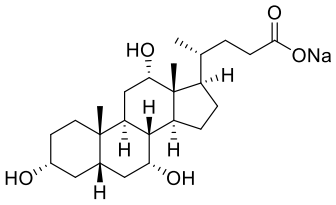

Sodium cholate

Figure 17. **Chemical structures of cholesterol derivatives.**

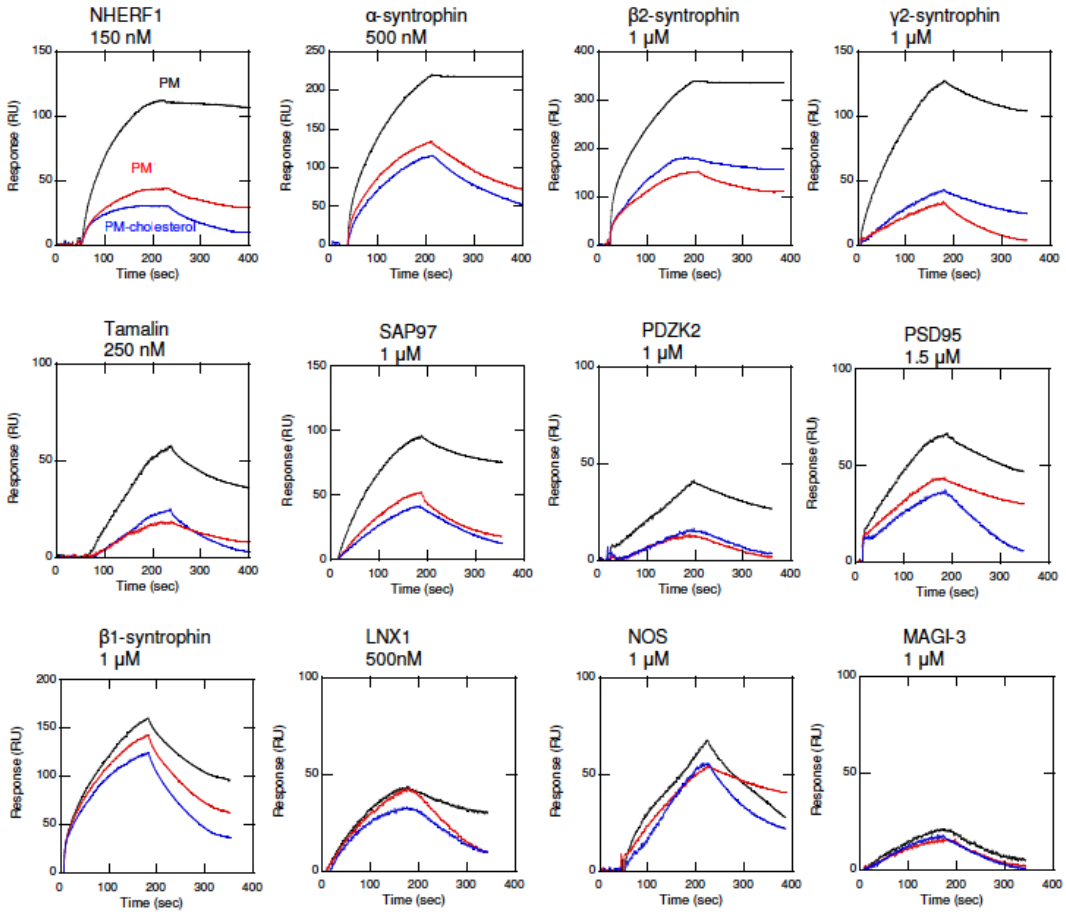

Figure 18. **Cholesterol-specific membrane binding of PDZ domains containing the CRAC motif.** [28]
For all PDZ domains the black curve is for PM-mimetic vesicles (POPC/POPE/POPS/POPI/Cholesterol/PtdIns(4,5)P_2 (12:35:22:8:22:1)), the blue curve for PM-cholesterol vesicles (POPC/POPE/POPS/POPI/PtdIns(4,5)P_2 (19:40:27:13:1)), and red one for PM-mimetic vesicles with a cholesterol derivative (POPC/POPE/POPS/POPI/5α,6β-dihydroxycholesterol/PtdIns(4,5)P_2 = (12:35:22:8:22:1) [28].

Many of these sterols are known to have similar effects on membrane structure to cholesterol. Therefore, high specificity of PDZ domains on cholesterol precludes the possibility that cholesterol controls the membrane binding and function of PDZ domains through non-specific membrane effects. Taken together, our findings suggest that upon cholesterol promote membrane binding of PDZ domains and their subsequent or concomitant interaction with other signaling proteins.

4. DISCUSSION

PDZ domains are the commonest protein-protein interaction modules abundantly presented in humans and other organisms. The structural features of PDZ domains allow them to interact with multiple binding partners simultaneously and thereby assembling supramolecular networks that mediate a broad range of regulatory functions, especially those involving in cell trafficking and synaptic formation and organization [6]. Most research groups adhere to the notion that the ability of PDZ domains to participate in these multidimensional processes relies on their binding capability to the specific ~5-residue motifs that occur at the carboxy-terminal of interacting proteins, therefore acting as a unit that holds the stability of the signaling platform [6]. Our research, on the other hand, focused on molecular mechanisms underlying association of PDZ domains with the plasma membrane and its impact on cell signaling. We revealed that PDZ domains harbor a putative "cholesterol recognition association/interaction consensus (CRAC)" motif and that specific substitutions of critical residues in the motif impair PDZs association with membranes without affecting peptide binding. Uniquely, our findings indicate that PDZ association with PM is dependent on membrane cholesterol content what provokes new insights into how cholesterol can control PDZ-mediated cellular activities simultaneously and yet specifically.

Our analysis showed that the interaction of PDZ domains, NHERF1-PDZ1 in particular, with cholesterol-containing membranes is multivalent and contains components of nonspecific electrostatic interactions. The large extended positive patch along one side of the domain seems crucial for the electrostatic interactions with the negatively charged cytosolic face of the plasma membrane. Mutation of these basic

residues (K32 and K43) to alanine reduced the binding to PM-vesicles proving that PDZ domain recruitment to cholesterol-enriched membranes is facilitated by nonspecific electrostatic interaction between the domain and lipid head groups. Furthermore, in the PDZ1 domain of NHERF1 clusters of positive residues is accompanied by a patch of hydrophobic residues (L41 and V42) (Figure 6B), which are suggested to enhance penetration of an amphipathic α-helix into the bilayer. Mutating the candidate residues to alanine and testing their ability to associate with plasma membrane by monolayer penetration assay reveled that L42A/V43A mutant cannot penetrate cholesterol rich membranes with the same effectiveness as the WT, again proving that unspecific hydrophobic association is essential for PDZ-membrane interactions. From these experimental data, it is obvious that NHERF1-PDZ1 structure harbors a specific docking site for plasma membrane and that this docking mechanism involves three steps: membrane recruitment through electrostatic interactions, membrane penetration, and specific cholesterol binding.

One of our main findings is particularly interesting, considering that some PDZ domains can simultaneously colocalize with cholesterol at the cellular membrane and directly interact with peptides. This points toward an intriguing possibility, coincident detection of peptide and cholesterol signaling by PDZ domains, with potentially important implications for the biology of PDZ-containing proteins. In the case of NHERF1, it may be of importance for its biological function in regulating the accumulation of various receptors at the cholesterol rich plasma membranes. The effect of peptide on the NHERF1-PDZ1–lipid interaction was evaluated by several biochemical approaches. Modeling and mutational analysis revealed that the membrane-interaction

surface of the NHERF-PDZ1 (Figure 6B) is positioned away from the putative peptide-binding site. When membrane-binding surface of PDZ1 is oriented towards a hypothetical plasma membrane surface, PDZ-peptide groove is completely available for peptide ligand binding and synchronized bimolecular binding of peptide and cholesterol can take place. Proven topological distinction between these two binding surfaces contributes directly to the specificity and affinity of PDZ interaction. Finally, by using pull-down assays with C-terminal peptide containing PDZ-binding motif of CFTR (-VQD**T**R**L**), we demonstrated that PM mimetic vesicles containing cholesterol could not interfere with the interaction between the PDZ domain and the CFTR binding partner. All these findings support the idea that both peptide and membrane binding can occur simultaneously and with high specificity.

We sought to further annotate how PDZ domains facilitate specific cholesterol-interaction and whether synergistic PDZ/CRAC motif/PM interaction is more than anecdotal. To determine whether the putative CRAC motif in PDZ1 of NHERF1 plays a role in enhancing affinity for cholesterol-containing membranes, we used site-directed mutagenesis to substitute critical residues in the identified consensus sequence. Mutants with alanine substitutions at Y38 and R40 were tested by SPR analysis. In contrast to wild type, double-site mutant Y38A/R40A of NHERF1-PDZ1 has impaired cholesterol-binding abilities and significantly reduced affinity to membranes. We further showed specifically that other PDZ domains with Y and K/R mutants were incapable of a normal interaction with cholesterol containing membranes. These studies highlighted the role of the CRAC motif in the cholesterol recognition, adding to the growing body of evidence on the functional importance of cholesterol as a signaling molecule in fundamental

interactions regulated by PDZ domains. We reasoned that if the association with cholesterol-containing membranes is required for scaffolding complex formation by PDZ domains, alterations in membrane cholesterol content could affect this activity, and our aspiration is to investigate this possibility by different *in vivo* strategies in the near future.

It is believed that even the smallest changes in chemical structure of cholesterol should significantly alter membrane functions and dynamics. Thus, it must be pinpoint that the sterol substitution strategy cannot be used by itself to absolutely prove or disprove PDZ domains specificity for cholesterol. As Figure 14 depicts, cholesterol derivatives can have a wide range of chemical structures and their variations will induce a conformational changes that will affect specific interactions with putative-lipid binding pocket on PDZ domains. Ultimately, these cholesterol-like structures alter spatial and temporal organization of plasma membrane by restricting proper lipid packing, H-bond formation, and membrane permeability, among others [45]. There is limited amount of experimental and computational data describing molecular details of sterols, oxysterols in particular, interactions with other lipids of mammalian cell membranes. Kulig et al. found that the two distinct groups of oxysterols: ring-oxidized sterols (profoundly produced by free radicals) and tail-oxidized sterols (mostly produced enzymatically) behave differently in a lipid membrane, influencing it in different ways [46]. Specifically, tail-oxidized sterols behave similarly to cholesterol in terms of membrane stiffening, indicating that their effect on biochemical processes in membranes will be similar to that of cholesterol [46]. In contrast, the ring-oxidized sterols that can adopt tilted conformations disturb the membrane structure more significantly in comparison with cholesterol and tail-oxidized sterols and as a result, they increase mobility of lipid

carbonyls. [46]. PDZ domain binds cholesterol in a fashion dependent upon cholesterol structure and this binding can be easily alternated by changes in membrane properties induced by replacement of cholesterol with other sterols. For example, some oxysterols such as 25 hydroxycholesterol by ordering neighboring acyl chains increases the membrane condensation and thickness. Thus, a PDZ domain with a function dependent upon membrane thickness might show different binding behavior and have enhanced affinity for such a membrane. And indeed, in our studies, we observed enhanced binding of some domains to PM vesicles containing 25-hydroxycholesterol and 22(S)-hydroxycholesterol (data not included). Based on this observation, one can believe that the affect of 5α,6β-dihydroxycholesterol, which belongs to the ring-oxidized sterols on membrane order is weaker than that of cholesterol, thus we see the difference in binding for majority PDZ domains. However, we concluded that proper stereochemistry of hydroxyl groups on the A ring of sterol is critical for discriminating between membrane effects and specific protein interactions. We believe that pivotal structural feature of cholesterol for its ability to affect the membrane binding of PDZ domain is the axial orientation of additional hydroxyl group at carbon-5. The relevance of stereospecificity, can be explained by comparing properties of two stereoisomers of cholesterol: epi-cholesterol, in which the orientation of the -OH group at carbon-3 is inverted and ent-cholesterol, which has inverted stereochemistry at all chiral positions (non-superimposable mirror image) [44]. Enantiomers have identical physical properties and as a result, membrane biophysical properties are same for native cholesterol and ent-cholesterol [47-50]. Conversely, the biophysical properties of epi-cholesterol and natural cholesterol are very different in membranes [47, 50]. The equatorial configuration of the

3-hydroxyl group in 5α,6β-dihydroxycholesterol is preserved and the degree to which the steroid affects membrane properties should not be accounted for the difference in binding of PDZ domains to PM. In our understanding, the addition of α-OH at C-5 alters "flatness" of sterol and this molecule is not able to adapt proper conformation to fit into cholesterol-binding pocket. This finding therefore further support the specificity of the interaction between PDZ domains and plasma membrane cholesterol.

Our work on PDZ containing proteins has contributed to a better understanding of the molecular mechanisms controlling the targeting of proteins to plasma membrane. The discovery of the cholesterol involvement in this process has been an important step in this comprehension. This important finding not only demonstrates that cholesterol can directly interact with major cellular regulatory proteins but also offers excellent systems to investigate the direct correlation between membrane cholesterol levels and cellular activities. Our main hypothesis is that the local cholesterol level in plasma membrane changes significantly in response to different pathophysiological stimuli and that tis change meditates diverse cellular processes such as cell signaling and intracellular cholesterol transport. Thus, we want to by measuring the local concentration of cholesterol and correlating this parameter with cellular activities such as cell signaling. To validate our hypothesis, we decided to develop a new fluorescence imaging technology for accurate *in situ* real-time quantification of membrane cholesterol. And this innovative process will be discussed next.

5. CITED LITERATURES

1. Good MC, Zalatan JG, Lim WA (2011) Scaffold proteins: hubs for controlling the flow of cellular information. Science 332: 680–686.

2. Belotti E, Polanowska J, Daulat AM, Audebert S, Thome V, et al. (2013) The Human PDZome: A Gateway to PSD95-Disc Large-Zonula Occludens (PDZ)-mediated Functions. Mol Cell Proteomics 12: 2587–2603.

3. Ivarsson Y, Wawrzyniak AM, Kashyap R, Polanowska J, Betzi S, Lembo F, Vermeiren E, Chiheb D, Lenfant N, Morelli X, Borg JP, Reboul J and Zimmermann P (2013) Prevalence, specificity and determinants of lipid-interacting PDZ domains from an in-cell screen and in vitro binding experiments. PLoS One 8, e54581.

4. Zimmermann P. (2006) The prevalence and significance of PDZ domain-phosphoinositide interactions. Biochim. Biophys. Acta **1**761, 947–956.

5. Luck K, Charbonnier S, Travé G (2012) The emerging contribution of sequence context to the specificity of protein interactions mediated by PDZ domains. FEBS Letters 586: 2648–2661.

6. Gallardo R, Ivarsson Y, Schymkowitz J, Rousseau F, Zimmermann P (2010) Structural diversity of PDZ–lipid interactions. ChemBioChem. 11: 456–467.

7. Nourry C, Grant SG, and Borg JP. (2003) PDZ domain proteins: plug and play! *Sci STKE 2003*: RE7.

8. London TB, Lee HJ, Shao Y, Zheng J (2004) Interaction between the internal motif KTXXXI of Idax and mDvl PDZ domain. Biochem. Biophys. Res. Commun. 322: 326–332.

9. Penkert RR, DiVittorio HM, Prehoda K E (2004) Internal recognition through PDZ domain plasticity in the Par-6-Pals1 complex. Nat. Struct. Mol. Biol. 11: 1122–1127.

10. Belotti E, Polanowska J, Daulat AM, Audebert S, Thome V, Lissitzky, JC, Lembo F, Blibek K, Omi, S, Lenfant N, Gangar, A, Montcouquiol M, Santoni MJ, l Sebbagh M, Aurrand-Lions M, Angers S, Kodjabachian L, Reboul J, and Borg JP (2013) The human PDZome: A gateway to PSD95-Disc Large-Zonula Occludens (PDZ)-mediated functions. Molecular and Cellular Proteomics. 12: 2587–2603.

11. Mohanty S, Ovee M, Banerjee M (2015) PDZ Domain Recognition: Insight from Human Tax-Interacting Protein 1 (TIP-1) Interaction with Target Proteins. Biology 4(1): 88-103.

12. Lee HJ, Zheng JJ (2010) PDZ domains and their binding partners: Structure, specificity, and modification. Cell Commun. Signal. 8: 8.

13. Ernst A, Appleton BA, Ivarsson Y, Zhang Y, Gfeller D, Wiesmann C, Sidhu SS (2014) A structural portrait of the PDZ domain family. J Mol Biol 426: 3509–3519.

14. Cho W, Stahelin RV (2005) Membrane-protein interactions in cell signaling and membrane trafficking. Annu Rev Biophys Biomol Struct. 34: 119–151.

15. Winters MJ, Lamson RE, Nakanishi H, Neiman AM, Pryciak PM (2005) A membrane binding domain in the ste5 scaffold synergizes with gbetagamma binding to control localization and signaling in pheromone response. Mol Cell. 20: 21–32.

16. Chen Y, Sheng R, Kallberg M, et al. (2012) Genome-Wide Identification and Functional Annotation of Dual Specificity Protein- and Lipid-Binding Modules That Modulate Protein Interactions at the Membrane. Molecular cell 46(2): 226-237.

17. Ivarsson Y (2012) Plasticity of PDZ domains in ligand recognition and signaling. FEBS Lett 586: 2638–2647.

18. Zimmermann P, Meerschaert K, Reekmans G, Leenaerts I, Small JV, et al. (2002) PIP(2)-PDZ domain binding controls the association of syntenin with the plasma membrane. Mol Cell 9: 1215–1225.

19. Balla T, Szentpetery Z ,Kim YJ (2009) Phosphoinositide Signaling: New Tools and Insights Physiology. 24(4): 231-244.

20. Wu H, Feng W, Chen J, Chan LN, Huang S, et al. (2007) PDZ domains of Par-3 as potential phosphoinositide signaling integrators. Mol Cell 28: 886–89

21. Schengrund C (2010) Lipid rafts: keys to neurodegeneration. Brain Res. Bull. 82 :7-17.

22. Lundbæk JA, Andersen OS, Werge T, Nielsen C (2003) Cholesterol-induced protein sorting: an analysis of energetic feasibility. Biophys. J., 84: 2080–2089.

23. Montero J, Morales A, Llacuna L, Lluis JM, Terrones O, Basañez G, Antonsson B, Prieto J, García-Ruiz C, Colell A, Fernández-Checa JC (2008) Mitochondrial cholesterol contributes to chemotherapy resistance in hepatocellular carcinoma Cancer Res. 68: 5246–5256.

24. Cho W, Trikha S, Jeremic AM (2009) Cholesterol regulates assembly of human islet amyloid polypeptide on model membranes J. Mol. Biol., 393: 765–775.

25. Arispe N, Doh M (2002) Plasma membrane cholesterol controls the cytotoxicity of Alzheimer's disease AßP (1–40) and (1–42) peptides FASEB J., 16: 1526–1536.

26. Goldstein JL, Brown M S (2001) Molecular medicine. The cholesterol quartet. Science. 292: 1310–1312.

27. Epand RM (2006) Cholesterol and the interaction of proteins with membrane domains. Prog Lipid Res. 45: 279–294.

28. Sheng, R, Chen, Y, Gee HY, Stec E., Melowic HR, Blatner NR, Tun MP, Kim Y, Kallberg M. Fujiwara T, Hong JH, Kim KP, Lu H, Kusumi A, Lee M G and Cho W (2012) Cholesterol Modulates Cell Signaling and Protein Networking by Specifically Interacting with PDZ Domain-Containing Scaffolding Proteins. Nature Communications. 1249(3).

29. Wawrzyniak AM, Wawrzyniak R, Kashyap P, Zimmermann P (2013) Phosphoinositides and PDZ domain scaffolds. Adv. Exp. Med. Biol., 991: 41–57.

30. Cho, W, Bittova, L and Stahelin, RV (2001) Membrane binding assays for peripheral proteins. Anal Biochem 296, 153-161.

31. Mulgrew-Nesbitt A, et al. (2006) The role of electrostatics in protein-membrane interactions. Biochim Biophys Acta. 1761: 812–826.

32. Hall RA, Ostedgaard LS, Premont RT, Blitzer JT, Rahman N, Welsh MJ, Lefkowitz RJ (1998) A C-terminal motif found in the β2-adrenergic receptor, P2Y1 receptor and cystic fibrosis transmembrane conductance regulator determines binding to the Na+/H+ exchanger regulatory factor family of PDZ proteins Proc. Natl Acad. Sci. USA, 95: 8496–8501.

33. Wang S, Raab RW, Schatz PJ, Guggino WB, Li M (1998) Peptide binding consensus of the NHE-RF-PDZ1 domain matches the C-terminal sequence of cystic fibrosis transmembrane conductance regulator (CFTR) FEBS Lett., 427: 103–108.

34. Riordan JR, Rommens JM, Kerem B, Alon N, Rozmahel R, Grzelczak Z, et al. (1989) Identification of the cystic fibrosis gene: cloning and characterization of complementary DNA Science, 245: 1066–1073.

35. Martínez-Abundis E, Correa F, Rodríguez E, Soria-Castro E, Rodríguez-Zavala JS, Pacheco-Alvarez D et al. CRAC-like motif in BAX sequence: relationship with protein insertion and pore activity in liposomes (2011) Biochim Biophys Acta 1808: 1888–1895.

36. Albrecht DE, Froehner SC (2002) Syntrophins and dystrobrevins: defining the dystrophin scaffold at synapses, Neurosignals 1: 123–129.

37. Kim MJ, Froehner SC, Adams ME, Kim HS (2011). α-Syntrophin is required for the hepatocyte growth factor-induced migration of cultured myoblasts. Experimental Cell Research, 317(20): 2914–2924.

38. Iwata Y, Sampaolesi M, Shigekawa M, Wakabayashi S (2004) Syntrophin is an actin-binding protein the cellular localization of which is regulated through cytoskeletal reorganization in skeletal muscle cells. Eur J Cell Biol. 83: 555–565.

39. Gardoni F (2008) MAGUK proteins: new targets for pharmacological intervention in the glutamatergic synapse. Eur J Pharmacol 585: 147–152

40. Gardoni F, Marcello E, Di Luca M (2009) Postsynaptic density-membrane associated guanylate kinase proteins (PSD-MAGUKs) and their role in CNS disorders. Neuroscience 158: 324–333

41. Elias GM, Nicoll RA (2007) Synaptic trafficking of glutamate receptors by MAGUK scaffolding proteins. Trends Cell Biol 17: 343–352

42. Sheng M, Kim E (2011) The postsynaptic organization of synapses. Cold Spring Harb Perspect Biol 3: a005678

43. Song Y, Kenworthy AK, Sanders CR (2014) Cholesterol as a co-solvent and a ligand for membrane proteins. Protein Sci., 23: 1–22.

44. Levitan I, Singh DK, Rosenhouse-Dantsker A (2014) Cholesterol binding to ion channels. Front. Physiol. 5: 65.

45. Kim JH, London E (2015) Using Sterol Substitution to Probe the Role of Membrane Domains in Membrane Functions. Lipids. DOI 10.1007/s11745-015-4007-y

46. Kulig W, Olżyńska A, Jurkiewicz P, Kantola AN, Komulainen S, Manna M, Pourmousa M, Vazdar M, Cwiklik L, Rog T, Khelashvili G, Harries, Telkki VV, Hof M, Vattulainen I, Jungwirth P (2015) Cholesterol under oxidative stress – how lipid membranes sense oxidation as cholesterol is being replaced by oxysterols. Free Radical Biology and Medicine, http://dx.doi. org/10.1016/j.freeradbiomed.2015.03.006

47. Westover EJ, Covey DF (2004) The enantiomer of cholesterol. J Membr Biol. 202: 61–72.

48. Westover EJ, Covey DF, Brockman HL, Brown RE, Pike LJ (2003) Cholesterol depletion results in site-specific increases in epidermal growth factor receptor phosphorylation due to membrane level effects. Studies with cholesterol enantiomers. J Biol Chem. 278: 51125–51133.

49. Mannock DA, McIntosh TJ, Jiang X, Covey DF, McElhaney RN (2003) Effects of natural and enantiomeric cholesterol on the thermotropic phase behavior and structure of egg sphingomyelin bilayer membranes.Biophys J. 84: 1038–1046.

50. Covey DF. (2009) *ent*-Steroids: novel tools for studies of signaling pathways. Steroids. 74: 577–585.

CHAPTER 2

TRASNBILAYER ASYMMETRY OF CHOLESTEROL IN THE PLASMA MEMBRANE ACCOUNTS FOR ITS SIGNALING FUNCTION

1. INTRODUCTION

Our increasing understanding of lipid-lipid interactions and of lipid key function in the signaling networks that lead the cell by recruiting proteins to specific membranes features the significance of the complexity of composition, structure, and fluidity of cell membranes [1,2]. The lipid composition of membranes differs among species, and also among different cell membranes within the species [3,4]. The lipid asymmetry of the extracellular and the intracellular leaflets of eukaryotic plasma membranes is very prominent [3-6]. The extracellular leaflet is enriched in phosphatidylcholine (PC) and sphyngomielin (SM), whereas most of phosphatidylethanolamine (PE) and practically all phophatidylserine (PS) and phosphoinositides including the di-phosphorylated lipid phosphatidylinositol-4,5-bisphosphate (PIP_2) face the cytosolic part [7]. The asymmetric property of the membrane is started during lipid synthesis and it is preserved by slow transbilayer diffusion, protein-lipid interactions, and a set of lipid translocases ("flippases") for example the energy-dependent ATP-binding cassette (ABC) transporters [8,9]. Lipid asymmetry and transmembrane translocation are a central aspect of the lipid economy of the cell that involves number of processes such as vesicle transport, protein recruitment and function, signal transduction, and physiological aspects like cell aging and death [10]. Because lipid asymmetry is fundamental to these processes, the preservation of this lipid asymmetry is essential in membrane function, if any alterations arise in asymmetry it will lead to cell activation or pathologic conditions. Cholesterol plays a major role in modulating membrane bilayer structure and important cellular functions such as membrane trafficking and cell signaling. We presumably have a general picture of how phospholipid asymmetry is generated, maintained, and disrupted in

cellular membranes, however, the transbilayer distribution of the cholesterol that makes up 10-45% [11] of the lipids in eukaryotic plasma membranes cannot be determined accurately by current methodologies. Within each membrane leaflet, cholesterol is not necessarily distributed homogeneously. Cholesterol binds to a verity of lipids in different ways forming transient structures that can segment into separate domains with diverse structural and dynamic properties [12]. Localized liquid-ordered domains called "lipid rafts" may have higher cholesterol concentrations than surrounding liquid-disordered domains, but since these structures cannot be visualized in cells, they remain controversial [2]. The transverse asymmetry in the distribution of cholesterol in biological membranes is also uncertain. Cholesterol can flip rapidly between the leaflets in a bilayer, and it has been shown that the $t_{1/2}$ for this is less than a second in erythrocytes [15]. Some models propose preferential interactions between cholesterol and sphingomyelin (which is found predominantly on the outer leaflet of the plasma membrane) [16,17], but studies of the transbilayer distribution of fluorescent sterols have indicated that most of the cholesterol is in the inner leaflet of human erythrocytes [18]. Regardless of the degree of steady-state transbilayer asymmetry, simultaneous determination of cholesterol in both leaflets of plasma membrane will provide us with valuable information about the dynamics and potential regulatory roles of cholesterol. This goal can be achieved with our innovative new lipid sensor technology for *in situ* quantification of signaling lipids in a spatiotemporally resolved manner in live cells. This technical breakthrough will enable us to directly correlate local cholesterol concentrations with various downsteam cellular processes.

Cholesterol is an atypical lipid found in eukaryotic membranes, having a one hydroxyl group giving it a slight dipole, a almost planar alignment of four fused rings, and a small isooctyl chain at the C17-position [19]. The verity of these molecular features give cholesterol a significant role in physicochemical properties of membranes, and the ability to translocate between two membrane leaflets. Cholesterol's physical effect gives membranes the ability to increase mechanical rigidity [20], produce a semipermeable barrier between inner and outer cellular environments, and adjust membrane fluidity [21,22]. On the molecular level, cholesterol has an interesting arrangement property of packing, adhesion, and condensing effects (cholesterol-lipid interaction). Several models attempt to explain the mechanisms of cholesterol–lipid interactions within cell membranes. The main ones are the "umbrella model" [23] and the "condensed complex model" [24]. The umbrella model suggests a mechanism in which phospholipids bearing relatively large polar headgroups, such as phosphatidylcholine (PC) or sphingomyelin (SM), favorably associate with cholesterol to provide additional shielding to its hydrophobic rings, which are insufficiently protected from aqueous environment by small hydroxyl head. Unshielded or poorly shielded cholesterol has a higher *chemical activity coefficient* [25] that increases availability of cholesterol to extramembrane acceptors (e.g., for transfer between membranes) or for interaction with membrane proteins (e.g., sterol-sensing or sterol-binding proteins) [26]. With headgroup size another factor is the level of acyl chain unsaturation and its effect in cholesterol stabilization of the umbrella model because of the effects on dynamic lipid geometry [27]. As portrayed in Figure 19, with increasing unsaturation a conical shape is formed due to the large cross section of acyl chains when compared to the headgroup; with saturated lipids a cylindrical shape

forms [27]. As a consequence, conical lipids, like dioleoyl-PC (DOPC), do not shield near by cholesterol molecules when compared to dipalmitoyl-PC (DPPC), which offers bettering shielding because of two saturated acyl chains. The condensed complex model, on the other hand, explains cholesterol tendency to associate with phospholipids encompassing long saturated acyl chains (e.g. SM or DPPC) through hydrogen bonding [25]. According to this model, compact packing between cholesterol and phospholipids orders the lipid acyl chains, lowers the chemical potential of cholesterol, and leads to its reduced extractability from the membrane [25]. Despite different frameworks for evaluation, in both models the cholesterol chemical activity (escape tendency) is anticipated to increase suddenly when cholesterol concentration goes beyond carrying capacity by phospholipids in the membrane bilayer [28]. Cholesterol molecules that exceeded the limit of complexing capacity of lipid molecules remain dispersed in the bilayer this confirmation of cholesterol is termed as “active” or “free” cholesterol [29]. A proportional fraction of this active (mobile) cholesterol is redistributed without the involvement of metabolic energy (down its activity gradient) including both its extracellular lipoproteins and its intracellular membranes, increasing their cholesterol content. It is crucial to note here that the amount of cholesterol in a plasma membrane is an important factor of the bilayers' physical properties and the level of free (non-esterified) cholesterol requires tight regulation at the cellular level.

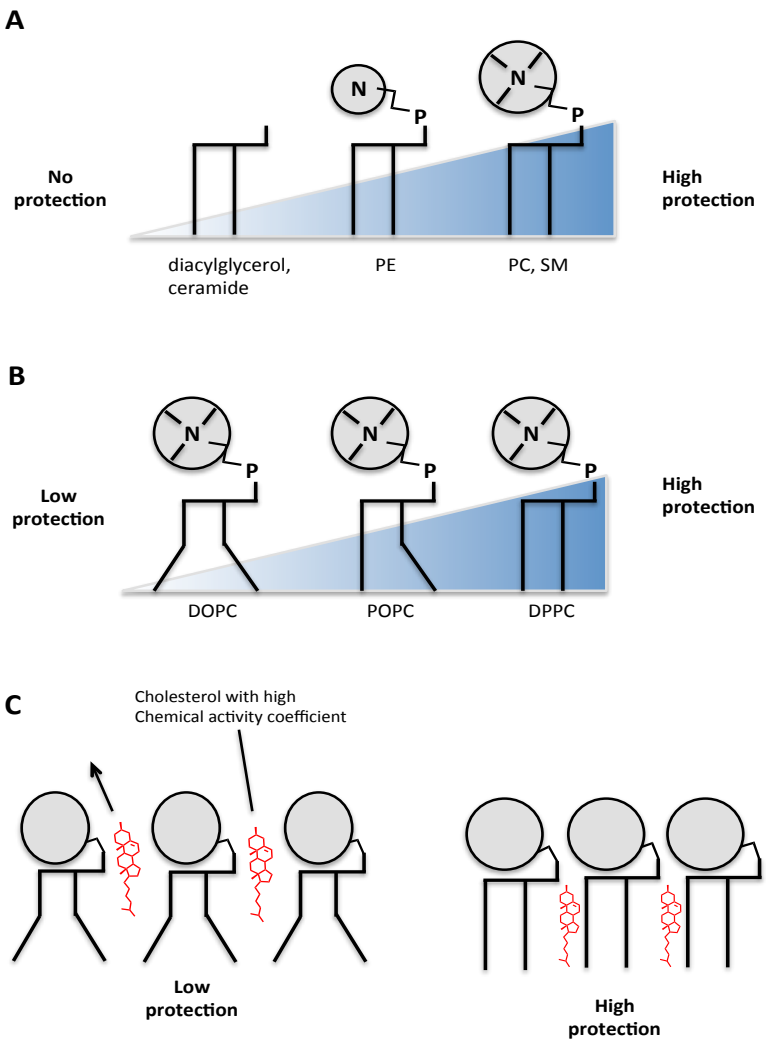

Figure 19. **Structural interactions between cholesterol and other lipids.** **(A)** As the lipid headgroup increases in size from PE to PC more protection from water is provided to the membrane surface and increases cholesterol integration into the membrane. **(B)** Keeping the size of the headgroup constant and modifying the acyl chain. By adding double bonds to the acyl chain kinks are introduced, the more double bonds the more kinks in the chain. This makes the membrane more fluid because it offers less protection from water and bulky lipids. While straight single bonded acyl chains have the opposite effect. **(C)** Bulky lipids (DOPC) display exposed cholesterol versus ordered cylindrical lipds (DPPC). With exposed cholesterol there is an increase in chemical activity. DOPC, dioleoyl-phosphatidylcholine (PC); POPC, palmitoyl-oleoyl-PC; DPPC, dipalmitoyl-PC.

Modified figure from: *Mesmin B, Maxfield FR (2009) Intracellular Sterol Dynamics. Biochimica et biophysica acta 1791(7): 636-645*.

Animal cells need to tightly regulate their level of cholesterol in the membranes; thus, an excess of active cholesterol needs to be transported to ER and mitochondria for inducing the homeostatic regulatory responses through which plasma membrane's cholesterol is restored to physiological set point (Figure 20). When the ER cholesterol rises above a sharp threshold of 5 mole% of total ER lipids [30], the Scap/SREBP complex (sterol regulatory element binding protein /SREBP cleavage activating protein-integral ER membrane proteins) binds to an ER anchor protein called Insig, and this prevents its transport to the Golgi [31]. As a result, cholesterol synthesis and uptake from LDL are reduced. If excess cholesterol accumulates, it is esterified by acyl-CoA:cholesterol acyltransferase (ACAT) for storage as cytoplasmic cholesteryl ester droplets and, when applicable, converted to steroids, oxysterols, bile acids, vitamin D3, and other functional byproducts [32]. Also analogous is increased mitochondrial cholesterol, which stimulates 27- hydroxycholesterol biosynthesis, and activates multiple feedback loops. 27-hydroxcholesterol interacts an ER protein called Insig, which then binds to 3-hydroxy-3-methyl-glutaryl-CoA reductase (HMGR) causing its degradation, while also binding sterol regulatory element binding proteins (SREBP) and preventing HMGR transcription [33]. It similarly stimulates the production of many homeostatic proteins, such as ATP binding cassette (ABCA1 and ABCG1) cholesterol pumps, which expel cholesterol from cells. Finally, 27-hydroxycholesterol-activated Liver X Receptors (LXRs) activate the expression of the inducible degrader of the LDL receptor, (IDOL) [34] by inhibiting the endocytosis of LDL receptor, which in turn limits the uptake of exogenous cholesterol.

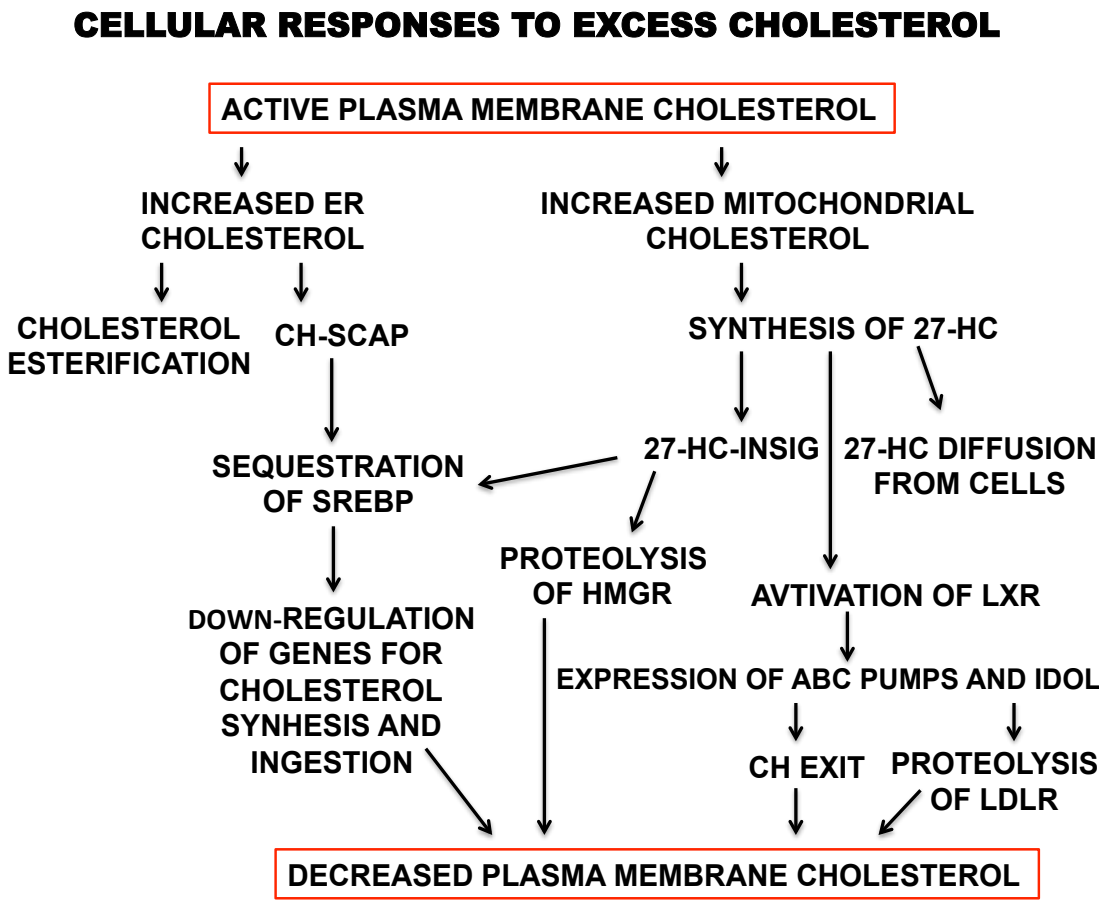

Figure 20. Cellular responses to excess cholesterol.
Pathways for lowering cholesterol concentration in the plasma membrane. Through equilibration mitochondrial cholesterol is increased and causes feedback loops of 27-HC. This starts to diffuse, pump out, and regulate receptors of cholesterol. In the ER esterification of cholesterol stops SREBP pathway and prevents cholesterol accumulation.

Modified figure from: *Steck TL, Lange Y (2010). Cell Cholesterol Homeostasis: Mediation by Active Cholesterol. Trends in Cell Biology, 20(11), 680–687.*

When ER cholesterol is less than ~5 mole% of total ER lipids [30], the Scap/SREBP-2 complex enters COPII-coated vesicles and localizes to the Golgi, where two proteases liberate the active fragment of SREBP-2 [35]. The active fragment enters the nucleus where it turns on transcription of the cholesterol-synthesizing genes and also the gene for low density lipoprotein (LDL) receptor, which supplies the cell with exogenous cholesterol [36]. LDL particles from the extracellular reservoir are internalized to endosomes and lysosomes through clathrin-dependent endocytosis; here cholesteryl esters (and triglycerides) are hydrolysed by acid lipase to supplement unesterified cholesterol for cellular processes [37]. The free cholesterol is then transported from late endosomes to plasma membrane, endoplasmic reticulum (ER), recycling endosomes, mitochondria, and other compartments [37]. Two proteins, NPC1 and NPC2, mediate efflux from late endosomal system [38]. The autosomal recessive Niemann-Pick Type C (NPC) disease is characterized in having malfunctioning NPC proteins; defective NPC proteins, either in one or both, resulted in cholesterol with lipids being retained in the organelles [38-40].

Cholesterol synthetic or the mevalonate pathway is accomplished by a series of enzymatic reactions (Figure 21). Acetyl-Coenzyme A is converted to HMG-CoA and mevalonate. The mevalonate is the rate-limiting step in this synthesis, and once produced its phosphorylated to isopentenyl pyrophosphate with an isoprenoid [41]. Condensation of isoprenoid forms squalene through rearrangement, and quickly modified to lanosterol, before ending up with cholesterol [4l]. On the completion of synthesis at ER, cholesterol is transported to plasma membrane in a relatively short time (half-life of ~10 min) [42]. Once cholesterol is localized to the membrane it is reallocated throughout the cell.

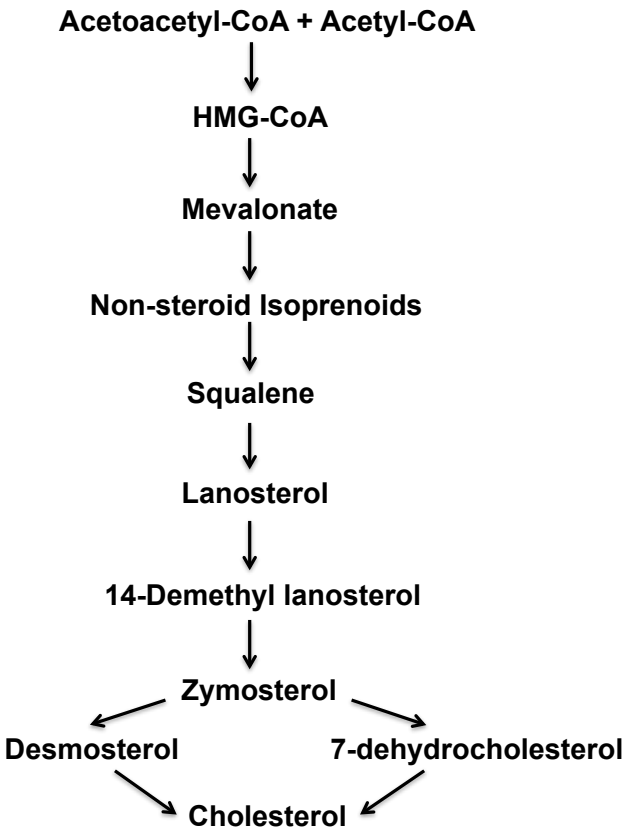

Figure 21. Simplified diagram revealing cholesterol synthesis in mammalian cells
The major steps in cholesterol or mevalonate pathway. A cascade of enzymatic reactions in the endoplasmic reticulum, with the rate-limiting step of mevalonate production, catalyzes theses steps.

Modified figure from: *Burns MP, Rebeck GW (2010) Intracellular cholesterol homeostasis and amyloid precursor protein processing.Biochim. Biophys. Acta1801, 853–859.*

The excess cholesterol removed by efflux into extracellular proteins. The cholesterol efflux is dependent mostly on energy driven ATP binding cassette (ABC) transporters present on the cell surface. The family of ABC transporters are known for cholesterol efflux, include ABCA1, ABCG1 and ABCG4 [43,44]. ABCA1 can deliver cholesterol directly to lipid free / lipid poor apolipoproteins (major apoproteins of HDL) fore example apoAI and apoE, however ABCG transporters function in transfer of partially lipidated particles produced by ABCA1 [45,46]. Cholesterols bound to HDL are transferred to the liver by scavenger receptor B1 (SR-B-1), are modified to bile salts and removed by the gastrointestinal tract [37].

The different localization and modifications of intracellular cholesterol primed us with this question: What regulates the heterogeneous distribution of cholesterol in the cell? It is seen clearly that intracellular cholesterol transport and distribution is an unsolved issue of vital importance to cell physiology. Mutations in transport pathways modify the cellular cholesterol metabolism, resulting in pathological conditions [38]. Irregular cholesterol levels were detected in several diseases, including Niemman-Pick type C disease [39], atherosclerosis [47], and Alzheimer's disease [48]. Therefore it is of importance in studying these pathways of intracellular cholesterol transport to better understand abnormal cholesterol levels in mammalian cells.

Even though cholesterol is able to transport bidirectionally between the plasma membrane and organelles, the path taken by cholesterol between any two membranes in the cell is not yet clear. While cholesterol is carried in the bilayers of cytoplasmic vesicles [49,50] these are not generally considered to be the principal vehicles for its transport. Non-vesicular cholesterol transfer uses cytosolic lipid transfer proteins as a

mechanism that shuttles cholesterol molecules between intracellular compartments the time scale minutes and does not require ATP as energy [51]. Several proteins such as the "steroidogenic acute regulatory protein (StAR)-related lipid-transfer (START) domain family" and the "oxysterol-binding protein (OSBP) family", which includes the "OSBP-related proteins (ORPs)," [52] are hypothesized to play a role in regulating intracellular transport and distribution of cholesterol but many aspects of this mechanism remains elusive. Furthermore, the mechanisms for preserving cholesterol asymmetry across bilayers remain even more theoretical. The information about cholesterol flip-flop kinetics and molecular basis of how translocators and exporters move cholesterol molecules across membrane is very limited and more methodological experiments are needed to clarify this issue.

To understand dynamics and functional roles of cholesterol in the plasma membrane, one has to study local cholesterol concentration in the inner and outer plasma membrane, cellular transport between different membranes, and the sensors and effectors that regulate this complex mechanism. Although significant advances have been made in studying cholesterol distribution and concentration in both leaflets of the plasma membrane, most methods used are indirect, which can lead to different interpretations. These methods are based on: (i) adjustment of cholesterol in plasma membrane by cholesterol oxidase, which unfortunately can disorder cell membranes (53), (ii) fluorescence microscopy of fluorescently-labeled cholesterol derivatives (54), and (iii) binding of fluorescent compounds like filipin, polyene macrolide (54). However, chemically altered cholesterol equivalents do not recollect all of the properties of the cholesterol molecule. In addition, any structural modification of cholesterol may induce

modifications in membrane organization and proteins function. Even filipin, the primary used sterol marker, has a serious restriction due to its reduced specificity; it can binds to other lipids present in the plasma membrane and cannot distinguish between cholesterol residing in cytosolic or exofacial leaflets. Although these probes remain useful in certain types of experiments, the development of alternative probes is highly desired.

To overcome these problems, we developed a new cholesterol-specific sensor and tested the notion of transbilayer asymmetry of cholesterol by simultaneous quantification of cholesterol in the two leaflets of the plasma membrane of various mammalian cells. A probe was used to enable the exposure of cholesterol levels in cell membranes and their dynamic relocation in response to metabolic and pathophysiological stimuli. We directly correlated these changes in the local cholesterol concentration with various cellular processes such as cell signaling and intracellular transport. Based on our recent findings that there are many cholesterol binding scaffold proteins and that the basal cholesterol concentration in the inner plasma membrane may be much more lower than previously thought, we hypothesize that cholesterol may serve as a local activation threshold that triggers diverse cellular responses through selective recruitment and activation of their cytosolic effectors. Here, we validated our hypothesis by measuring the local concentration of cholesterol according to our established analysis protocols [55] and correlating this parameter with cellular activities such as cell signaling.

2. EXPERIMENTAL PROCEDURES

2.1. Materials

Cayman Chemical was used to purchase PtdIns(4,5)P_2 and the other lipids were supplied by Avanti Polar Lipids. The thiol-reactive acrylodan and thrombin were purchased from Invitrogen. The methyl-β-cyclodextrin (MβCD) and *S. aureus* SMase were obtained from Sigma.

2.2. Plasmid construction

Bacterial and mammalian cell expression vectors used were pET21a (+) from Invitrogen and pEGFPC1 from BD Clonetech, respectively. cDNA libraries of NHERF1 were subcloned into both vectors along with PDZ1 domain. pET21a (+) vector was used to prepare the other PDZ domains or tagged with enhanced green fluorescent protein (EGFP) on the C-terminus and then subcloned into pRSET-b vector (Invitrogen). The D4 domain (residue K391-N500) of perfringolysin O was subcloned into the pGEX-4T-1 (Invitrogen) vector to generate bacterial expression plasmid containing an N-terminal glutathione S-transferase (GST) fusion. Mutations were done with a QuickChange kit from Stratagene. After positive results each construct was sent and verified by DNA sequencing.

2.3. Preparation of Cholesterol Sensor Constructs

The D4 domain (residue K391-N500) of perfringolysin O was subcloned into the pGEX-4T-1 (Invitrogen) vector to generate bacterial expression plasmid containing an N-terminal glutathione S-transferase (GST) fusion. To improve membrane affinity of the

protein, D434 was mutated to Ala, A463 to Trp, and Y415 to Ala yielding D434A/A463W/Y415A or just single mutant D434A. One endogenous cysteine residue was left for labeling. Mutations were done with a QuickChange kit from Stratagene. After positive results each construct was sent and verified by DNA sequencing.

2.4. Protein Expression, Purification, and Labeling

D434A and D434A/A463W/Y415A were expressed as GST-tagged proteins. E. coli BL21 RIL codon plus (Stratagene) cells were used for protein expression. Growth of E. coli was initiated by inoculating 1 L flask of sterile Difco Luria broth (containing 100 μg/mL ampicillin) with 10ml of an overnight culture grown at 37°C. The 1L culture was incubated at 37°C with constant shaking. To induce expression of the D4 domain 0.2 mM isopropyl β-D-thiogalactopyranoside (IPTG) was added when optical density A_{600}nm was equal to 7.0 absorbance units. The induced culture was further grown for 16 h at room temperature, and then centrifuged for 10 min at 5000 rpm in 4`C. 20ml lysis buffer (50mM Tris, 300mM NaCl, 10mM Immidazole, 10%(v/v) Glycerol, pH=7.9) containing 20 μl of 2-mercaptoethanol was added to resuspend the cells and subjected to tip sonication with a cell disruptor (Branson Sonifier 450) at cycles of 15 seconds on and off while over ice, and then cooled further for 15s. 10 cycles were used for sonication. The total lysate was centrifuged for 30 minutes at 16,000 rpm in 4`C. The supernatant from this step was incubated for 1 h at 4°C while mixing with 1 ml glutathione S-transferase tag™ resin (Novagen, Madison, WI). The mixture was applied to a column and the column was washed with 150ml washing buffer (20mM Tris, 160mM NaCl, pH=7.4) with occasional pipetting. For labeling of the proteins, stock solutions of acrylodan or NR3 in dimethyl sulfoxide were prepared and >100 μg of acrylodan or NR3

supplemented to the resin. The mixture was subjected to light shaking at room temperature for 2 hours. Washing the resin with the buffer several times was done to remove excess resin. The resins were incubated with thrombin (Life Technologies) at 4^0C over night to cleave the labeled protein from the GST tag. The labeled protein was collected from the resin by centrifugation. Purity and the concentration of the recombinant proteins were determined by sodium dodecylsulfate-polyacrylamide gel electrophoresis and Bradford (BioRad) assay, respectively.

2.5. Lipid vesicle prepertion

Plasma membrane-mimetic vesicles are formulated with 1-palmitoyl-2-oleoyl-sn-glycero-3- phosphocholine (POPC), 1-palmitoyl-2-oleoyl-sn-glycero-3-phosphoethanolamine (POPE), 1-palmitoyl-2-oleoyl-sn-glycero-3-phosphoserine (POPS), cholesterol, 1-palmitoyl-2-oleoyl-sn-glycero-3-phosphoinositol (POPI), and 1,2-dipalmitoyl derivatives of PtdIns(4,5)P_2 using a molar ratio 12:35:22:22:8:1. Solution for PM-cholesterol vesicles contains POPC/POPE/POPS/PI/PtdIns(4,5)P_2 in a molar ratio of 23:46:22:8:1. To prepare different large unilamellar vesicles (LUVs) Liposofast (Avestin) microextruder with a 100-nm polycarbonate filter was used. Giant unilamellar vesicles (GUVs) were prepared by the electroformation. The lipid mixture (POPC/POPS/cholesterol= 80-x:20:x, x = 0-30 mole%) was dissolved in chloroform to the final concentration of 100 µg/ml. The lipid solution was spread onto the indium-tin oxide electrode surface and dried under vacuum for 1.5 hour. By applying an electric field at 3V with 20 Hz frequency vesicles were developed in 350 mM sucrose rich solution at room temperature for 4 hours. 1µl sucrose-loaded GUV solution was added into a well containing 200 µl of buffer (20 mM Tris, 0.16 M NaCl, pH 7.4). Protein was added after GUVs were sedimented at the bottom of

the well, and the entire well was scanned with an automated x-y stage (2-min scan time).

2.6. Surface Plasmon Resonance (SPR) Measurement

All SPR measurements were performed at 23°C in running buffer (20 mM Tris, pH 7.4, containing 0.16 M NaCl). Lipids were immobilized on L1 chip in the BIACORE X system purchased from GE Healthcare. The active channel (Fc-2) was coated with PM-mimetic (or others) vesicles and control surface with POPC vesicles (Fc-1). Equilibrium SPR measurements required extended time for association equilibration for reliable R_{eq} results, thus a flow rate of 5 μL per minute was used. Each sensorgram was background-corrected by subtracting the response units (RU) of control surface from the active surface ones. The Langmuir-type binding, represented as P + M <--> PM, is concerning the protein, P, and vesicle binding site for protein, M, was used to analyze sensograms. A plot was generated comparing the equilibrium values, R_{eq}, and concentration of protein, P_0. Using the binding isotherm curve and nonlinear least-squares analysis, R_{eq} = Rmax/(1 + Kd/Po), was solved for dissociation constant, K_d. Kinetic SPR measurements were preformed at 30 μL per minute flow rate for both association and dissociation phases. The measurement was repeated three times to obtain average and standard deviation values.

2.7. Spectrofluorometric Measurements

Horiba Flurolog-3 spectrofluorometer was used for all cuvette-based fluorescence measurements. Lipid sensors (typically 500 nM) were added to large unilamellar vesicles with various lipid compositions and the emission spectra of DAN labeled sensor and NR3 labeled sensor were measured with excitation wavelength set at 392 nm and 520 nm, respectively.

2.8. Calibration of Lipid Sensors by Fluorescence Microscopy

All fluorescence microscopy measurements were carried out at 37 ºC with by two-photon microscope equipped with four-channel detection with two femtosecond-pulsed laser sources (Newport). Both instrument control and data analysis were performed by PrairieView (Bruker). In vitro calibration of DAN-D434A and NR3-D434A/A463W/Y415A was performed using GUVs composed of POPC/POPS/cholesterol (100-x:20:x) (x = 0-60 mole%). These GUV were mixed with DAN-D434A (or NR3-D434A/A463W/Y415A) in the concentration range of 0-500nM. DAN-D434A and NR3- D434A/A463W/Y415A were two-photon excited at 780nm and 950nm, respectively. 436 ± 10 and 525 ± 25 band pass filters were employed for the blue channel and the green channel, respectively, whereas 600 ± 19 and 635 ± 20 band pass filters were used for the orange channel and the red channel, respectively. For DAN-D434A, blue channel fluorescence signals derive from membrane-bound sensors only whereas green channel signals are from both membrane-bound and sensors. Likewise, orange channel fluorescence signals derive from membrane-bound sensors only whereas red channel signals are from both membrane-bound and sensors for NR3-D434A/A463W/Y415A. Using Peltier-cooled 1477P style Hamamatsu photomultiplier instrument, at each time point, an image of 512 x 512 pixels was gathered with dwell time of 20 milliseconds. At each cholesterol concentration, 10 GUVs were selected for image analysis by MATLAB (MathWorks, Inc) or Image-Pro Plus (Media Cybernetics, Inc). For data analysis, each cross-sectional two-dimensional vesicle image was read into M x N (typically 256 x 256) matrix. The region of interest (the membrane in our case) was selected by setting a threshold intensity (or brightness) value on the basis of the

intensity distribution profile of the image obtained using a virtual line drawn over the vesicle and rotated 360 degree around it. Typically, 15% of the maximal brightness (in the center) was set as a threshold to distinguish the membrane region from the non-membrane region (by graythresh function in MATLAB or by the automatic intensity cutoff function in Image-Pro Plus) and a virtual mask was drawn to cover the selected membrane region. Since the orange channel (or blue channel for DAN-D434A) always gives stronger membrane signals than the red channel (or green channel for DAN-D434A) for NR3- D434A/A463W/Y415A, we first selected the mask from the orange (or blue) channel and superimposed it onto the same image in the red (or green) channel. The estimated membrane region of the vesicle was validated by comparing it with the membrane region in the differential interference contrast image of the vesicle. The total photon counts of GUV (F_B(total) and F_G(total) for DAN-D434A and F_O(total) and F_R(total) for NR3- D434A/A463W/Y415A) is then divided against total area of pixels that contain each GUV to produce average intensities, F_B and F_G for DAN-D434A and F_O and F_R for NR3- D434A/A463W/Y415A (counts/m^2), which were then used to prepare the calibration curves for ratiometric analyses. For DAN-D434A, K_d and $(F_B/F_G)_{max}$ values were calculated from non-linear least-squares analysis of the (F_B/F_G) versus PS plot using the equation; $(F_B/F_G) = (F_B/F_G)max/(1 + K_d/[cholesterol]) + C$ where $(F_B/F_G)_{max}$, K_d, and C indicate the maximal F_B/F_G value, the equilibrium dissociation constant (in terms of mole%), and the arbitrary instrumental parameter, respectively. The theoretical calibration curve was then constructed using these values (see Figure 31) and [cholesterol] from an unknown sample was calculated using the calibration curve. The same calibration was performed for NR3-D434A/A463W/Y415A.

2.9. Cellular Culture, Methyl-β-cyclodextrin, and Sphyngomielinase Treatments

NIH 3T3, HeLa, and HEK 293T cells were seeded into 50 mm round glass-bottom plates, grown at 37^{o}C in a humidified atmosphere of 95% air and 5% CO2. Growth medium was composed of Dulbecco's modified Eagle's medium (DMEM) (Life Technologies) and supplemented with 10% (v/v) fatal bovine serum (FBS), 100 units per milliliter penicillin G, and 100 microgram per milliliter streptomycin sulfate (Life Technologies) and passaged every other day. For cholesterol depletion, HEK 293 cells were incubated in 5 mM MβCD, methyl-β-cyclodextrin, (Sigma) for 60 minutes in serum free media. For cholesterol supplementation, cholesterol was added to cells by incubating cells for 1 h at 37°C with 50 mg/ml cholesterol complexed with 1.5 mg/ml MβCD in serum-free medium. To hydrolyze sphyngomielin, 100 milliunits/ml of SMase was added to the growth medium and cells were incubation for 30 min at 37°C.

2.10. Cellular Lipid Quantification

For cholesterol quantification in the inner and outer PM of NIH 3T3 or HeLa cells, NR3-D434A/A463W/Y415A was delivered into NIH 3T3 cells by microinjection and DAN-D434A was added to the growth media. Microinjection was performed using the Eppendorf InjectMan NI 2 system. P-97 Pipette Puller was used for microinjection micropipette preparation. To minimize cell damages by microinjection, we used the calcium-free media and gave enough time for cells to recover after injection, and selected only healthy cells for further fluorescence measurements. Cholesterol sensor concentrations were adjusted to give strong enough fluorescence signals for robust data analysis. Typically, 20-30 femtoliter of 0.5-1 μM sensor solution was microinjected into

the cell. All microscopy measurements and imaging data analysis were performed as described above. The local lipid concentration on the cell membrane was determined from the observed local (F_B/F_G) or (F_O/F_R) values using the in vitro calibration curves determined using GUVs with corresponding cholesterol compositions. The three-dimensional display of local cholesterol concentration was obtained using the surf function in MATLAB. Briefly, two binary image masks were created: the first one was around the PM as described above and the second one was a triangular mask that connects the center of the cell, any position on the PM and the second position on the PM that is advanced from the first position by 2 (or any discrete number) degree. The average local intensity was calculated by multiplying the two masks and the cell's image matrix. The same operation was repeated for every 2 degrees around the PM in a counter-clockwise manner.

3. RESULTS

3.1. Perfringolysin O and its C-terminal domain as a potential cholesterol sensor candidate.

To acquire an effective tool for analyzing transbilayer distribution of cholesterol in plasma membrane, a cholesterol sensor, termed D4, was developed based on the fourth domain of Clostridium perfringens O-toxin (PFO), which recognizes cholesterol in the plasma membrane and organelles. Among a number of extensively studied cholesterol binding domains, we selected the D4 domain of perfringolysin O as a potential sensor candidate because of its rigorous cholesterol specificity. PFO belongs to a family of bacterial pore forming toxins called "thiol-activated cytolysins" also termed cholesterol-dependent cytolysins (CDCs) [56]. PFO is an 115Å long molecule encompassing four domains from which only the residues of the domain 4 (termed D4) possess membrane cholesterol binding activity [57]. As Figure 22A depicts, D4 contains cholesterol recognition motif (CRM), 11-residue long undecapeptide region, and two L2 and L3 short loops [58]. It has been reported that tryptophan-rich motif with adhered sequence (ECTGLAWEWWR) [58] is a region that plays a significant role in the membrane binding of D4 doamin. The binding of D4 domain to a membrane surface involves two steps: the initial non-specific association and specific cholesterol recognition, which leads to the formation of a tightly bound complex. In this binding process, tryptophan residues located in the undecapeptide region make first contact with membrane, L2 and L3 insert into the bilayer surface, and upon cholesterol recognition by the CRM D4 domain is anchored perpendicularly to the membrane [59].

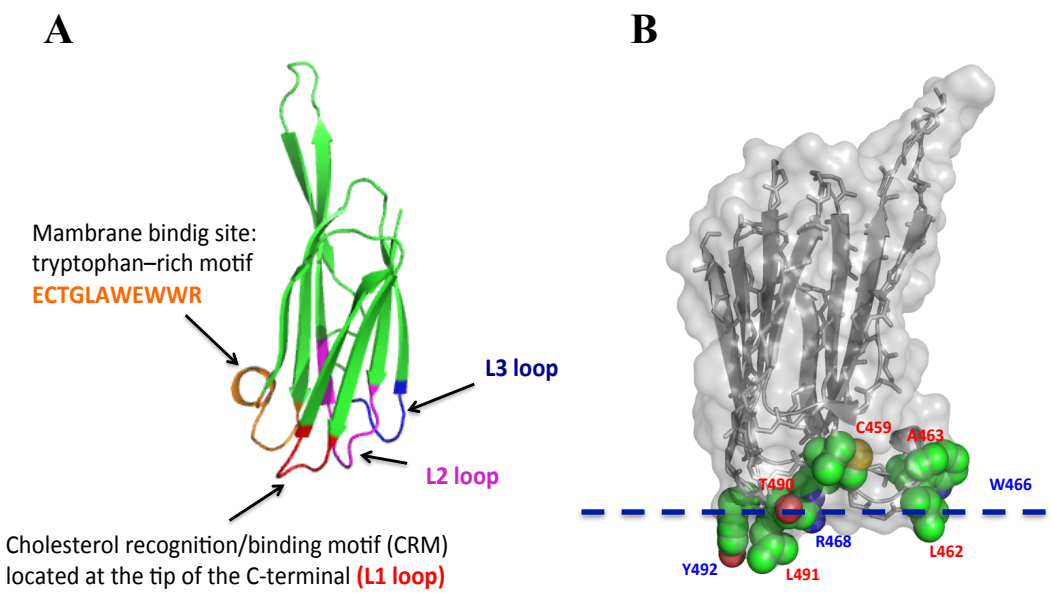

Figure 22. The crystal structure of the D4 domain of perfringolysin O.
(A) The localization of regions pertinent to this study is specified by arrows **(B)** Key residues involved in membrane affinity and cholesterol recognition are highlighted. Also shown is C459 that is used for fluorophore labeling. The dotted line indicates the putative location of membrane surface.

According to the literature, although the side chains of several residues of both loops and undecapeptide embed into the membrane, they do not breaks through the bilayer core [60,61]. Based on our experience with membrane binding proteins, we predicted that residues: L462, W466, R468 located in the undecapeptide region and Y492 in L1 loop, most likely facilitate membrane binding (Figure 22B). Moreover, recent studies suggested that two highly conserved among species residues T490 and L491 located in L1 loop are critical for cholesterol recognition [62]. Finally, D4 has very distinct structure from other cholesterol-binding proteins, implying the presence of unique molecular mode of action. We believe that D4 with these unique structural properties can give rise to drastic difference in the ability to uncover the fundamental nature of membrane cholesterol.

To understand the nature of D4-cholesterol interaction in the context of membrane lipids, we first investigated binding of the isolated toxin fragment to cholesterol and other sterols by surface plasmone resonance (SPR) analysis. D4 recognized cholesterol with high sensitivity and selectivity, as demonstrated in Figure 23A. One issue is that the D4 binding to PM-mimetic vesicles increases very non-linearly as cholesterol content increases. The cholesterol content of plasma membrane at which the rapid increase in binding is observed exceeds 30% of cholesterol (Figure 23B). Furthermore, the D4 domain showed fast membrane association and dissociation-a property critically required in time-resolved lipid quantification technique. These preliminary data suggest that D4 domain of perfringolysin O toxin can serve as

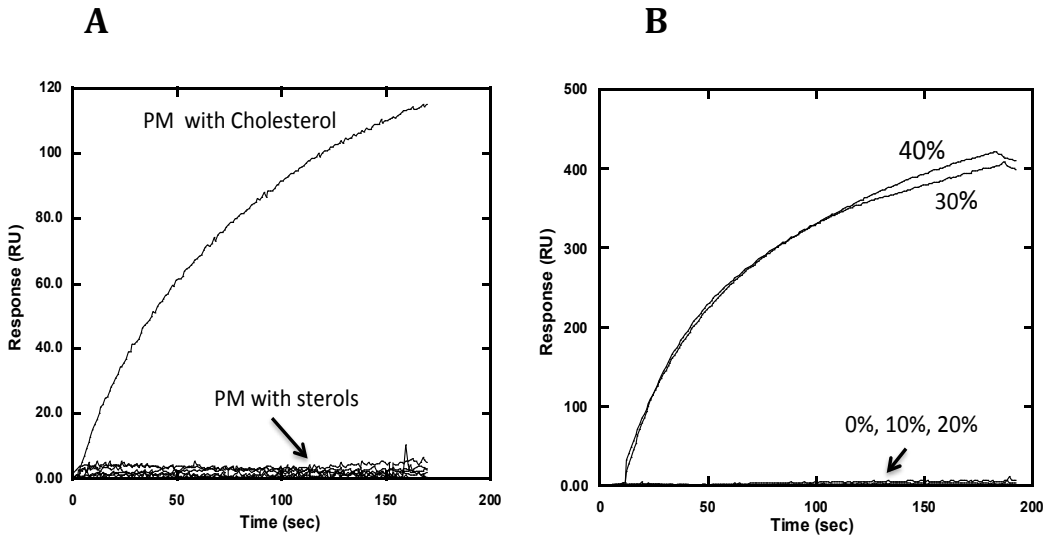

Figure 23. **Membrane-binding properties of perfringolysin O - D4 domain by SPR analysis.**
(A) Specificity of perfringolysin O – D4 domain to PM-mimetic vesicles containing a mixture of POPC/POPE/POPS/PI/cholesterol/PtdIns(4,5)P2 in molar ratio (12:35:22:8:22:1) and PM-mimetic with cholesterol derivatives (POPC/POPE/POPS/POPI/cholesterol derivatives/PtdIns(4,5)P2 =12:35:22:8:22:1. Cholesterol derivatives were: 25-hydroxycholesterol, ergosterol, dexamethasone, cholate, and 5α,6β- dihydroxycholestanol and protein concentration was 400nm. Note that the D4 domain shows strict selectivity for cholesterol over other derivatives.
(B) Cholesterol dependency. The D4 domain (400 nM) was allowed to interact with POPC/cholesterol/POPS (80-x:x:20) vesicles. D4 is highly dependent on cholesterol content.

an appropriate and selective probe for membranes enriched with cholesterol, but is not suitable for quantification of membrane cholesterol in intact cells due to its narrow dynamic range. Hence, we decided to improve its properties by mutagenesis analysis and use it as a template for a cholesterol sensor.

3.2. Spectral properties of the D4 WT fluorescence sensor

To observe the subcellular distribution of lipids in living cells our research group has developed sophisticated fluorescence imaging techniques. In our strategy, a selected potential candidate is first engineered for optimal membrane affinity and high lipid selectivity. Then the engineered domain is converted into a fluorescence sensor by cysteine labeling with solvatochromic fluorophores that displays desired spectral attributes upon lipid binding (Figure 24) [55]. A model PtdIns(4,5)P_2 sensor that serves as a template for the lipid sensor development in our laboratory was obtained from engineered ENTH domain. When labeled with 2-dimethylamino-6-acyl-naphthalene (DAN)[63], it undergoes a large increase in fluorescence intensity with a "blue-shift" upon lipid binding, enabling accurate quantification of PtdIns(4,5)P_2 by ratiometric analysis [55]. Once delivered to mammalian cells by microinjection, the sensor allows for rubust and sensitive measurements of local PtdIns(4,5)P_2 concentration with high spatiotemporal resolution under physiological conditions. Assertively we believe that the same technology can be applied to *in situ* quantification of cellular cholesterol in mammalian cells.

To check the feasibility of cholesterol quantification using DAN-labeled D4 WT, we first measured its spectral properties by spectrofluorometry. As Figure 8C shows, WT D4 fluorescence spectra confirmed our previous findings that native form of D4 can only

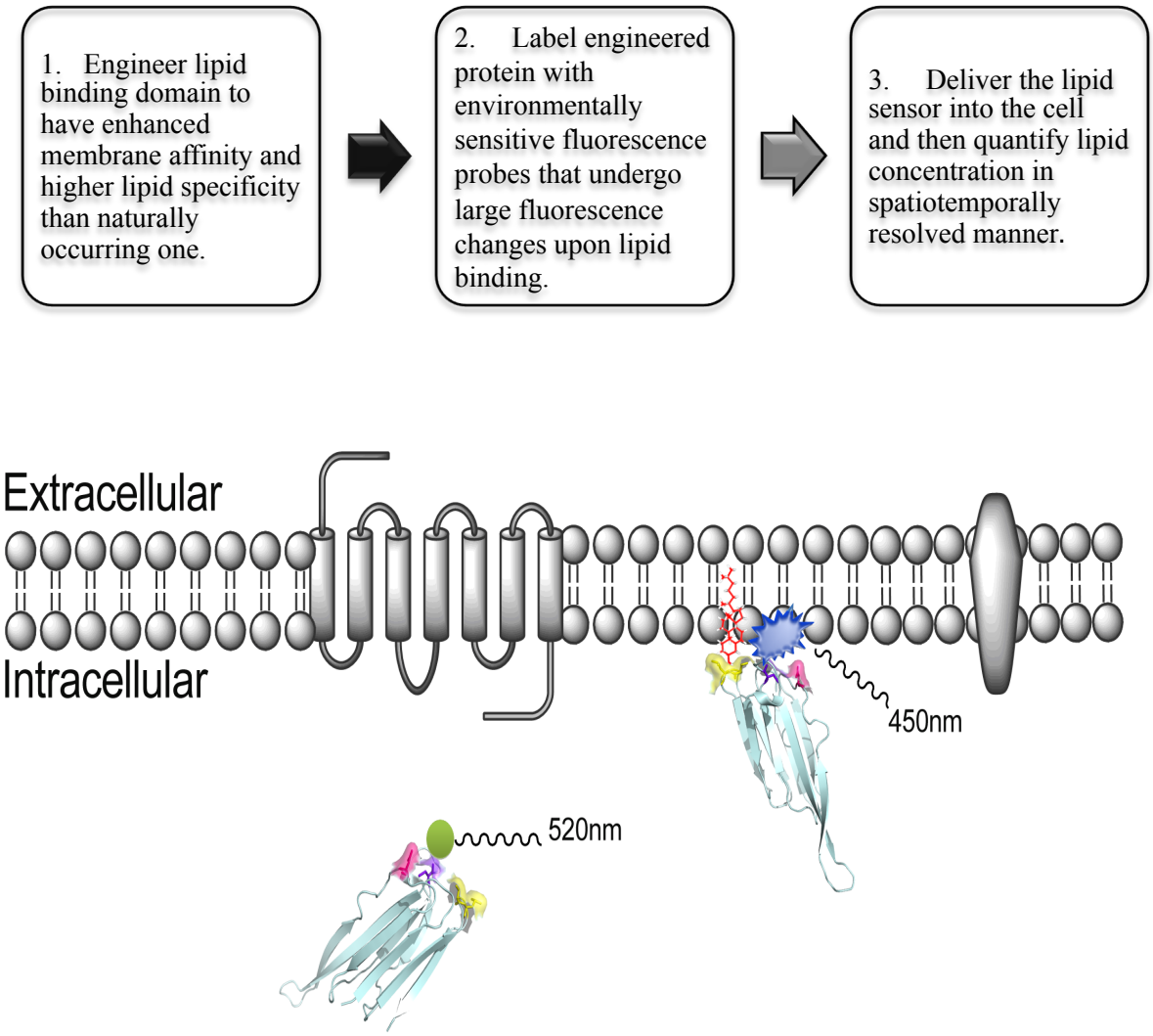

Figure 24. **General strategy for cellular lipid quantification using an engineered lipid binding domain labeled with a single fluorophore (e.g., DAN).**
Environment-sensitive fluorophores possess spectral properties that are responsive to physical changes in the local environment, solvent polarity in particular. In our approach, a fluorophore is engineered into a membrane-binding surface of a protein that undergoes a change in its environment upon lipid binding. Upon association with membrane, the polarity around the fluorophore changes and this is reflected in altered fluorescence properties of the probe. Thus, hybridized cholesterol binding domain with appropriate dye can be used for ratiometric determination of cholesterol concentration.

detect very narrow range of cholesterol concentrations. When a cysteine residue (C459) of D4 domain is labeled with DAN group, resulting sensor experiences blue-shifted fluorescence emission spectra with only a subtle increase in emission intensity (F) at 455nm (F_{455}) corresponding to increase of cholesterol mol% in LUVs. This unfavorable spectral change suggests that cholesterol concentration cannot be determined by ratiometric analysis using this sensor and further sensor engineering is required.

3.3. Cholesterol sensor protein engineering

As we previously reported, introducing labeling site on the most exposed protein surface while removing an endogenous cysteine can drastically change the lipid concentration threshold required for binding [55]. We conceptualized that moving cysteine to positions near D4 membrane interacting surface might yield variants that associate with membranes containing less cholesterol than the native domain. Because D4 has endogenous cysteine (C459) buried inside (Figure 22B), exposing it to aqueous environment would not only improve its spectral properties but also increase labeling efficiency. Therefore, we generated mutants: L462C, A463C, Y492C, D434, S399C, G488C, H398C, G400C, A401C, Y402C, V403C, A404C, Q405C, F406C, among others. Unfortunately, cysteine mutants had adverse affects. When labeled with DAN, new sensors neither exhibit a ‘blue shift’ upon membrane binding nor increase in fluorescence emission intensity (F) at 455nm. They also destabilized protein and lowered labeling yield, thus, we concluded that endogenous cysteine is crucial for protein stability and functionality.

To further improve cholesterol affinity of the D4 domain, we created a panel of new mutants. Our first candidate for decreasing the cholesterol threshold was D434

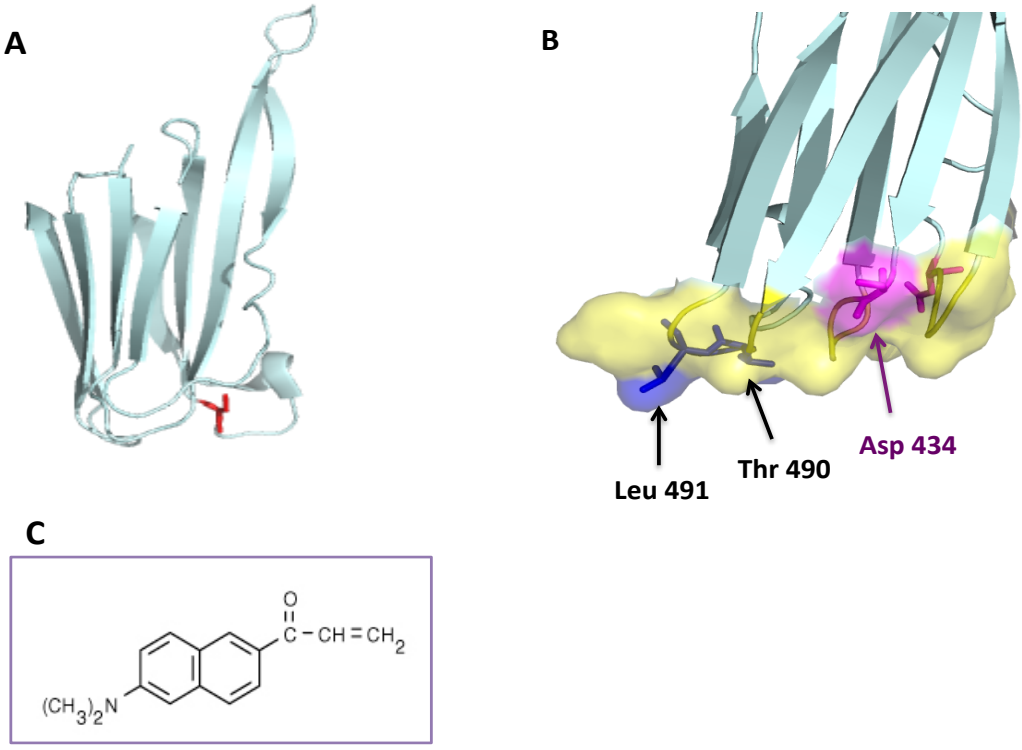

Figure 25. Engineering D4 Domain of perfringolysin O into cholesterol sensor.
(**A**) Crystal structure of D4 Domain of perfringolysin O generated by Pymol. Labeling site Cysteine 459 is shown in red.
(**B**) Enhancing membrane binding of D4 domain by introducing D434A mutation.
(**C**) Chemical structure of acrylodan.

residue positioned in L3 of D4 domain (Figure 25B). Once Asp was mutated to Ala, the change in the mole percent of cholesterol for resulting D434A decreased by 10%. As shown in Figure 26B, DAN-D434A displayed significantly lower cholesterol threshold (and wider dynamic range) than the WT (Figure 26C) and larger fluorescence changes upon cholesterol binding. D434A was also more stable than the WT. Since our spectral analysis was satisfactory, we checked the feasibility of DAN-D434A sensor in the living cells. When DAN–D434A was delivered into NIH 3T3 cells by microinjection, however, no membrane localization was observed. The addition of D434A to the extracellular medium, on the other hand, resulted in its instantaneous membrane binding to the NIH 3T3 cell surface (Figure. 27A). To verify whether this outer membrane binding is cholesterol dependent, we mutated T490 and L491 (Figure 25B), which are involved in cholesterol recognition, to alanine. The resulting double-site mutant was added to the medium at varying concentrations but no signal was observed on the plasma membrane, as Figure 26B and C depicts, even after extended incubation time. Our preliminary results showed that in situ cholesterol quantification of cholesterol for the outer PM could be achieved with DAN-D434A (first generation mutant); however, quantification of cholesterol in the inner PM may require a sensor with higher cholesterol affinity. Thus, we further optimized the technique for robust and versatile determination of cholesterol in a wider concentration range and applied it to determination of the cholesterol concentration and its changes at two layers of PM.

Since our preliminary results revealed that the cholesterol concentration in the inner PM is significantly lower than that in the outer PM, we aimed to enhance the D4 domain affinity for cholesterol-containing vesicles and thereby prepare a panel of sensors

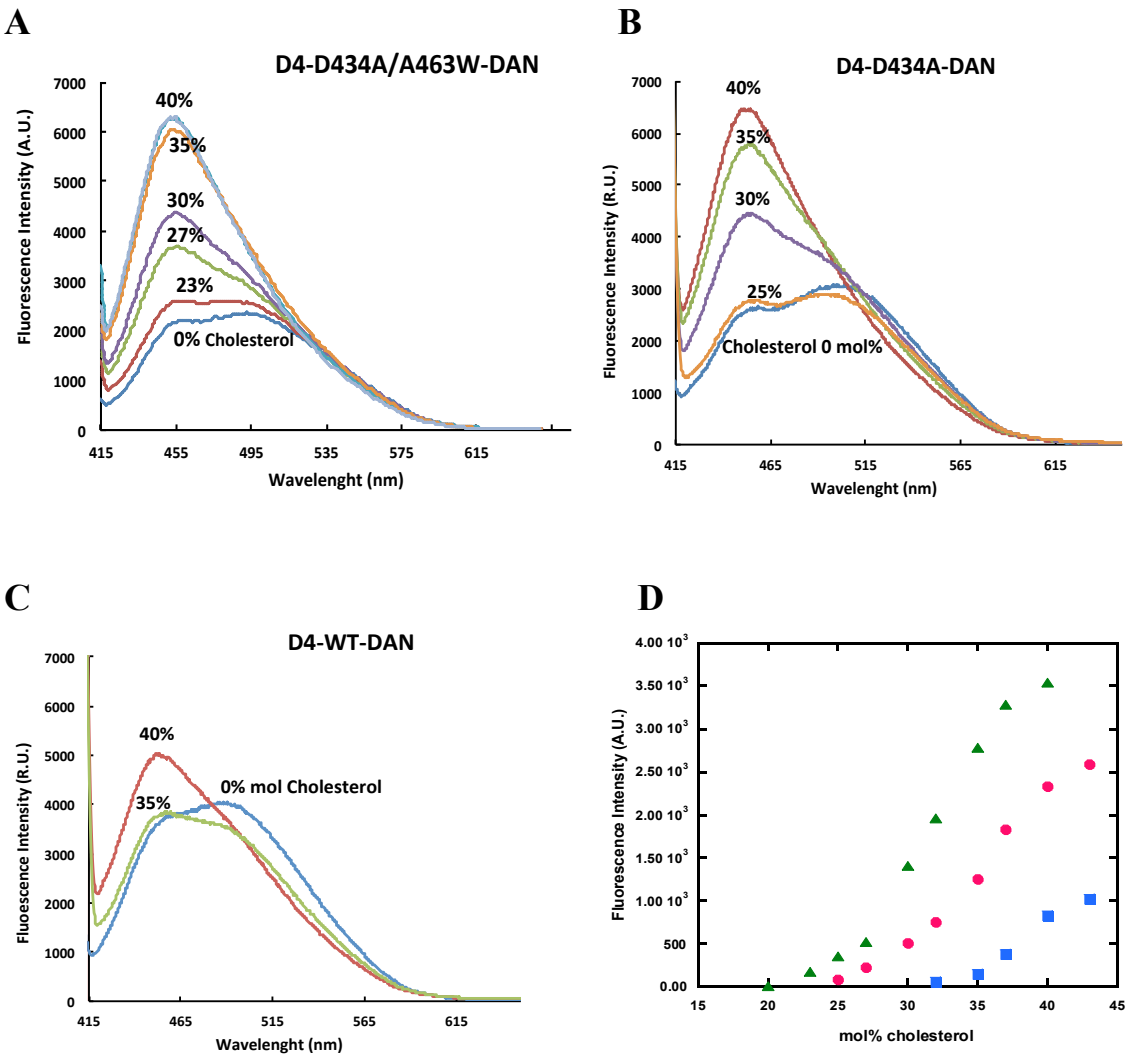

Figure 26. Spectral properties of cholesterol sensors.
Fluorescence emission spectra of **(A)** DAN-D434A/A463A, **(B)** DAN-D434A, and **(C)** DAN WT (sensors concentration 400 nM) in the presence of vesicles containing a mixture of cholesterol (25-43%), POPS (20%), and POPC (80%-chol%) LUVs measured spectrofluorometrically. (**D**) Plot fluorescence intensity versus mol % cholesterol used as a calibration curve for ratiometric determination of cholesterol concentration.

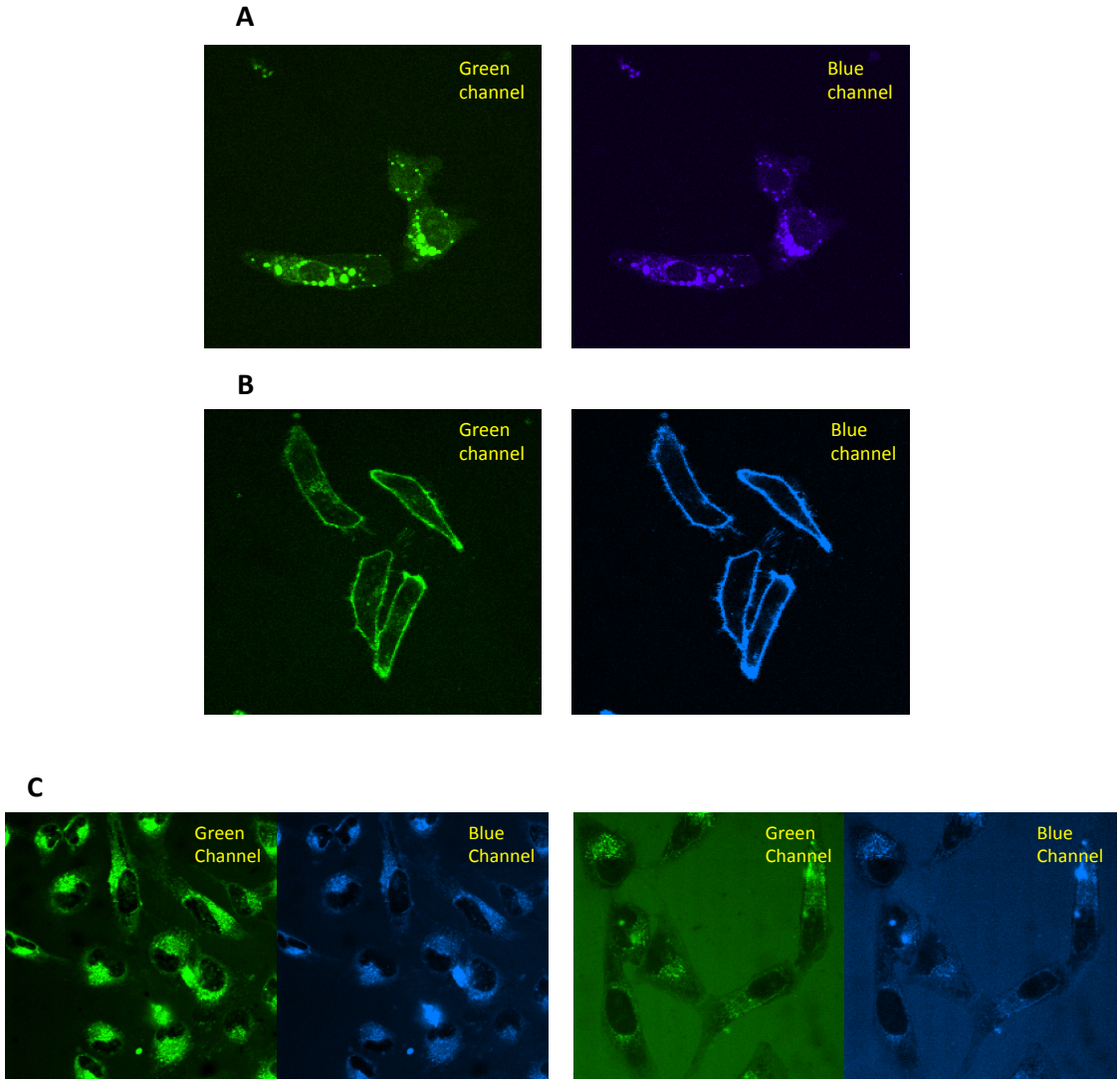

Figure 27. **Subcellular localization of DAN labeled D434A and its mutant D434A/T490A/L491A in NIH 3T3 cells.**
(A) Two-channel image of cell showing relatively random cytosolic distribution of the D434A-DAN sensor after microinjection. **(B)** Cholesterol distribution in the exofacial leaflets of the plasma membrane monitored by DAN-D434A added to extracellular medium. **(C)** Media-added DAN-D434A mutant (D434A/T490A/L491A) was mainly localized in the cytosol, proving that Thr490 and Leu491 are crucial for cholesterol-dependent membrane binding.

that cover a wide range of cholesterol concentration. In general, membrane binding of a protein has two components, specific recognition of a lipid in the pocket and non-specific interaction between protein and membrane surface. Our previous studies with other lipid domains showed that it is much easier to improve membrane affinity of a protein by engineering its membrane binding surface than its specific binding pocket [64]. Indeed, all mutations reported to improve the affinity of the D4 domain for cholesterol-containing vesicles were performed on or near its membrane binding surface. To decrease the cholesterol threshold of the D434A mutant even further, we targeted residues which are located near the membrane-binding surface and are thus expected to be involved in nonspecific interaction with the membrane surface. We substituted these residues with tryptophan, which is known for enhancing membrane binding. When A463 was substituted with Trp, resulting DAN-D434A/A463W mutant bound to LUVs containing around 20% cholesterol. The cholesterol threshold was decreased by 5% and the spectral properties of this so-called second-generation mutant closely resemble the spectral properties of DAN-D434A (Figure 26). The addition of DAN-D434A/A463W to the extracellular medium resulted in cholesterol-dependent binding to the outer plasma membrane. Concentration of cholesterol in the outer membrane can be quantified (supplementary material Fig S2A) and it shows a significant degree of spatiotemporal heterogeneity. However, when microinjected, sensor was mainly localized in the cytosol, suggesting that either the probe has insufficient affinity to detect the low concentration of cholesterol in the plasma membrane and/or it has low stability and thus loses its integrity after microinjection. To overcome these potential limitations, we decided to stabilize this domain by further mutational analysis. By replacing Y415 with alanine, we created

D434A/A463W/Y415A mutant, which is believed to sense cholesterol concentration as low as 5% and display high stability.

3.4. In search for environmental sensitive probes

Visualization and quantification of cholesterol in both membranes is an important tool for monitoring its local fluctuations but most commonly available probes are not well suited for this purpose. Thus, we developed dual-color fluorescence-analysis to evaluate the distribution of fluorescent-labeled cholesterol sensor in live cells. An approach for the selective detection of cholesterol in the inner and outer plasma membrane requires orthogonal lipid sensors that allow simultaneous dual lipid quantification in the context of living systems. The limited availability of environment-sensitive fluorescent turn-on probes (ESF) makes the extrinsic synthesis of orthogonal lipid sensors very challenging [65]. Our group, thus, investigated specific class of solvatochromic fluorophores demonstrating emission attributes that are highly sensitive to the immediate environment and that can be paired with thiol-reactive acrylodan (6-acryloyl-2-dimethylaminonaphthalene). Since DAN shows a spectral shift from green to blue upon lipid binding it requires a conjugated partner with no overlapping spectra and we believe that Nile Red dye and its maleimide derivatives is a perfect match [66]. However, one major limitation of labeling proteins with Nile Red is its low water solubility and high fluorescence background, which necessitate extensive washing steps to remove unreacted fluorophore and destabilize protein. With collaborative effort this limitation was overcome by conjugating Nile Red core to another molecule to enhance solubility. Among 13 tested Nile Red acrylate derivatives [65] (structures in supplementary material Fig. S1) NR3 had the highest quantum yield when coupled with

the D434A/A463W mutant and its concentration-dependent emission spectra were orange-shifted upon cholesterol binding. Generating 3rd generation sensor with the threshold for binding to cholesterol-containing vesicles as low as 5%, turned out to be much more time consuming than anticipated. Thus, to test feasibility of NR3 dye, we used D434A/W434A mutant.

To validate NR3-D434A/A463W effectiveness in vivo, we added it to the extracellular medium and as expected, the addition of NR3 labeled sensor led to the outer plasma membrane localization. But this time, its distribution was not as uniform as for DAN labeled senor and showed a distinctive punctate pattern, suggesting uneven cholesterol distribution within the outer plasma membrane (Figure 28A). This result revealed a potential increase in sensitivity of NR3 labeled D434A/A463W as oppose to DAN labeled sensor. To investigate this possibility, we microinjected NR3-D434A/A463W into various mammalian cell lines. After several trials, as Figure 28B illustrates, we finally observed inner plasma membrane localization. With agreement to our preceding results, cholesterol distribution in the cytosolic leaflet is also heterogeneous and most likely organizes itself into microdomains. NR3-D434A/A463W was also shown to quantify cholesterol concentration as a molecular sensor in the dynamic range from 15–40% cholesterol by ratiometric analysis (supplementary material Fig. S2; Fig. S3).

Since D4 domain comes from the family of pore-forming toxins, it may penetrate eukaryotic membranes. To preclude this possibility, we added NR3-D434A/A463W to the outer plasma membrane of HeLa cells and then incubated the mixture for 4 hours at

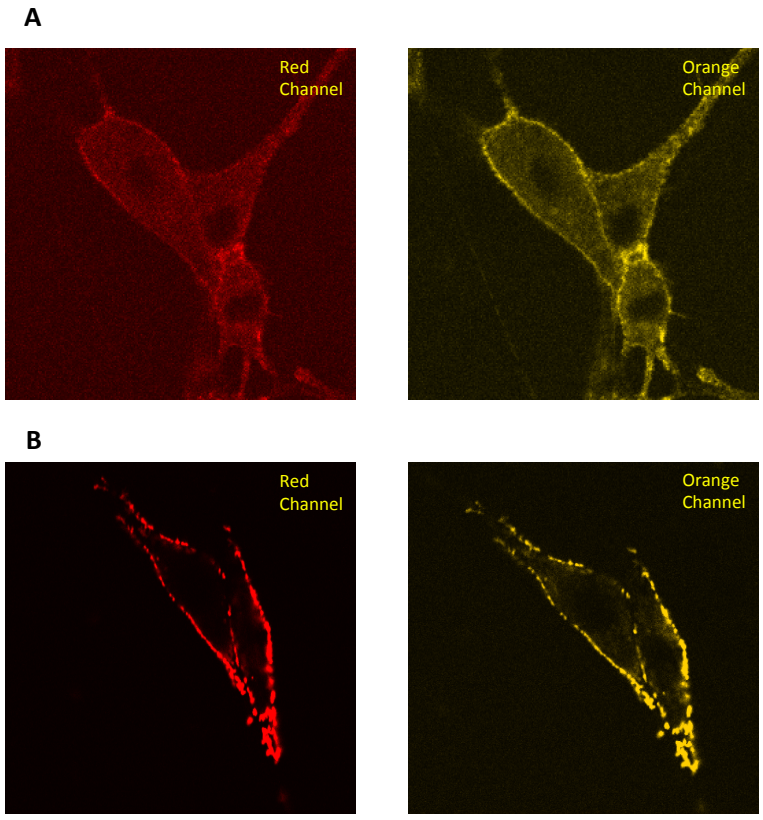

Figure 28. **NR3-D434A/A463W can detect cholesterol in both the cytosolic and the exofacial leaflet of the plasma membrane of NIH 3T3 cells.**
(A) Two-channel image of outer plasma membrane localization of media-added NR3-D434A/A463W sensor. **(B)** Two-channel image of a representative cell showing pronounced inner plasma membrane localization of the microinjected NR3-D434A/A463W sensor.

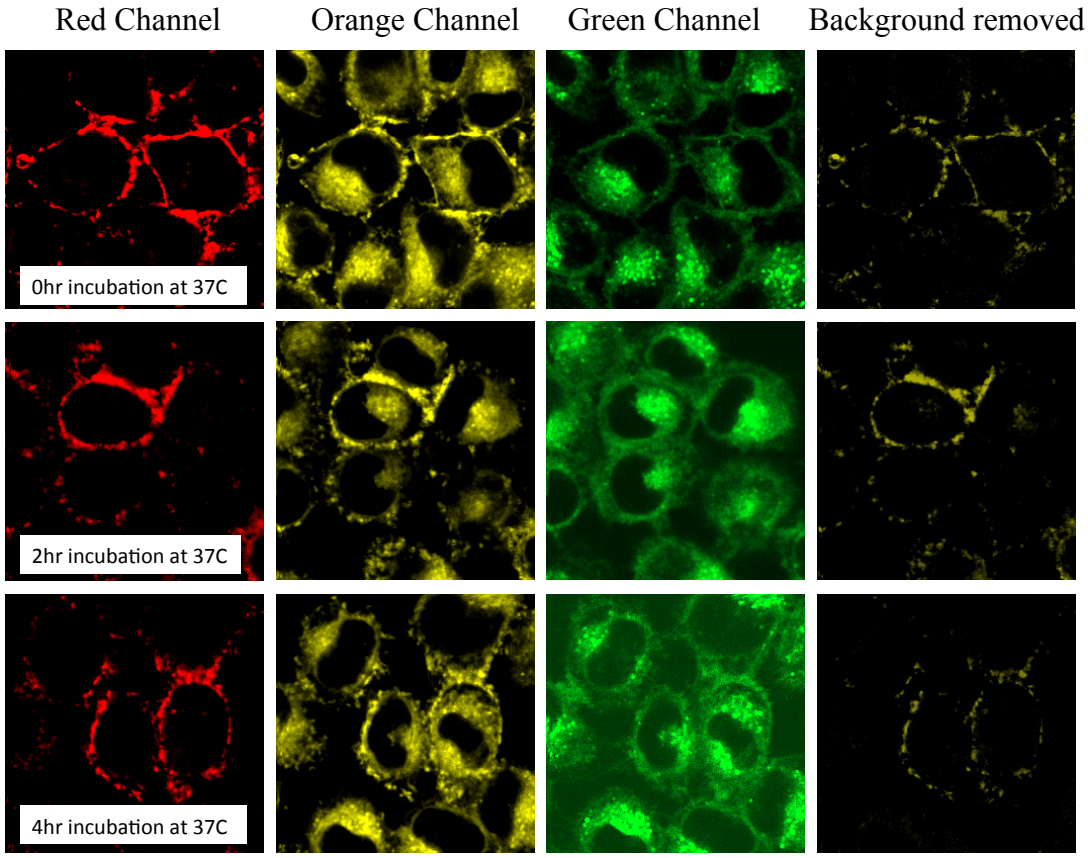

Figure 29. **Four-channel images of cholesterol in the outer plasma membrane monitored using media-added NR3 labeled D434A/A463W.**
It should be noted here that cells' autofluorescence bleeds through from the green to yellow channel and therefore is the source of "internalization" illusion. However, after background removal (yellow – green channel), it is clear that the probe localization is entirely restricted to the plasma membrane.

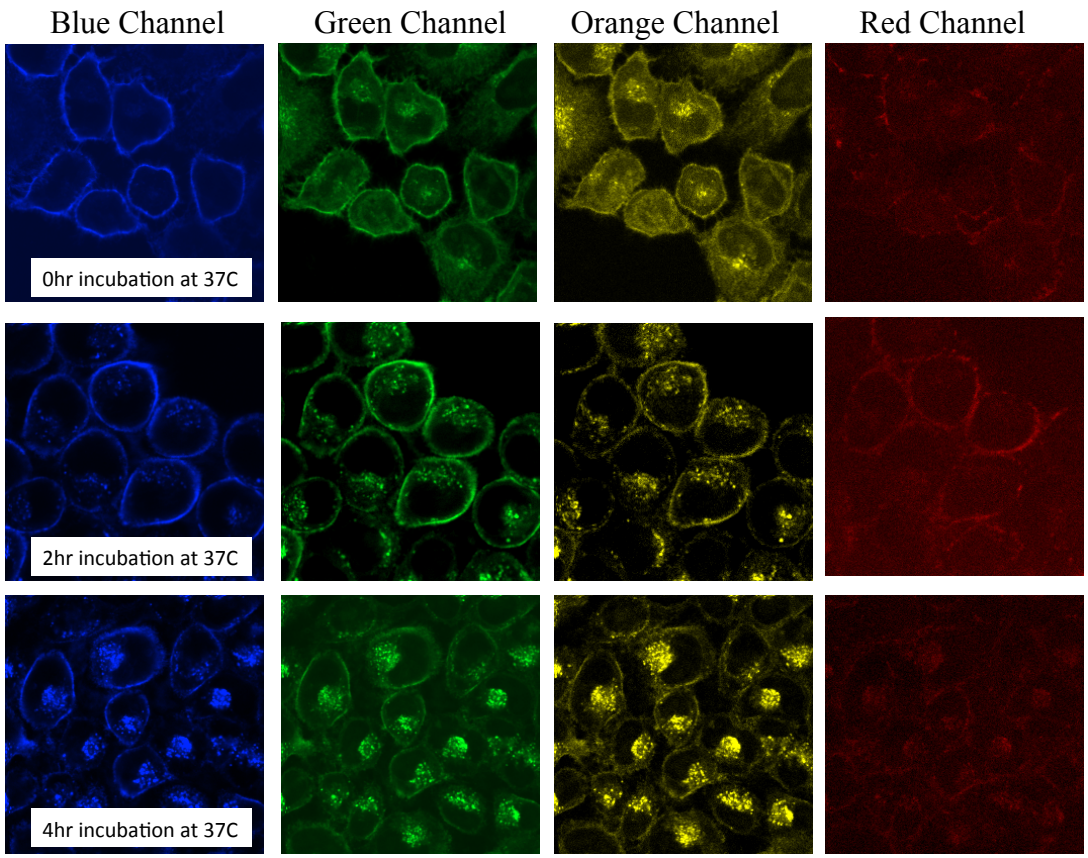

Figure 30. **Four-channel images of cholesterol in the outer plasma membrane monitored using media-added DAN-labeled D434A/A463W.** Sensor cannot be internalized by incubation.

37C. As seen in Figure 29, the sensor remained on the outer plasma membrane even after extended incubation period, proving that the probe cannot cross the cell membrane and lacks toxicity. It should be noted that cells' autofluorescence bleeds through from the green to yellow channel and therefore is the source of "internalization" illusion. However, after background removal, the probe localization is entirely restricted to the plasma membrane. In parallel, we found that DAN labeled D434A/A463W could not be internalized by incubation at 37°C (Figure 30). Taken together, DAN and NR3 labeled D4 can be used as an orthogonal cholesterol sensor for simultaneous dual-color imaging using our two-photon 4-channel microscope.

3.5. Cholesterol in the Inner and Outer Leaflets of Plasma Membrane

To perform simultaneous quantification of cholesterol in outer and inner plasma membrane, we labeled D434A/A463W/Y415A with NR3 and D434A with DAN. Both DAN-D434A and NR3- D434A/A463W/Y415A showed desired spectral properties upon association with LUVs in a concentration-dependent manner (Figure 31A,B). These favorable spectral changes of both sensors suggest that cholesterol concentration can be obtained by ratiometric analysis.

To calibrate DAN–D434A and NR3 D434A/A463W/Y415A for cellular cholesterol quantification, we equilibrated sensors with giant unilamellar vesicles and measured the fluorescence intensity by two-photon microscope with four channel detection. For this measurement purposes, 436 ± 10 and 525±25 band pass filters were employed for the blue channel and the green channel, respectively, whereas 600 ± 19 and 635 ± 20 band pass filters were used for the orange channel and the red channel, respectively. For DAN-D434A, blue channel fluorescence signals derive from membrane-bound sensors only

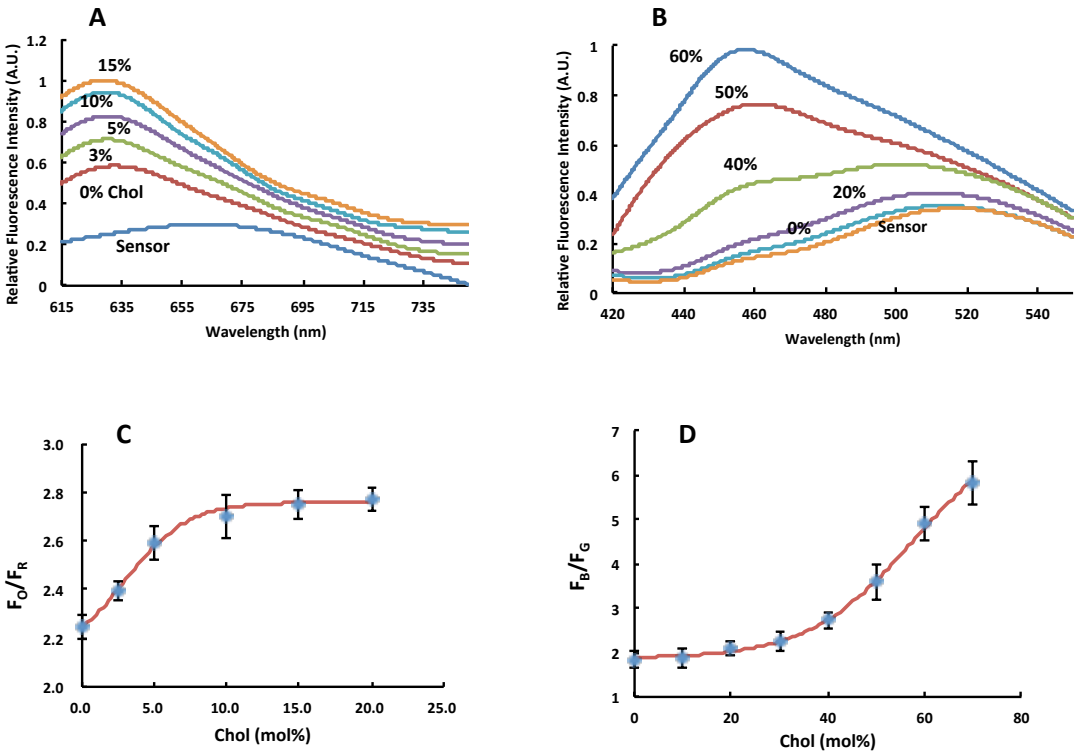

Figure 31. **Spectral properties and ratiometric calibration for cholesterol sensors.** **(A)** Fluorescence emission spectra of NR3-D434A/A463W/Y415A and **(B)** DAN-434A in the presence of phosphatidylcholine (PC)/PS/Cholesterol (80–x:20:x) large vesicles measured spectrofluorometrically. The excitation wavelength was 392 nm for DAN-D434A and 520 nm for NR3-D434A/A463W/Y415A. DAN exhibited a dramatic blue shift upon cholesterol binding whereas fluorescence emission spectra for NR3 are orange-shifted. **(C)** Ratiometric calibration curves of NR3 D434A/A463W/Y415A and **(D)** DAN-D434A for cholesterol quantification. The cholesterol sensors were monitored by a two-photon microscope in the presence of POPC/POPS/Cholesterol (80–x:20:x) LUVs. Nonlinear least-squares analysis of the plot using the equation (for DAN-D434A); $F_B/F_G=(F_B/F_G)$ max$/(1+K_d/[\text{cholesterol}])+C$ yields K_d, $(F_B/F_G)_{max}$, and C values and the calibration curves are constructed using these parameters. F_B, F_G, F_o, and FR indicate fluorescence intensities of the blue, green, orange, and red channels, respectively. K_d, $(F_B/F_G)_{max}$, and C are the equilibrium dissociation constant (in mole%), the maximal F_B/F_G value, and the arbitrary instrumental parameter. Error bars indicate standard deviations calculated from at least three independent sets of measurements. For all measurements buffer with 20 mm Tris buffer and 0.16m KCl adjusted to pH=7.4 was used.

whereas green channel signals are from both membrane- bound and sensors. Likewise, orange channel fluorescence signals derive from membrane-bound sensors only whereas red channel signals are from both membrane-bound and sensors for NR3-D434A/A463W/Y415A. The GUVs containing different mol% of cholesterol were added into the wells that contained DAN-D434A and NR-D434A/A463W/Y415A respectively, mixed well, and then the image data was collected by 10 times scan by two-photon microscope. The images were analyzed and the photon counts of each pixel were extracted by MATLAB software. The F_B (intensity at 430nm) and F_G (intensity at 520nm) of DAN-D434A and F_O (intensity at 600nm) and F_R (intensity at 630nm) of NR-D434A/A463W/Y415A on GUV membrane were converted to the photon counts of each pixel, and then they were plotted versus known mol% cholesterol. These two curves (Figure 31C,D) were used to quantify concentration of cholesterol on cytosolic and exofacial surface of plasma membrane.

After sensor calibration, we microinjected NR- D434A/A463W/Y415A into fibroblast cells and added DAN-D434A to the extracellular medium to quantitatively determine concentration of cholesterol live cells. Almost instantaneously, we observed distinctive signals from the outer and the inner PM (Figure 32), which were unambiguously distinguished by fluorescence analysis in a time-resolved manner. Our spatially resolved quantification revealed surprisingly low cholesterol concentration in the inner plasma membrane. We found that the inner leaflet of e.g. NIH 3T3 cells contains as little as 2.4% of cholesterol while the outer plasma membrane cholesterol content is 57.7%; but these percent's vary among different cell lines (Figure 33). In terms of integrative strategy, these cholesterol probes validate the usefulness of our fluorescent

A

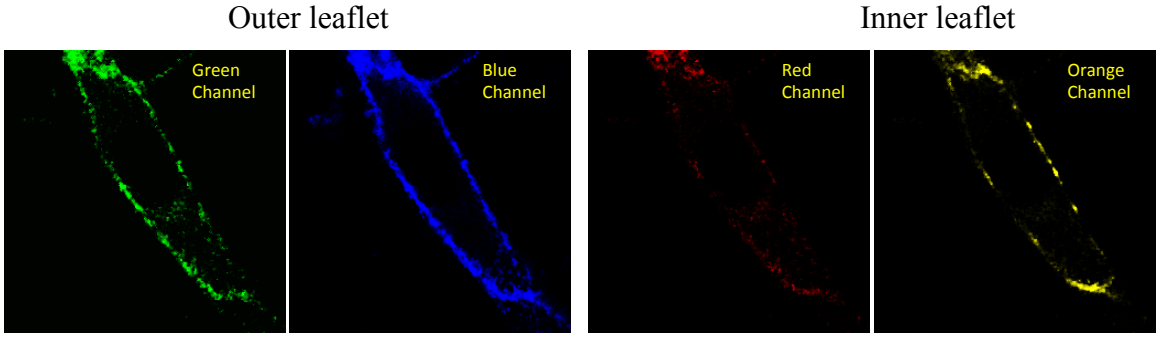

B

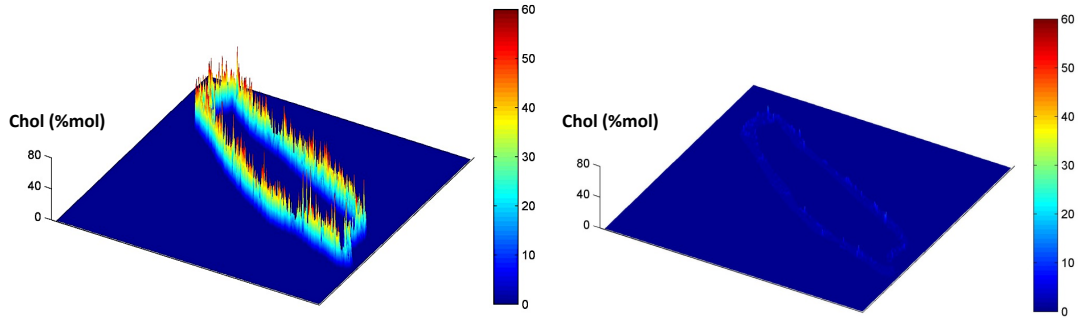

Outer leaflet = 57.7% cholesterol

Inner leaflet = 2.4% cholesterol

Figure 32. **Simultaneous in situ quantification of cholesterol in the inner and outer PM of NIH 3T3 cells.**
(A) Four-color images of cholesterol in the inner and outer plasma membrane monitored using microinjected NR3-D434A/A463W/Y415A (red and orange channels) and media-added DAN-D434A (green and blue channels) sensors, respectively. Membrane-bound sensors are monitored in blue and orange channels while membrane-bound plus free sensors in green and red channels. **(B)** Spatially resolved quantification of cholesterol in the plasma membrane by ratiometric analysis of F_B/F_G and F_O/F_R using the calibration curve in Figure 13. Pseudo-coloring is used for the images (red, highest concentration; blue, lowest). DAN-D434A and NR3-D434A/A463W were two-photon excited at 780 nm and 950 nm, respectively.

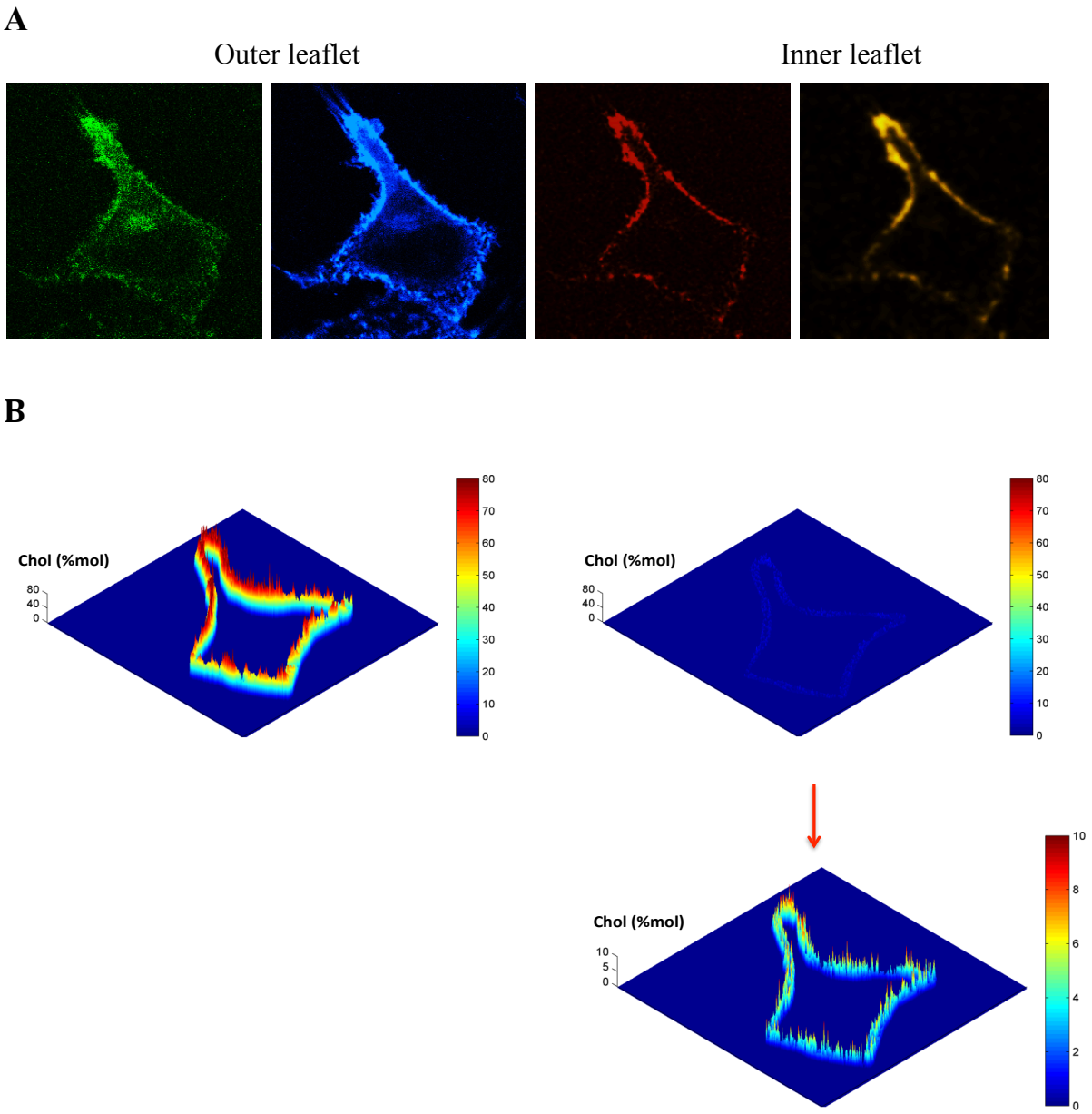

Figure 33. **Simultaneous in situ quantification of cholesterol in the inner and outer PM of Hela cells.**
(A) Four-channel images of cholesterol in the inner and outer PM monitored using microinjected NR3-D434A/A463W/Y415A (red and yellow channels) and media-added DAN-D434A (green and blue channels) sensors, respectively. Membrane-bound sensors are monitored in blue and orange channels whereas green and red channels show membrane-bound plus free sensors. **(B)** Measuring cholesterol concentration in spatially resolved manner. NR3-D434A/A463W/Y415A and DAN-D434A were quantified through ratiometric calibration shown in Figure 13.

lipid sensor technology affording greater flexibility in the excitation/emission wavelengths and evoke a reconceptualization on the cholesterol transbilayer distribution.

3.6. Monitoring cholesterol changes under patho-physiological conditions

Changes in the cholesterol concentration can be determined in the two PM leaflets after treatment with MβCD-cholesterol mixtures. Although not physiologically relevant, this measurement would allow us to test the feasibility of our sensor technology in *in situ* quantification of cholesterol changes, and also reveal how this popular treatment affects PM cholesterol distribution. The cholesterol dependence of D4 sensor binding to the cytosolic leaflet of the plasma membrane was confirmed by the use of methyl β-cyclodextrin (MβCD). We demonstrated in Figure 34C that the capacity for D4 binding could be enhanced if cells were enriched with cholesterol. When NR3-D434A/A46W/Y415A was microinjected to the cells previously treated with cholesterol-loaded MβCD, we observed enhancement of the signal, which indicates an increase in abundance of cholesterol in the inner leaflet. We also examined the consequences of cholesterol depletion; when cells were treated with MβCD, microinjected NR3-D434A/A46W/Y415A binding to inner plasma membrane was not observed (Figure 34B).

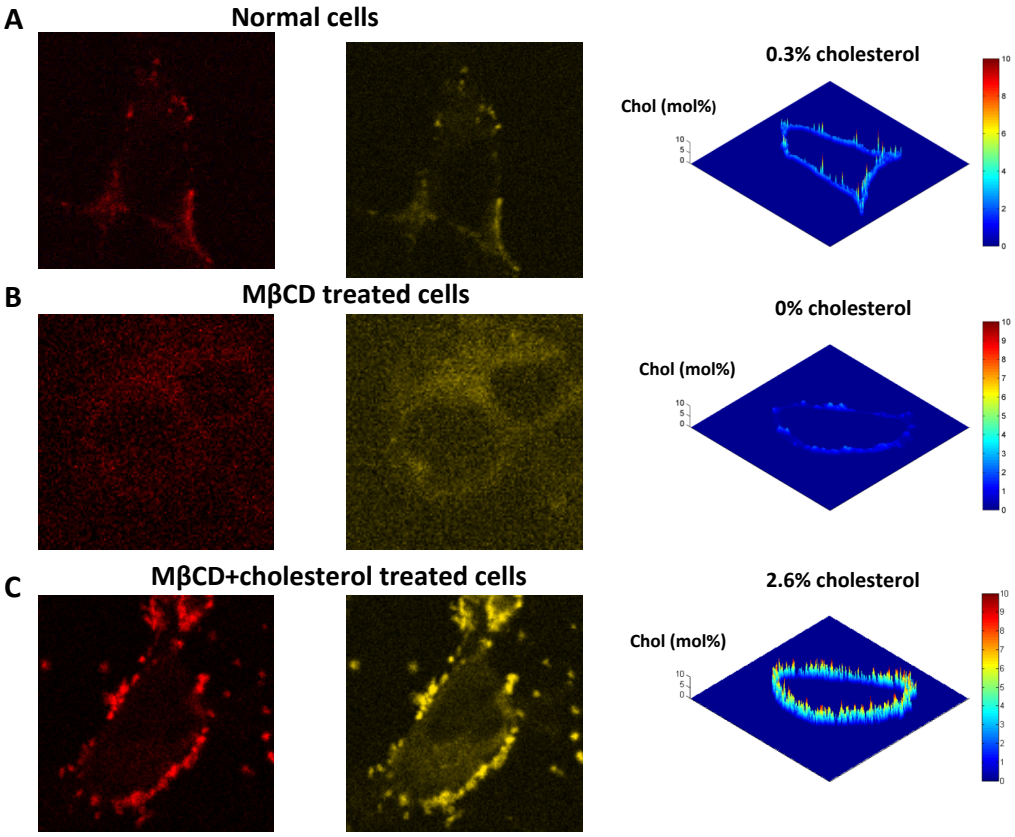

Figure 34. **The effect of methyl β-cyclodextrin (MβCD) treatment on the cholesterol dependence binding of NR3-D434A/A463W to the cytosolic leaflet of the plasma membrane.**
(A) Typical two-channel image showing inner plasma membrane cholesterol distribution after microinjection in normal HEK 293T cell. **(B)** In cholesterol-depleted cells from cholesterol, probe did not localize on the plasma membrane. **(C)** Addition of cholesterol by cholesterol–MβCD complex led to increased NR3-labeled probe signal intensity and the enhancement of signal in the inner plasma membrane.

3.7. Sphyngomielin is required to retain cholesterol in the outer leaflet of the plasma membrane

Our observations lead us to believe that cholesterol is organized in nanodomains. The umbrella and condensed complex models are two related hypotheses to explain the interactions between cholesterol and other lipids in the plane of the membrane. Essentially, owing to its small headgroup, cholesterol associates closely with lipids with large headgroups and primarily saturated acyl chains to maintain itself in a low-energy state [23,24]. Based on our microscopy results, we postulated that sphyngomielin (SM) would be the most likely candidate to interact with cholesterol in the exofacial leaflet of the plasma membrane. In addition, a reduction in sphyngomielin would potentially lead to enrichment of cholesterol in outer plasma membrane. To test this hypothesis, we made use of sphyngomielinase (SMase) that hydrolyses SM to ceramide. Treating HEK 293 cells with sphyngomielinase (SMase) causes relocalization of liberated cholesterol from the outer plasma membrane to the inner through an uncharacterized mechanism. As Figure 35 depicts, in cholesterol-replete cells, NR3-D4 binding to the inner leaflet was abounded, and SMase treatment increased inner membrane cholesterol content from 0.3% to 1.3%. Our results indicate that, in the absence of SM, the outer leaflet of the plasma membrane has less ability to retain cholesterol with high chemical activity, which consequently, due to its elevated mobility translocate or “flips” to the inner membrane. This phenomenon is facilitated by ceramides, which displace cholesterol from phospholipid complexes. Worth to note that this coincident localization of sphyngomielin with cholesterol have confirmed the existence of nanoscale liquid-ordered microdomains predicted by the raft hypothesis [67].

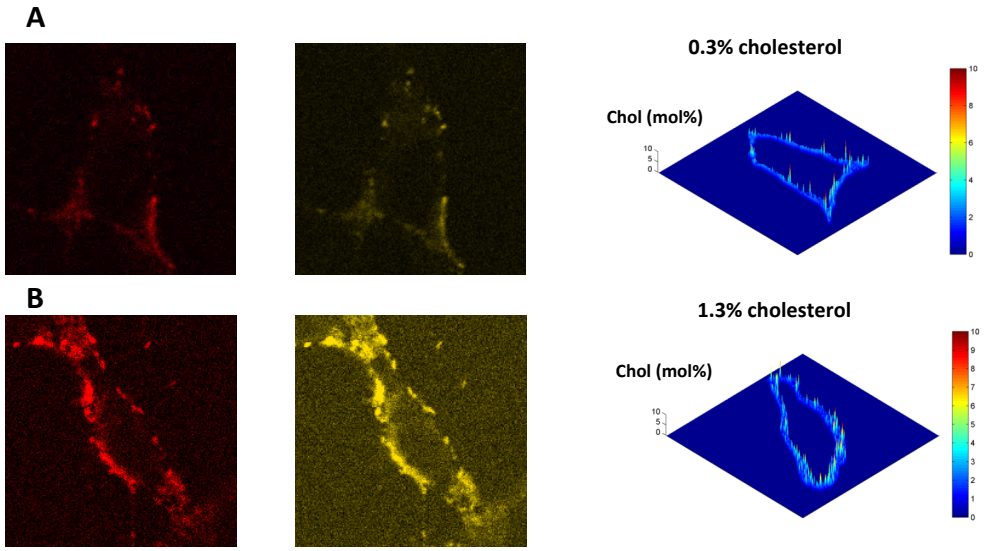

Figure 35. Effect of sphyngomielinase (SMase) treatment on cholesterol distribution in the cytosolic leaflet of plasma membrane in HEK 293T cells.
(A) Typical two-channel image showing inner plasma membrane cholesterol distribution in normal HEK 293T cell. **(B)** HEK 293T treated with SMase displayed elevated cholesterol content in the inner plasma membrane.

Having demonstrated the presence of dynamic cholesterol-rich membrane microdomains that incorporate lipids with saturated acyl chains (lipid-lipid interaction), we next want to determine cholesterol-protein interactions and their involvement in formation of raft domains. For these experiments, we decided to choose caveolin-1 and follotin-1, membrane nanodomain-associated proteins that have been implicated in endocytosis and signaling [68,69]. They both localize to the plasma membrane in a cholesterol-dependent manner through scaffolding region that induces the assembly of plasma membrane domains enriched in cholesterol and sphyngomielin [68,69]. We aim to test whether the local cholesterol concentration in the inner plasma membrane changes significantly in response to altered cholesterol distribution produced by disruption of nanodomain-associated proteins.

4. DISCUSSION

Our ultimate goal was to acquire and validate a pair of probes that allow profound cholesterol quantification with spatial and temporal resolution under physiological and patho-physiological conditions in the living cells. The specific and sensitive cholesterol quantification was achieved by engineered sensor derived from the D4 domain of perfringolysin O toxin and favorable spectral and membrane-binding properties of DAN and Nile Red 3 probes. This probe offers advantages over the e.g. canonical cholesterol stain, filipin, which is typically used with fixed cells to stain cholesterol in cellular membranes, regardless of its transbilayer distribution [54]. First, D4 has an adaptable fluorescent property that makes the incorporation of variety of fluorescent dyes with distinctive fluorescence spectra comparable easy. Second, D4 probe is suitable for live-cell imaging. In this regard, microinjected or media-added D4 proved to be adequate for examination of the dynamics and organization of cholesterol in the exofacial and cytosolic leaflet of the plasma membrane simultaneously due to its low permeability. Finally, molecular structure of D4 domain is very different from other sterol-binding molecules, suggesting the existence of unique molecular modes of action.

High sensitivity of our sensor allowed accurate ratiometric cholesterol quantification in the inner and outer plasma membrane in various living cells. Our investigation revealed that cholesterol distributes asymmetrically between the two leaflets with 2.4% and 57.7% of the total cholesterol in the inner and outer leaflet of NIH 3T3 cells, respectively (Figure 32). To validate the effectiveness of the D4 probe in measuring such a low cholesterol concentration in the cytofacial plasma membrane, we used methyl β-cyclodextrin (MβCD) treatment to increase or decrease levels of cholesterol. We

demonstrated that the capacity for NR3-D4 binding could be enhanced if cells were loaded with cholesterol or completely abolished when cholesterol was depleted from the plasma membrane (Figure 34). Collectively, our data revealed that D4 probe could serve as a cholesterol sensor to monitor the distribution of cholesterol in the outer plasma membrane.

Based on our microscopic observations cholesterol is also asymmetrically distributed in the plane of the bilayer, forming patches with slightly increased or decreased cholesterol densities. Formation of lower/higher density cholesterol regions is more prominent in the inner plasma membrane as shown by our sensor injection that had punctate pattern. Furthermore, our in vivo studies revealed that binding affinity of the D4 to cholesterol that resides in the inner plasma membrane is influenced by its local environment (e.g.neighboring phospholipids and proteins). These findings led us to consider an alternative hypothesis that the chemical activity of cholesterol in the inner leaflet of the plasma membrane is altered and, as a result, less accessible to the D4 probe. Our, SMase data (Figure 35) suggested that the removal of sphingomyelin increased the chemical activity of cholesterol and made more accessible to the probe in the inner plasma membrane. Notably, we believe this evidence indicate that, the inner leaflet of the plasma membrane has higher ability to retain cholesterol and that the levels of available cholesterol dip below the minimal threshold required for detection by the D4 probe. Moreover, recent evidence suggests that cholesterol might act as an allosteric regulator for many proteins embedded in membrane, ion channels and scaffolding proteins, which will likely influence the amount of freely accessible cholesterol [70-72]. Additionally, the presence of soluble carriers of cholesterol, such as the steroidogenic acute regulatory-

related lipidtransfer (START) proteins and oxysterol-binding protein (OSBP)-related protein (ORP) family suggest that the concerted actions of these types of proteins might help to regulate the co-segregation of cholesterol [73-75]. As presented, despite the advantages of our D4 probe, it does have the same limitation that applies to all of these types of biosensors, in that they only have access to available "free" cholesterol.

Cholesterol has various physiological functions in cell signaling and vesicular trafficking, as well as in pathophysiological states such as atherosclerosis and Alzheimer's disease [38,48,76,77]. However, it is currently unclear to what extent cytosolic leaflet cholesterol is involved in these processes. Clearly, understanding the organization of the plasma membrane is required to understand proteins and signaling hubs that reside here. The existence of lipid rafts or nanodomains in the exofacial leaflet of the plasma membrane remains remains controversial, although electron and super-resolution microscopy has revealed lipid clusters [78,79]. Our results suggest that a number of the same organizing principles exist for the cytosolic leaflet cholesterol as well. Thus, it is possible that they influence the trafficking of other lipids or their retention in a given organelle. We hypothesize that segregation of PtdSer and cholesterol in the cytosolic leaflet of organelles could generate nanoscale enrichments of anionic charge that in turn could be recognized by sorting or vesiculating machinery. To examine the presence of the nanodomains of PtdSer and cholesterol in the cytosolic leaflets of the plasma membrane, cluster analysis will be required using high-resolution electron microscopy or super-resolution light microscopy with the Lact-C2 (PS sensor) and D4 probes.

Plasma membrane cholesterol level is tightly controlled by complex cellular homeostatic mechanisms. Varieties of membrane and cytosolic proteins are also believed to be involved in redistribution and re-organization of cholesterol in the plasma membrane. Therefore, deciphering how translocators and exporters move cholesterol molecules across membranes on molecular level is crucial step in understanding of how cholesterol asymmetry is generated, maintained, and disrupted in cellular plasma membranes. The large family of plasma membrane ABC transporters facilitates cholesterol export from the cell to diverse acceptors. The ABC transporters: ABCA1 and ABCG1 are believed to be major determinants of cholesterol level in plasma membrane [43-45]. But how these pump proteins drive the transfer of cholesterol to extracellular acceptors? This topic became an ultimate goal of our investigation. Our recent studies established that ABCA1 and ABCG1 synergistically facilitate movement of cholesterol from the inner to the outer plasma membrane. Knockdown of both ABCA1 and ABCG1 in HEK293 cells led to dramatic increase in cholesterol deposition in the inner plasma membrane, proving that ABC transporters induce changes in membrane cholesterol distribution. Nevertheless, there are many other possibilities on what causes the cholesterol level changes in both layers of plasma membrane but we feel that it is premature at present and beyond the scope of this investigation to at least partially untangle the mechanism of intracellular cholesterol trafficking. As we learn more about the cholesterol dynamics in the plasma membrane through our investigations and as more information about the intracellular cholesterol trafficking is available, we will be in a better position to address the mechanistic questions.

In this study, we presented recent advances in the development, incorporation, and application of our innovative cholesterol sensor technology. Our technique allows simultaneous in situ quantification of plasma membrane cholesterol in the context of living systems in a spatiotemporally resolved manner. This simultaneous quantification of cholesterol provides valuable information regarding physiological importance of this signaling lipid in membrane biology that was unachievable by conventional methodologies. Collectively, it represents an important technical advance toward understanding of complex cholesterol-mediated cell regulation and hereby, helps to develop new and more efficient strategies to diagnose, treat, and prevent human diseases caused by dysfunctional cholesterol-dependent cell function and regulation.

5. CITED LITERATURES

1. Quinn PJ (2012) Lipid-lipid interactions in bilayer membranes: Married couples and casual liaisons.Progress Lipid Res 51: 179–198.

2. Lingwood D, Simons K (2010) Lipid rafts as a membrane-organizing principle. Science 327: 46-50.

3. van Meer G, Voelker DR, Feigenson GW (2008) Membrane lipids: where they are and how they behave.Nature Rev Mol Cell Biol 9: 112–124.

4. van Meer G, de Kroon AIPM (2011) Lipid map of the mammalian cell. J Cell Sci 124: 5–8.

5. Coskun U, Simons K (2011) Cell membranes: the lipid perspective. Structure: 1543–1548.

6. Shevchenko A, Simons K (2010) Lipidomics: coming to grips with lipid diversity. Nature Rev Molec Cell Biol 11: 593–598.

7. Kiessling V, Wan C, Tamm LK (2009) Domain coupling in asymmetric lipid bilayers. Biochim Biophys Acta 1788:64–71.

8. Daleke DL (2003) Regulation of transbilayer plasma membrane phospholipid asymmetry. J Lipid Res. 44: 233–242.

9. Sprong H, van der Sluijs P, van Meer G (2001) How proteins move lipids and lipids move proteins. Nat Rev Mol Cell Biol. 2: 504–513.

10. Fadeel B, Xue D (2009) The ins and outs of phospholipid asymmetry in the plasma membrane: roles in health and disease. Critical reviews in biochemistry and molecular biology 44(5): 264-277.

11. Yeagle PL (1985) Cholesterol and cell membrane. Biochim Biophys Acta 822: 267-287.

12. McConnell HM, Vrljic M (2003) Liquid-liquid immiscibility in membranes. Annu Rev Biophys Biomol Struct. 32:469–492.

13.Veatch SL, Keller SL (2003) A closer look at the canonical 'Raft Mixture' in model membrane studies. Biophys. J. 84:725–726.

14. Chiang YW, Zhao J, Wu J, Shimoyama Y, Freed JH, Feigenson GW (2005) New method for determining tie-lines in coexisting membrane phases using spin-label ESR. Biochim. Biophys. Acta 1668:99–105.

15. Steck TL, Ye J, Lange Y (2002) Probing red cell membrane cholesterol movement with cyclodextrin.Biophys. J. 83: 2118–2125.

16. Simons K and Ikonen E (1997) Functional rafts in cell membranes. Nature 387:569–572.

17. McConnell HM and Radhakrishnan A (2003) Condensed complexes of cholesterol and phospholipids. Biochim. Biophys. Acta 1610: 159–173.

18. Schroeder F, Nemecz G, Wood WG, Joiner C, Morrot G, Ayraut-Jarrier M and Devaux PF (1991) Transmembrane distribution of sterol in the human erythrocyte. Biochim. Biophys. Acta 1066: 183–192.

19. van Meer G (2005) Cellular lipidomics. EMBO J. 24: 3159–3165.

20. Bloom M, Evans E, Mouritsen OG (1991) Physical properties of the fluid lipid-bilayer component of cell membranes: a perspective Q. Rev. Biophys. 24: 293–397.

21. Subczynski WK, Wisniewska A, Yin J-J, Hyde JS, Kusumi A (1994) Hydrophobic barriers of lipid bilayer membranes formed by reduction of water penetration by alkyl chain unsaturation and cholesterol. Biochemistry 33: 7670–7681.

22. Mouritsen OG, Jørgensen K (1994) Dynamical order and disorder in lipid bilayers Chem. Phys. Lipids 73: 2–35.

23. Huang J, Feigenson GW (1999) A microscopic interaction model of maximum solubility of cholesterol in lipid bilayers. Biophys. J. 76: 2142–2157.

24. McConnell HM, Radhakrishnan A, (2003) Condensed complexes of cholesterol and phospholipids. Biochim. Biophys. Acta 1610: 159–173.

25. Mesmin B, Maxfield FR (2009) Intracellular Sterol Dynamics. Biochimica et biophysica acta 1791(7): 636-645.

26. Bielska AA. Schlesinger P, Ory DS (2012) Oxysterols as non-genomic regulators of cholesterol homeostasis. *Trends Endocrinol. Metab*. 23: 99–106.

27. Ali MR, Cheng KH, Huang J (2007) Assess the nature of cholesterol-lipid interactions through the chemical potential of cholesterol in phosphatidylcholine bilayers. Proc Natl Acad Sci U S A 104:5372–5377.

28. McConnell HM, Radhakrishnan A (2003) Condensed complexes of cholesterol and phospholipids. Biochim Biophys Acta. 1610: 159–173.

29. Lange Y, Steck TL (2008) Cholesterol homeostasis and the escape tendency (activity) of plasma membrane cholesterol. Prog Lipid Res. 47:319–332.

30. Radhakrishnan A, Goldstein JL, McDonald JG, Brown MS (2008) Switch-like control of SREBP-2 transport triggered by small changes in ER cholesterol: a delicate balance. Cell Metabolism 8:512–521.

31. Goldstein JL, DeBose-Boyd RA, Brown MS (2006) Protein sensors for membrane sterols. Cell 124:35–46.

32. Brown MS, Goldstein JL (1986) A receptor-mediated pathway for cholesterol homeostasis. Science 232:34–47.

33. DeBose-Boyd RA (2008) Feedback regulation of cholesterol synthesis: sterol-accelerated ubiquitination and degradation of HMG CoA reductase. Cell Res.18:609–621.

34. Zelcer N, Hong C, Boyadjian R, Tontonoz P (2009) LXR Regulates Cholesterol Uptake Through Idol-Dependent Ubiquitination of the LDL Receptor. Science 325:100–104.

35. Sun L-P, Seemann J, Brown MS, Goldstein JL (2007) Sterol-regulated transport of SREBPs from endoplasmicreticulum to Golgi: Insig renders sorting signal in SCAP inaccessible to COPII proteins. Proceedings of the National Academy of Sciences of the United States of America 104:6519–6526.

36. Brown MS, Goldstein JL (1997) The SREBP pathway: regulation of cholesterol metabolism by proteolysis of a membrane-bound transcription factor. Cell 89:331–340.

37. 2. Ikonen E (2008) Cellular cholesterol trafficking and compartmentalization. Nat Rev Mol Cell Biol. 9: 125–138.

38. Maxfield FR, Tabas I (2005) Role of cholesterol and lipid organization in disease. Nature 438:612–621.

39. Vance JE (2006) Lipid imbalance in the neurological disorder, Niemann-Pick C disease. FEBS Lett. 580:5518–5524.

40. Mukherjee S, Maxfield FR (2004) Lipid and cholesterol trafficking in NPC. Biochim Biophys Acta 1685:28–37.

41. Burns MP, Rebeck GW (2010) Intracellular cholesterol homeostasis and amyloid precursor protein processing.Biochim. Biophys. Acta1801, 853–859.

42. DeGrella RF, Simoni RD (1982) Intracellular transport of cholesterol to the plasma membrane. J. Biol. Chem. 257:14256–14262.

43. Bojanic DD, Tarr PT, Gale GD, Smith DJ, Bok D, Chen B, Nusinowitz S, Lovgren-Sandblom A, Bjorkhem I, Edwards PA (2010) Differential expression and function of ABCG1 and ABCG4 during development and aging. J. Lipid Res. 51:169–181.

44. Burns MP, Vardanian L, Pajoohesh-Ganji A, Wang L, Cooper M, Harris DC, Duff K, Rebeck GW (2006) The effects of ABCA1 on cholesterol efflux and Abeta levels in vitro and in vivo. J. Neurochem. 98:792–800.

45. Wang N, Lan D, Chen W, Matsuura F, Tall AR (2004) ATP-binding cassette transporters G1 and G4 mediate cellular cholesterol efflux to high-density lipoproteins. Proc. Natl. Acad. Sci. U. S. A. 101:9774–9779.

46. Vaughan AM, Oram JF (2005) ABCG1 redistributes cell cholesterol to domains removable by high density lipoprotein but not by lipid-depleted apolipoproteins. J. Biol. Chem. 280:30150–30157.

47. Tabas, I. (2005) Consequences and therapeutic implications of macrophage apoptosis in atherosclerosis: The importance of lesion stage and phagocytic efficiency. Arterioscler. Thromb. Vasc. Biol. 25: 2255−2264.

48. Puglielli, L., Tanzi, R. E., and Kovacs, D. M. (2003) Alzheimer's disease: The cholesterol connection. Nat. Neurosci. 6: 345−351.

49. Prinz WA (2007) Non-vesicular sterol transport in cells. Prog Lipid Res. 46:297–314.

50. Yancey PG, Bortnick AE, Kellner-Weibel G, de la Llera-Moya M, Phillips MC, Rothblat GH (2003) Importance of Different Pathways of Cellular Cholesterol Efflux. Arterioscler Thromb Vasc Biol. 23:712–719.

51. Baumann NA, Sullivan DP, Ohvo-Rekilä H, Simonot C, Pottekat A, Klaassen Z, Beh CT, Menon AK (2005) Transport of newly synthesized sterol to the sterol-enriched plasma membrane occurs via nonvesicular equilibration. Biochemistry. 44:5816–5826.

52. Clark BJ (2012) The mammalian START domain protein family in lipid transport in health and disease. J Endocrinol. 212(3): 257-75.

53. Lange Y (1992) Tracking cell cholesterol with cholesterol oxidase. J Lipid Res 33(3): 315–321.

54. Gimpl G, Gehrig-Burger K (2011) Probes for studying cholesterol binding and cell biology. Steroids 76(3):216–231.

55. Yoon Y, Lee P, Kurilova S, Cho W (2011) In situ quantitative imaging of cellular lipids using molecular sensors. Nat Chem 3:868-874.

56. Tweten RK (2005) Cholesterol-dependent cytolysins, a family of versatile pore-forming toxins. Infect Immun. 73:6199–6209.

57. Czajkowsky DM, Hotze EM, Shao Z, Tweten RK (2004) Vertical collapse of a cytolysin prepore moves its transmembrane beta-hairpins to the membrane. EMBO J. 23: 3206–3215.

58. Dowd KJ, Tweten RK (2012) The Cholesterol-Dependent Cytolysin Signature Motif: A Critical Element in the Allosteric Pathway that Couples Membrane Binding to Pore Assembly. Koehler TM, ed. PLoS Pathogens. 8(7):e1002787.

59. Heuck AP, Moe PC, Johnson BB (2010) The cholesterol-dependent cytolysin family of gram-positive bacterial toxins. Subcell Biochem. 51:551-77.

60. Ramachandran R, Heuck AP, Tweten RK, Johnson AE (2002) Structural insights into the membrane-anchoring mechanism of a cholesterol-dependent cytolysin. Nat Struct Biol 9: 823–827.

61. Heuck AP, Hotze E, Tweten RK, Johnson AE (2000) Mechanism of membrane insertion of a multimeric b-barrel protein: Perfringolysin O creates a pore using ordered and coupled conformational changes. Molec Cell 6: 1233–1242.

62. Farrand A J, LaChapelle S, Hotze EM, Johnson AE, Tweten RK (2010) Only two amino acids are essential for cytolytic toxin recognition of cholesterol at the membrane surface. Proc. Natl. Acad. Sci. U.S.A. 107, 4341−4346.

63. Weber G, Farris FJ (1979) Synthesis and spectral properties of a hydrophobic fluorescent probe: 6-propionyl-2-(dimethylamino)naphthalene. Biochemistry 18(14): 3075–3078.

64. Cho W, Stahelin RV (2005) Membrane-protein interactions in cell signaling and membrane trafficking. Annu Rev Biophys Biomol Struct. 34: 119-151.

65. Liu S, Sheng R, O'Connor MJ, Cui Y, Yoon Y, Kurilova S, Lee D, Cho W (2014) Simultaneous In Situ Quantification of Two Cellular Lipid Pools Using Orthogonal Fluorescent Sensors. Angew Chem Int Ed Engl. 53(52):14387-91.

66. Black SL, Stanley W, Filipp,FV, Bhairo M, Verma A, Wichmann O, Sattler M, Wilmanns M, Schultz C (2008) Probing lipid- and drug-binding domains with fluorescent dyes. Bioorg. Med. Chem. 16: 1162−1173.

67. Hancock JF (2006) Lipid rafts: contentious only from simplistic standpoint. Nature Rev. Mol. Cell Bio. 7: 456-462.

68. Wanaski SP, Ng BK, Glaser M (2003) Caveolin scaffolding region and the membrane binding region of SRC form lateral membrane domains. Biochemistry 42: 42-56.

69. Liu J, Deyoung SM, Zhang M, Dold LH, Saltiel AR (2005). The stomatin/prohibitin/flotillin/HflK/C domain of flotillin-1 contains distinct sequences that direct plasma membrane localization and protein interactions in 3T3-L1 adipocytes. J. Biol. Chem. 280, 16125–16134.

70. Levitan I, Singh DK, Rosenhouse-Dantsker A (2014) Cholesterol binding to ion channels. Front. Physiol. 5: 65.

71. Sheng R, Kim H, Lee H, Xin Y, Chen Y, Tian W, Cui Y, Choi JC, Doh J, Han JK, Cho W (2014) Cholesterol selectively activates canonical Wnt signalling over non-canonical Wnt signalling. Nat. Commun. 5: 4393.

72. Sheng R, Chen Y, Gee HY, Stec E, Melowic HR, Blatner NR, Tun MP, Kim Y, Kallberg, M, Fujiwara T, Hong JH, Kim KP, Lu H, Kusumi A, Lee MG, Cho W (2012) Cholesterol Modulates Cell Signaling and Protein Networking by Specifically Interacting with PDZ Domain-Containing Scaffolding Proteins. Nature Communications. 3: 1249.

73. Maeda K, Anand K, Chiapparino A, Kumar A, Poletto M, Kaksonen M, Gavin, AC (2013). Interactome map uncovers phosphatidylserine transport by oxysterol-binding proteins. Nature 501: 257-261.

74. Mesmin B, Pipalia NH, Lund FW, Ramlall, TF, Sokolov A, Eliezer D, Maxfield FR (2011). STARD4 abundance regulates sterol transport and sensing. Mol. Biol. Cell 22: 4004-4015.

75. Olkkonen VM, Li S (2013). Oxysterol-binding proteins: sterol and phosphoinositide sensors coordinating transport, signaling and metabolism. Prog. Lipid Res. 52: 529-538.

76. Simons K, Toomre D. (2000). Lipid rafts and signal transduction. Nat. Rev. Mol. Cell Biol. 1: 31-39.

77. Simons K, Ehehalt R (2002). Cholesterol, lipid rafts, and disease. J. Clin. Invest. 110: 597-603.

78. Mizuno H, Abe M, Dedecker P, Makino A, Rocha S. Ohno-Iwashita, Y, Hofkens J, Kobayashi T, Miyawaki A(2011). Fluorescent probes for superresolution imaging lipid domains on the plasma membrane. Chem. Sci. 2: 1548-1553.

79. Zhou Y, Liang H, Rodkey T, Ariotti N, Parton RG, Hancock JF (2014). Signal integration by lipid-mediated spatial cross talk between Ras nanoclusters. Mol. Cell. Biol. 34: 862-876.

SUPPLEMENTERY MATERIALS

Table S1. Mouse PDZ domains with the CRAC Motif[a] [28]

No.	Protein Name	Residue Number	Sequence	K_d(nM)[b] for PM[c]
1	BC034090 - PDZ1	33-45	LDTAKLYSGLLR	
2	Card14 - PDZ1	35-42 63-73	VDYKPTK VNGSCYLSVK	
3	Cnksr2 - PDZ1	11-17	LGMYIK	
4	Cnksr3 - PDZ1	11-17	LGMYIK	
5	Dlg1 - PDZ1	78-84	VRLYVK	
6	Dlg2 - PDZ2	77-82	VVYLK	
7	Dlg4 - PDZ2	71-82	LKNTYDVVYLK	
8	Dlg5 - PDZ4	44-55 58-68	LILEYGSLDMR VEDVYVEMLK	
9	Gipc1 - PDZ1	52-63	LLGCRHYEVAR	
10	Gipc2 - PDZ1	18-26	VGYAFIKR	
11	Gipc3 - PDZ1	53-63	VGCRHYEVAK	
12	Gorasp2 - PDZ	61-70	VKMLIYSSK	
13	Grid2ip - PDZ	1-9	VRVYKGNK	
14	Grip1 - PDZ1	41-49	LDVGDYIK	
15	Grip1 - PDZ4	19-31 37-46	LLEKGVYVKNIR VGGLKPYDR	
16	Grip1 - PDZ7	19-31 37-46	LLEKGVYVKNIR VGGLKPYDR	
17	Htra1 - PDZ1	6-16	VTKKKYIGIR	
18	Inadl - PDZ4	2-8 53-65	LQKYSK VNGMQLYGKSRR	
19	Lnx1 - PDZ1	239-246	VPHNYAVRLLR	960 ± 120
20	Lnx1 - PDZ4	15-26 33-46	VGGYEEYSGNK VEGTPAYNDGRIR	180 ± 40
21	Lnx2 - PDZ1	33-46	VLGTPAYYDGRLK	670±100
22	Lnx2 - PDZ4	33-46	VLGTPAYYDGRLK	
23	Magi2 - PDZ1	34-42	VAYESGSK	NM[d]
24	Magi3 – PDZ5	1042-1051 1141-1146	LGCYPVELER LCSYVK	610±190
25	Mast4 - PDZ1	37-48	VVSMYCSFETR	
26	Mllt4 - PDZ1	25-35	LGIYVKSVVK	
27	Mpdz - PDZ12	24-30	LPIYVK	
28	Mpp4 - PDZ1	38-45	LLYAGDK	
29	NHERF1-PDZ1	35-40	LCQYIR	48±9
30	Pard6a - PDZ1	11-17	LGFYIR	
31	Pard6b - PDZ1	1-9 11-17	VRLCKYGTEK LGFYIR	
32	Pdzd3 - PDZ1	60-67	VVVRYIR	
33	Pdzd3 - PDZ2	56-68	VEKLTYNQLNRK	
34	Pdzd9 - PDZ1	54-61	VLGYTLR	
35	Pdzk1 - PDZ2	6-12	LCYLVK	
36	Pdzk1 - PDZ4	52-64	VQEEPYDRVVER	
37	Pdzk2 - PDZ2	211-218	LTYNQLNR	320±32
38	Prex2 - PDZ2	61-73	VTACRKYKRPMK	
39	Ptpn4 - PDZ1	14-22	VKGGYDQK	

40	Ptpn13 - PDZ1	21-30	VRHGGIYVK	
41	PSD95 PDZ2	238-242	VVYLK	930±120
42	PSD95 PDZ3	436-441	LFD**Y**D**K**	390±30
43	Radil - PDZ1	57-65	LRGVSYMR	
44	SAP97-PDZ3	588-593	LFD**Y**D**K**	620±70
45	SAP102-PDZ3	527-532	LFD**Y**D**R**	140±5
46	Shank3 - PDZ1	12-24	LTSHSDYVIDDK	
47	Shroom3 - PDZ1	68-78	LVKGSYKTLR	
48	Snx27 - PDZ1	3-15	VKSESGYGFNVR	
49	Synpo2 - PDZ1	57-65	LTYPEVIK	
50	α-syntrophin PDZ	158-164	LEVK**Y**M**K**	860±70
51	β1-syntrophin PDZ1	188-194 245-252	LEVK**Y**M**R** LKMCYVTR	1440±180
52	β2-syntrophin PDZ1	200-205	VTP**Y**I**K**	320±80
53	γ2-syntrophin PDZ	152-156	VE**Y**L**R**	530±140
54	Tamalin-PDZ1	183-192 196-204	LETL**Y**GTSI**R** LEARLQ**Y**L**K**	90±8
55	Tiam2 - PDZ1	18-31	LPDSLAYGGGLRK	
56	Tjp2 - PDZ3	62-71	VLYLLEIPK	

[a]L/V-(X)(1–5)-Y-(X)(1–5)-R/K-, in which (X)(1–5) represents between one and five residues of any amino acid

[b]Mean ± S.D. values determined by equilibrium SPR analysis

[c]PM-mimetic vesicles = POPC/POPE/POPS/PI/cholesterol/PtdIns(4,5)P2 (12:35:22:8:22:1)

[d]NM, not measurable

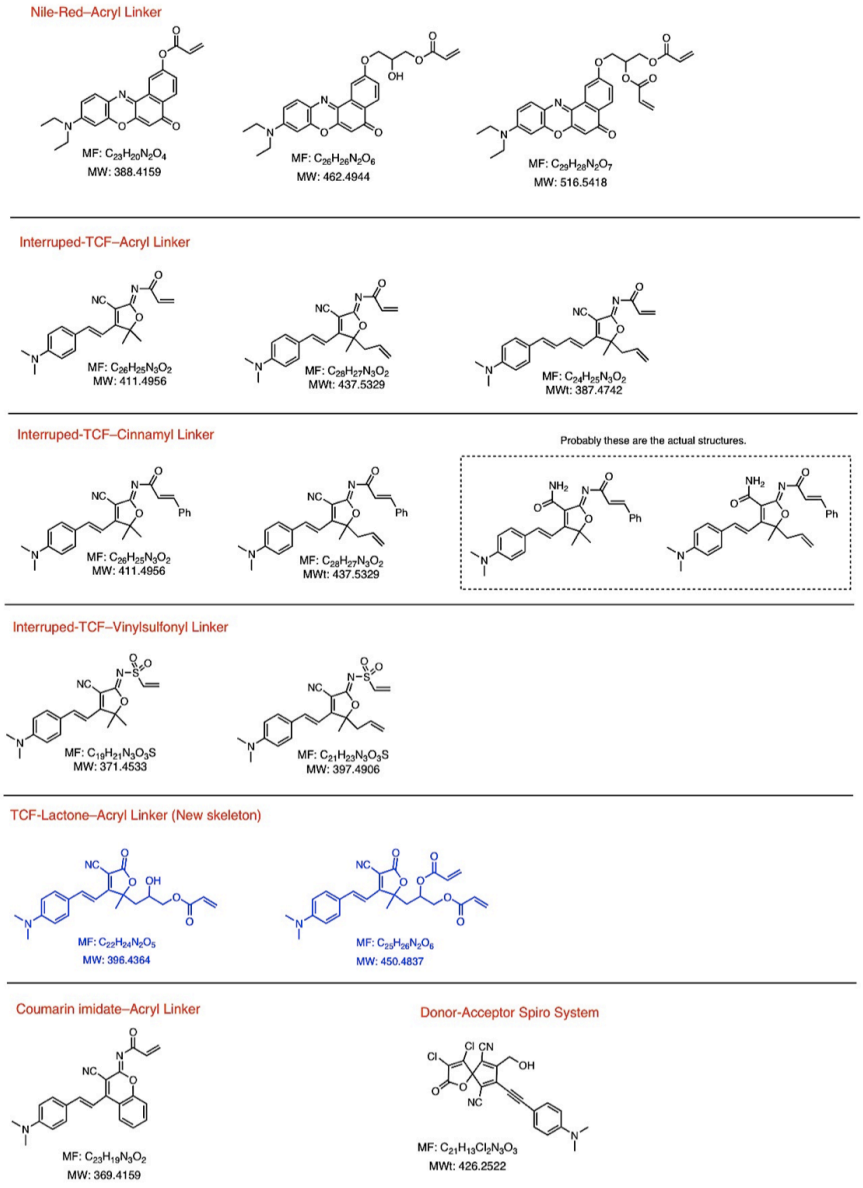

Figure S1. Chemical structures of Environmental Sensitive Fluorophores

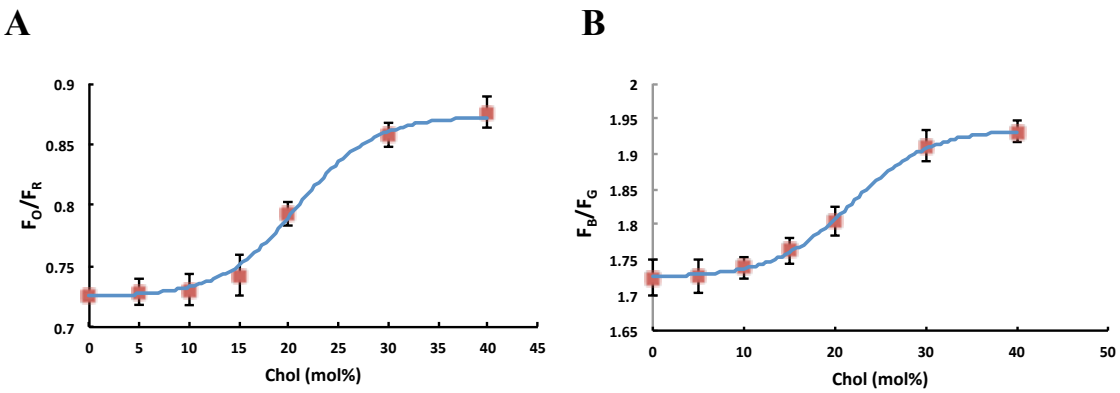

Figure S2. **Ratiometric calibration of D434A/A463W cholesterol sensors.** **(A)** Ratiometric calibration curves of NR3 D434A/A463W and **(B)** DAN-D434A/A463W for cholesterol quantification. The cholesterol sensors were monitored by a two-photon microscope in the presence of POPC/POPS/Cholesterol (80–x:20:x) LUVs. Nonlinear least-squares analysis of the plot using the equation (for DAN-D434A); $F_B/F_G=(F_B/F_G)$ max$/(1+K_d/[\text{cholesterol}])+C$ yields K_d, $(F_B/F_G)_{max}$, and C values and the calibration curves are constructed using these parameters. F_B, F_G, F_o, and FR indicate fluorescence intensities of the blue, green, orange, and red channels, respectively. K_d, $(F_B/F_G)_{max}$, and C are the equilibrium dissociation constant (in mole%), the maximal F_B/F_G value, and the arbitrary instrumental parameter. Error bars indicate standard deviations calculated from at least three independent sets of measurements. For all measurements buffer with 20 mm Tris buffer and 0.16m KCl adjusted to pH=7.4 was use

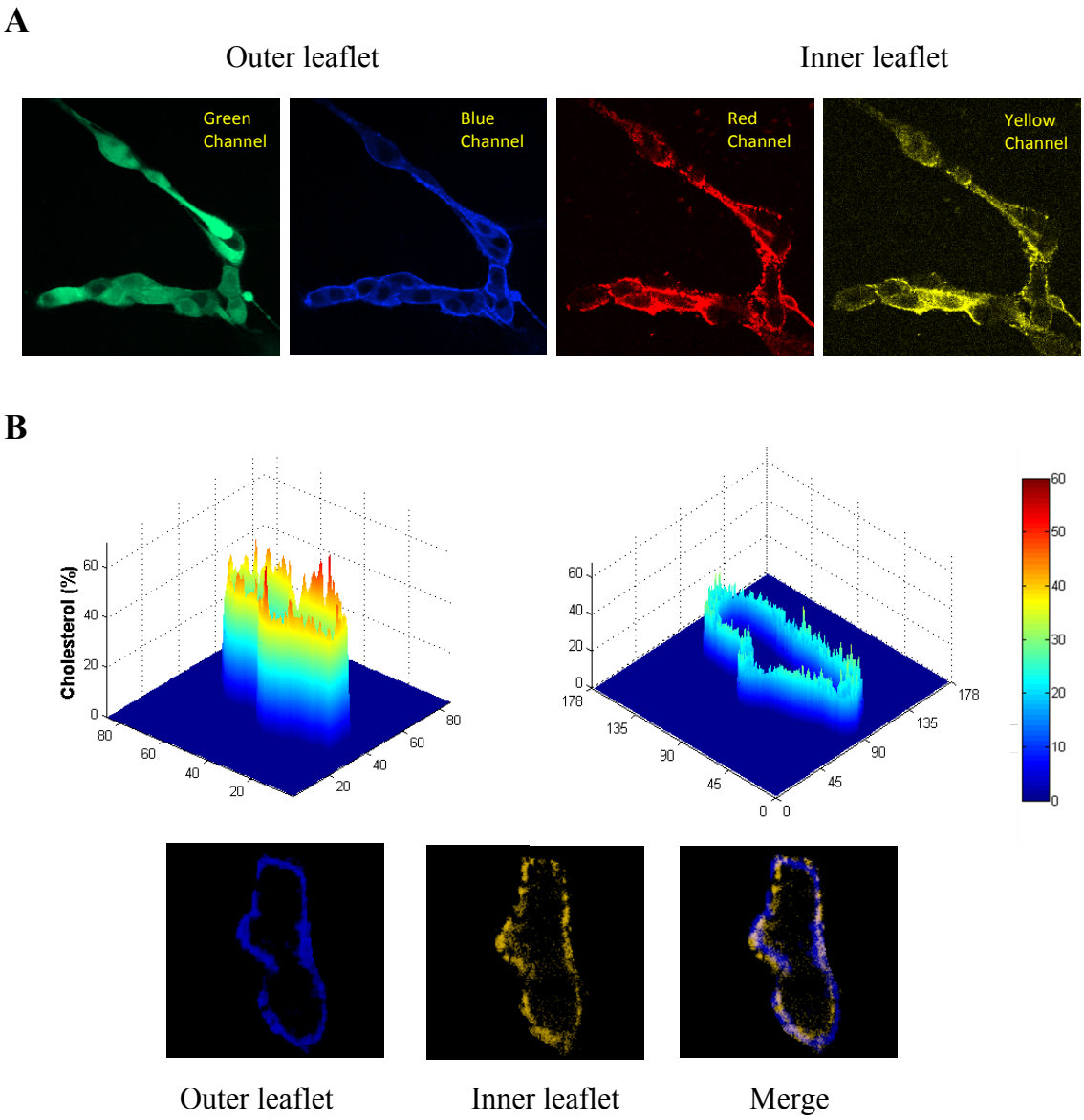

Figure S3. **Simultaneous in situ quantification of cholesterol in the inner and outer PM of NIH 3T3 cells.**
(A) Four-channel images of cholesterol in the inner and outer PM monitored using microinjected NR-D434A/A463W (red and yellow channels) and media-added DAN-D434A/A463W (green and blue channels) sensors, respectively. Membrane-bound sensors are monitored in blue and orange channels while membrane-bound plus free sensors in green and red channels. **(B)** Spatially resolved quantification of cholesterol in the plasma membrane by ratiometric analysis of F_B/F_G and F_O/F_R using the calibration curve in Fig. S. Pseudo-coloring is used for the images (red, highest concentration; blue, lowest). DAN-D434A and NR3-D434A/A463W were two-photon excited at 780 nm and 950 nm, respectively.

The publisher's copyright permission statement

RightsLink®

Home | Account Info | Help | Live Chat

Title: Cholesterol modulates cell signaling and protein networking by specifically interacting with PDZ domain-containing scaffold proteins

Author: Ren Sheng, Yong Chen, Heon Yung Gee, Ewa Stec, Heather R. Melowic, Nichole R. Blatner

Publication: Nature Communications

Publisher: Nature Publishing Group

Date: Dec 4, 2012

Logged in as:
Ewa Stec
LOGOUT

Author Request

If you are the author of this content (or his/her designated agent) please read the following. If you are not the author of this content, please click the Back button and select an alternative Requestor Type to obtain a quick price or to place an order.

Ownership of copyright in the article remains with the Authors, and provided that, when reproducing the Contribution or extracts from it, the Authors acknowledge first and reference publication in the Journal, the Authors retain the following non-exclusive rights:

a) To reproduce the Contribution in whole or in part in any printed volume (book or thesis) of which they are the author(s).

b) They and any academic institution where they work at the time may reproduce the Contribution for the purpose of course teaching.

c) To reuse figures or tables created by them and contained in the Contribution in other works created by them.

d) To post a copy of the Contribution as accepted for publication after peer review (in Word or Text format) on the Author's own web site, or the Author's institutional repository, or the Author's funding body's archive, six months after publication of the printed or online edition of the Journal, provided that they also link to the Journal article on NPG's web site (eg through the DOI).

NPG encourages the self-archiving of the accepted version of your manuscript in your funding agency's or institution's repository, six months after publication. This policy complements the recently announced policies of the US National Institutes of Health, Wellcome Trust and other research funding bodies around the world. NPG recognises the efforts of funding bodies to increase access to the research they fund, and we strongly encourage authors to participate in such efforts.

Authors wishing to use the published version of their article for promotional use or on a web site must request in the normal way.

If you require further assistance please read NPG's online author reuse guidelines.

For full paper portion: Authors of original research papers published by NPG are encouraged to submit the author's version of the accepted, peer-reviewed manuscript to their relevant funding body's archive, for release six months after publication. In addition, authors are encouraged to archive their version of the manuscript in their institution's repositories (as well as their personal Web sites), also six months after original publication.

v2.0

BACK CLOSE WINDOW

VITA

NAME **EWA STEC**

EDUCATION

2010-present	Ph.D	University of Illinois at Chicago	Chemistry
2006 - 2010	B.S.	University of Illinois at Chicago	Biochemistry

CAREERS

2010-present	Research Assistant	University of Illinois at Chicago

TEACHING

2010-2012	Graduate Teaching Assistant	University of Illinois at Chicago
2012-present	Teaching Assistant Coordinator	University of Illinois at Chicago

ABSTARACTS **Poster presentation:**

Ewa Stec, Ren Sheng, Hamid Samareh Afsari, Svetlana Kurilova, and Wonhwa Cho
In situ Quantification of Cellular Cholesterol using a Molecular Sensor
Experimental Biology 2013, Boston MA.

Oral presentation:

Ewa Stec and Wonhwa Cho
Characterization of Cholesterol Binding Domains by SPR
Chicago Biacore and MicroCal User's Day,
Northwestern University, 2013. Evanston IL.

PUBLICATIONS

*Sheng, R., *Liu, S-L., ***Stec, E**., Wang, L., Song, S., Levitan, I., and Cho, W. Transbilayer asymmetry of cholesterol in the plasma membrane accounts for its signaling function manuscript in preparation (*equal contribution)

Sheng, R., Chen, Y., Gee, H. Y., **Stec, E**., Melowic, H.R., Blatner, N.R., Tun, M.P, Kim, Y., Kallberg, M., Fujiwara, T., Hong, J.H., Kim, K.P., Lu, H., Kusumi, A., Lee, M.G., and Cho, W. Cholesterol Modulates Cell Signaling and Protein Networking by Specifically Interacting with PDZ Domain-Containing Scaffolding Proteins. Nature Communications. 2012; 1249(3).